Efficient Beamspace Design and Waveform Optimization for RadCom

By

Ahmed Saleem
11-FET/PhDEE/S18

A dissertation submitted to IIU in partial fulfilment of the requirements for the degree of

DOCTOR OF PHILOSOPHY

Department of Electrical & Computer Engineering
Faculty of Engineering and Technology
INTERNATIONAL ISLAMIC UNIVERSITY
ISLAMABAD

2024

LIST OF PUBLICATIONS

1. **Ahmed Saleem**, Abdul Basit, Muhammad Fahad Munir, Athar Waseem, Wasim Khan, Aqdas Naveed Malik, Salman A. AlQahtani, Amil Daraz, and Pranavkumar Pathak, 2023. "Alternating Direction Method of Multipliers-Based Constant Modulus Waveform Design for Dual-Function Radar-Communication Systems" Entropy 25, no. 7 : 1027.
$https://doi.org/10.3390/e25071027$

2. **Ahmed Saleem**, Abdul Basit, Muhammad Fahad Munir, Wasim Khan, and Aqdas Naveed Malik, "Optimizing Penalty Parameter Selection of Alternating Direction Methods of Multipliers for an Improved Joint Radar-Communication Waveform Design",
(Submitted to "Digital Signal Processing", Elsevier)

3. **Ahmed Saleem**, Abdul Basit, Muhammad Fahad Munir, Athar Waseem, Wasim Khan, and Aqdas Naveed Malik, "Beamspace Design for Joint Radar-Communication Systems"
(Submitted to " Wireless Personal Communications", Springer Limited.)

4. Muhammad Fahad Munir, Abdul Basit, Wasim Khan, Athar Waseem, Muhammad Mohsin Khan, **Ahmed Saleem**, Salman A. AlQahtani, Amil Daraz, and Pranavkumar Pathak. 2023. "Hybrid FSK–FDM Scheme for Data Rate Enhancement in Dual-Function Radar and Communication", Sensors $23, no.12 : 5440$. $https://doi.org/10.3390/s23125440$

5. Muhammad Fahad Munir, A. Basit, W. Khan, A. Waseem, **Ahmed Saleem** and Abdulrehman Al-Salehi, "Frequency Quadrature Amplitude Modulation based Scheme for Dual Function Radar and Communication Systems," 2022 International Conference on Engineering and Emerging Technologies (ICEET), Kuala Lumpur, Malaysia, 2022, pp. $1-5$, doi: $5.1109/ICEET56468.2022.10007302$.

6. Muhammad Fahad Munir, Abdul Basit, Wasim Khan, **Ahmed Saleem**, and Abdulrehman Al-salehi, A Comprehensive Study of Past, Present, and Future of Spectrum Sharing and Information Embedding Techniques in Joint Wireless Communication and Radar Systems. Wireless Communications and Mobile Computing 2022. DOI: $https://doi.org/10.1155/2022/9642849$

7. Muhammad Fahad Munir, Abdul Basit, Wasim Khan, **Ahmed Saleem**, and Nauman Anwar Baig, "Deep Learning-Enabled Design of Joint Cognitive Radar and Communication System for Interference Mitigation in Noisy Channels", Computers and Electrical Engineering (Submitted)

This dissertation includes the research articles from S. No 1 to 3.

 It is declared that the research work presented in this dissertation 'Efficient Beamspace Design and Waveform Optimization for RadCom', is solely my work.

DEDICATED

to the memories of late Dr. Ijaz Mansoor Qureshi

Abstract

Dual-function radar-communication (DFRC) is a crucial technology that integrates radar and communication by sharing frequency resources and hardware. Recent advancements have expanded the scope of information embedding using a unified aperture. This technology now extends beyond military and surveillance to a wide range of civilian and commercial uses. However, beamspace and waveform design have not received enough attention. Further investigation is needed to fully realize the potential of DFRC systems.

This dissertation comprises two major sections. The first section focuses on the design of constant modulus waveforms for DFRC systems based on a multi-input multi-output (MIMO) configuration of sensors deployed in the far-field. Initially, a non-convex optimization problem is formulated to minimize interference power while maintaining a constant modulus constraint. An iterative solution is proposed based on the alternating direction method of multipliers (ADMM). The designed waveforms achieve improved beams for both radar and communication while maintaining low sidelobes. These waveforms ensure enhanced detection probability and bit error rate (BER) for radar and communication, respectively. The effectiveness of the proposed method is demonstrated through extensive simulations.

Another waveform design strategy is proposed for MIMO radar-communication systems, focusing on optimization with constraints on waveform similarity and

constant power. ADMM is also applied to this problem, leading to a novel method of selecting penalty parameters to enhance performance. This strategy prioritizes the power of the main beam in desired directions, such as the radar target and communication receiver, while minimizing sidelobes. The synthesized waveforms are simulated, and the results validate their effectiveness.

The second section of the research addresses beamspace design, with a novel contribution being the development of a beamspace transformation matrix tailored for DFRC systems within a MIMO framework. An optimization problem is formulated to minimize power emissions in undesired locations while preserving the desired power levels toward targets under a constant modulus constraint. The non-convex optimization in this case is also carried out using ADMM. The algorithm produces improved beams for radar and communication while maintaining low sidelobes. This approach enhances radar detection probability and improves BER performance for the DFRC system. Simulation results demonstrate the effectiveness of the proposed approach.

Acknowledgements

The course of my PhD journey has been a challenging yet rewarding experience. I am deeply thankful to Allah Almighty, the Benevolent, the Compassionate, for giving me the strength and capability to persevere through this path. His seen and unseen support guided me throughout, leading me to the right people and right resources.

I would like to express my deepest gratitude to my supervisor, Dr. Aqdas Naveed Malik, for his invaluable guidance and continuous encouragement throughout my research. He also supervised me during my Master's degree. I extend my sincere gratitude to my co-supervisor, Dr. Abdul Basit, who closely monitored my progress through weekly meetings, supported me in times of difficulty, corrected my mistakes, and patiently endured my failures. Dr. Wasim Khan, my unofficial co-supervisor, provided significant support during this time. Muhammad Fahad Munir, my old friend and research buddy, a key member of our research team, provided many opportunities for technical discussions on relevant topics, helping me better understand my research problems and develop optimal solutions. Adeel Jadoon and Umair Hafeez, two other colleagues from our team, also contributed by listening to my presentations and providing constructive feedback. Ebrahim Shahzad, Ahmad Saeed, and Muhammad Umer Naseer, my department fellows, were a constant support system for me. We had many intellectual discussions on various topics during these long years.

Imran Iftikhar, from the Graduate Studies Office, provided invaluable help by easing the non-academic tasks and facilitating my dealings with administrative issues through his excellent coordination. I am also indebted to my cousin, Dr. Israr Ullah, for his selfless support, both technical and non-technical, during this journey. I would also like to thank Muhammad Fahad Khan Shinwari, my childhood friend, for his companionship during this time.

I gratefully acknowledge the financial support provided by the Higher Education Commission (HEC) for both my PhD and my previous degree (MS in Electronic Engineering). The HEC not only covered my tuition and other university fees but also provided a stipend to support my living expenses, allowing me to fully focus on my studies and research work.

My family deserves my utmost gratitude for their unwavering love, patience, and support. My mother, is my paradise. My father, of whom I am an extension both biologically and intellectually, is my hero. My brothers, sister, cousins, our extended family played important roles in my life. Above all, my loyal wife's support has been invaluable. She and our children are the pillars of my life. May Allah keep them happy. I must thank Allah for blessing me with such a wonderful family.

Lastly, I dedicate this thesis to the late Dr. Ijaz Mansoor Qureshi, whose memories continue to inspire me every day. He was my supervisor, advisor, and mentor at the beginning, though his journey with me was brief. May Allah bless his soul.

Ahmed Saleem

Contents

List of Tables

List of Figures

List of Abbreviations

Abbreviation	**Full Form**
ADMM	Alternating Direction Method of Multipliers
ALM	Augmented Lagrangian Method
AM	Amplitude Modulation
ATC	Air Traffic Control
AWGN	Additive White Gaussian Noise
BER	Bit Error Rate
BSP	Beamspace Precessing
CM	Constant Modulus
CMC	Constant Modulus Constraint
CRSS	Communication-Radar Spectrum Sharing
CW	Continuous Wave
DFRC	Dual-Function Radar Communication
DoA	Direction of Arrival
DSSS	Direct-Sequence Spread Spectrum
EW	Electronic Warfare
FANET	Flying Ad hoc Network
FDA	Frequency Diverse Array
FFRED	Far-Field Radiated Emission Design

FM	Frequency Modulation
FHSS	Frequency Hopping Spread Spectrum
FMCW	Frequency-Modulated Continuous Wave
FSK	Frequency Shift Keying
GA	Genetic Algorithm
IO-AW	Iterative Optimization with Amplitude Weighting
IRCS	Integrated Radar and Communication System
ISAC	Integrated Sensing and Communication
JRC	Joint Radar-Communication
LFM	Linear Frequency Modulation
MIMO	Multi-Input Multi-Output
mMIMO	Massive MIMO
mmWave	Millimeter Wave
MTI	Moving Target Identification
NOMA	Non-Orthogonal Multiple Access
OFDM	Orthogonal Frequency Division Multiplex
PAPR	Peak-to-Average Power Ratio
PAR	Phased Array Radar
PCM	Pulse Code Modulation
PRI	Pulse Repetition Interval
PSK	Phase Shift Keying
QAM	Quadrature Amplitude Modulation
QoS	Quality of Service
QPSK	Quadrature Phase-Shift Keying
RCC	Radar-Communication Coexistence
RIS	Reconfigurable Intelligent Surfaces

SAR	Synthetic Aperture Radar
SNR	Signal-to-Noise Ratio
SER	Symbol Error Rate
UAV	Unmanned Aerial Vehicle
ULA	Uniform Linear Array
V2I	Vehicle to Infrastructure
WS	Waveform Synthesis

Chapter 1

Introduction

The convergence of radar and communication technologies, known as dual-function radar-communication (DFRC), represents a transformative synergy at the intersection of wireless communication and radar systems. This integration, also referred to as RadCom, joint DFRC, integrated sensing and communication (ISAC), seeks to harness the complementary strengths of radar sensing and communication functionalities to enhace the capabilities of modern wireless systems. By combining radar's ability to detect objects and measure distances with communication's prowess in transmitting data, RadCom promises enhanced spectrum utilization, improved efficiency, and the facilitation of multifunctional applications that were previously challenging to achieve.

However, the realization of RadCom presents several technical challenges that must be addressed to fully exploit its potential. One significant challenge lies in waveform design, where the waveform characteristics must be optimized to support both radar sensing and communication requirements simultaneously. This entails balancing considerations such as pulse duration, modulation scheme, and bandwidth allocation to ensure robust radar performance while accommodating high-speed data transmission. Another critical aspect is beamspace design, which involves the efficient utilization of antenna arrays to form and steer beams for both radar and communication purposes. Beamspace techniques enable spatial multiplexing, enhancing spectrum efficiency and enabling spatially selective communication and radar operations.

Navigating these challenges requires innovative approaches and methodologies that integrate radar and communication functionalities seamlessly. This chapter explores the background of joint radar-communication, delving into waveform design principles, beamspace techniques, and the overarching objectives and contributions of research in this emerging field. By addressing these fundamental aspects, this research aims to pave the way for advanced RadCom systems capable of supporting diverse applications across industries, from autonomous vehicles to military and telecommunications sectors.

1.1 Background

1.1.1 Joint Radar-Communication

Radar and communication systems have historically developed separately. Radar systems are designed to detect objects, measure distances, and track movement by emitting radio waves and analyzing their reflections. Initially developed for military use during World War II, radar has since expanded to civilian applications like air traffic control, weather monitoring, and remote sensing.

Communication systems, in contrast, focus on transmitting information between two or more points using electromagnetic waves. These systems evolved from basic telegraphy to modern digital communication, improving data rates and reliability through advancements in modulation and signal processing.

The combination of radar and communication into RadCom or dual-function radar-communication (RadCom/DFRC) systems represents a major advancement. RadCom/DFRC merges radar's ability to detect objects with communication's capacity to send data. This integration allows systems to simultaneously detect objects and transmit data, improving decision-making in real-time environments like autonomous vehicles and smart cities. RadCom/DFRC systems also make better use of radio frequencies, helping to alleviate spectrum scarcity, while shared hardware reduces costs and improves flexibility.

1.1.2 Waveform Design

A waveform refers to the shape or structure of a signal used to carry information in communication or radar systems. In radar , waveforms are short bursts of energy designed to improve detection range, accuracy, and resolution. By adjusting pulse duration, frequency, and modulation, radar systems can better detect objects and measure distances.

In communication , waveforms encode data for transmission. Modern communication waveforms use advanced modulation schemes like phase-shift keying (PSK), quadrature amplitude modulation (QAM), or orthogonal frequency-division multiplexing (OFDM) to transmit data efficiently and minimize errors.

In RadCom/DFRC systems , waveforms must perform both radar and communication tasks. These RadCom/DFRC waveforms are designed to detect objects and transmit data simultaneously. The radar side processes reflected signals to detect objects, while the communication side decodes the transmitted data. Parameters like pulse duration, frequency, and modulation are adjusted to balance radar detection and communication needs. Advanced modulation schemes like PSK and OFDM are typically used for the communication side.

Designing waveforms for RadCom/DFRC systems is challenging because both radar and communication functions must share the same spectrum and hardware. The waveforms need to balance precise radar detection with reliable data transmission. This requires innovative designs that adapt to changing environments and operational needs.

For RadCom/DFRC systems, waveform design focuses on optimizing parameters like pulse duration and modulation to achieve both radar and communication goals. Adaptive waveforms, for example, can adjust pulse characteristics in real-time based on environmental feedback, enhancing radar detection while maintaining efficient data transmission. By integrating radar and communication functions into a single waveform, RadCom/DFRC systems maximize spectrum utilization and improve system efficiency.

1.1.3 Beamspace Design

Beamspace processing is a technique used in radar and communication systems to control the spatial characteristics of antenna arrays. In radar systems, beamspace processing helps focus antenna beams on specific directions, improving target detection and accuracy. This technique also reduces interference from other signals, enhancing radar performance.

In communication systems, beamspace processing enables spatial multiplexing and beamforming, which improves signal strength and spectral efficiency. By directing signals to intended receivers and reducing interference from other directions, beamspace processing enhances communication quality and range.

In RadCom/DFRC systems , beamspace processing is crucial because it allows the same antenna arrays to be used for both radar and communication. This technique dynamically allocates antenna resources between radar sensing and communication tasks. RadCom/DFRC systems can switch between radar beamforming for object detection and communication beamforming for data transmission, optimizing spectrum usage and system efficiency.

Beamspace processing in RadCom/DFRC involves designing algorithms to manage antenna arrays effectively. This includes beamforming algorithms that adjust beam directions in real-time to track moving objects or establish stable communication links. By using beamspace processing, RadCom/DFRC systems increase operational flexibility, improve spectral efficiency, and reduce hardware complexity by sharing antenna resources for both radar and communication functions.

1.1.4 Summary of Background

The motivation for RadCom/DFRC systems is to improve spectrum efficiency and reduce hardware costs. These systems combine radar's object detection with communication's data transmission, useful for real-time applications like autonomous vehicles. The main challenge is designing waveforms and antenna systems that can handle both radar and communication functions at the same time. This must be done within the same spectrum and hardware. The solution lies in creating composite waveforms and beamspace techniques . These methods allow DFRC systems to adapt in real-time, optimize spectrum use, and reduce interference, improving overall system performance.

1.2 Problem Statement

DFRC systems face significant challenges in meeting the increasing performance demands in waveform and beamforming design. Moreover, the convergence of radar and communication technologies on a single platform introduces additional complexities such as increased computational demands and the need to mitigate mutual interference.

Efficient waveform designs are vital for minimizing mutual interference and ensuring effective co-existence by maintaining a constant modulus. The designed waveforms play a pivotal role in achieving a seamless balance of integration of functionalities under the constraints of spectrum and hardware capabilities. Therefore, a thorough investigation is imperative for designing new waveforms that optimize the overall performance of integrated radar-communication systems.

Moreover, modern radar and communication systems are increasingly adopting MIMO configurations to enhance performance. Consequently, a robust beamspace design capable of efficiently managing complex antenna arrays is critical. Given that computational complexity significantly escalates during the joint operation of radar and communication systems, effective beamspace processing techniques are crucial for optimizing resource allocation.

Effective waveform and beamspace designs will enable RadCom systems to operate efficiently in diverse and dynamic environments. This technology will benefit a wide range of applications, including autonomous vehicles, military surveillance, and independently operating robots in remote areas.

1.3 Objectives of Research

The objectives of this research aim to tackle the challenges outlined in the Problem Statement.

- The first objective is to optimize joint waveforms tailored for radar and communication functionalities to mitigate mutual interference. This involves designing uncorrelated waveforms that are optimized using convex optimization techniques, while adhering to specified performance constraints.

- The second objective is to propose optimized beamspace designs to enhance system performance and reduce computational complexity in DFRC systems. These designs will focus on efficiently managing antenna arrays and beamforming processes to optimize resource utilization.

1.4 Contributions of the Research

The contributions of this research encompass three main papers, each addressing different aspects of waveform and beamspace design in MIMO-based joint radar-communication systems:

1. **Constant Modulus Waveform Design for DFRC Systems** This paper focuses on the design of constant modulus waveforms for Dual Function Radar-Communication (DFRC) systems operating in a far-field scenario with a multi-input multi-output (MIMO) sensor configuration. The research begins by formulating a non-convex optimization problem aimed at synthesizing waveforms that minimize interference power while adhering to a constant modulus constraint. The problem is tackled using the alternating direction method of multipliers (ADMM) algorithm, iteratively optimizing the waveforms to approximate a desired beampattern with high radar beam gain and slightly elevated communication beam gain, while maintaining low sidelobe levels. Simulation results validate that the designed waveforms significantly enhance detection probability

for radar and reduce bit error rate (BER) for communication components, demonstrating the effectiveness of the proposed methodology.

2. **Constant Power Waveform Design Strategy for MIMO-Based DFRC Systems** This paper presents a novel waveform design strategy tailored for MIMO-based DFRC systems, focusing on the challenge of constant power waveforms. The research formulates an optimization problem aimed at minimizing power radiation in undesired directions while ensuring waveform similarity and adherence to constant power constraints. Utilizing the ADMM algorithm as the computational framework, the approach introduces a new method for selecting penalty parameters to optimize waveforms that approximate desired beampatterns. The designed waveforms achieve high radar and communication main-beam gains in target directions while effectively reducing sidelobes elsewhere. Simulation results validate the efficacy of the strategy in generating intended radar and communication signals within the far-field of the antenna array, offering a promising solution for dual-function radar-communication systems.

3. **Constant Modulus Beamspace Design for MIMO-Based DFRC Systems** This paper addresses the constant modulus beamspace design problem for MIMO-based DFRC systems, proposing an efficient solution methodology. The research formulates the beamspace design as a challenging non-convex optimization problem due to the constant modulus constraint, making conventional methods impractical. The paper employs the ADMM algorithm to iteratively tackle this problem, leveraging the augmented Lagrangian method and dual decomposition principles for enhanced performance. The proposed method enhances radar detection probability and

improves BER for communication components by synthesizing optimized beampatterns. Simulation results demonstrate the effectiveness of the design approach across various metrics, highlighting its convergence properties and capability to synthesize desired beampatterns effectively.

These contributions advance the state-of-the-art in waveform and beamspace design for MIMO-based DFRC systems, offering novel methodologies and demonstrating their effectiveness through comprehensive simulation studies.

1.5 Thesis Outlines

This dissertation investigates the convergence of radar and communication functionalities within a unified system, focusing on optimizing system performance through waveform design and beamspace processing. The research is structured into four chapters, briefly introduced as follows.

Chapter 1 offers an overview of the thesis, discussing the background of joint radar-communication and the motivation for addressing research challenges such as waveform design and beamspace processing in this domain. It defines the research problem, outlines research objectives, and discusses the contributions of the study.

Chapter 2 provides a comprehensive review of relevant literature on radar, communication, and joint radar-communication, covering historical developments and recent trends. It also examines literature related to waveform design and beamspace processing, supported by citations from reports and articles discussing various techniques and methodologies.

Chapter 3 delves into detailed discussions on two waveform design methods for joint radar-communication. Both methods utilize ADMM-based optimization techniques to achieve specific objectives while adhering to various constraints. The first method focuses on designing constant-modulus waveforms for MIMO-based dual-function radar-communication systems. Meanwhile, the second method is dedicated to designing constant-power waveforms for similar integrated systems.

Chapter 4 explores a beamspace design method for joint radar-communication. This approach employs ADMM-based optimization techniques to achieve defined objectives while addressing multiple constraints. Specifically, the method concentrates on designing a constant-modulus beamspace transformation matrix for MIMO-based dual-function radar-communication systems.

Chapter 5 concludes the thesis by presenting the outcomes of the research and evaluating the extent to which the research objectives have been achieved. It compares these results with contemporary research findings, highlighting the significant contributions made. The chapter also proposes future research directions in the field, emphasizing opportunities for further advancements in dual-function radar and communication systems. Additionally, it includes a list of publications resulting from this work.

Chapter 2

Background and Related Literature

This chapter provides a comprehensive introduction to dual-function radar-communication (DFRC) systems, emphasizing their historical development and a thorough review of relevant literature, including recent trends. It also delves into the waveform design problem and beamspace processing within the context of DFRC systems. Additionally, the chapter offers an introduction to the alternating direction method of multipliers (ADMM), highlighting its significance and applications in optimizing DFRC systems.

2.1 Joint Radar-Communication

Although some early research on DFRC exists [6; 7], the current widespread interest in this field is a relatively new phenomenon [8–10]. Historically, radar and communication technologies have evolved along separate paths, each with its own unique advancements and applications. Therefore, to fully appreciate the significance of their convergence, it is essential to first provide a brief overview of their individual developments. This foundational understanding will set the stage for a deeper exploration of the innovative merging of radar and communication technologies into integrated DFRC systems.

2.1.1 Radar

The term radar, derived from radio detection and ranging, was coined by the U.S. Navy in 1940 to describe systems that utilize radio waves for detecting and tracking a wide range of objects, from spacecraft and aircraft to ships, guided missiles, weather formations, and motor vehicles. Radar systems play a crucial role by providing essential information such as range, direction, altitude, speed, and velocity of these objects. Modern radar design integrates advanced signal processing, control systems, information theory, probability theory, and statistical techniques to enhance robustness, adaptability, and overall effectiveness [11].

Originally developed in the early twentieth century for detecting ships and preventing collisions, radar technology experienced significant advancements during the two World Wars. A pivotal milestone was the patenting of a functional radar system by Sir Robert Watson-Watt in 1935, which laid the foundation for practical radar applications. These advancements greatly enhanced radar capabilities, allowing for more effective detection and tracking of various objects [12]. During the second World War, German radar systems pioneered mechanical beam steering techniques, rotating directional antennas to scan entire surveillance regions, marking a pivotal advancement in radar capabilities [13]. Evolving from these early developments, radar systems have progressed considerably, now incorporating technologies like phased array radar (PAR) [14]. PAR systems utilize multiple antenna elements to steer radiation patterns, offering advantages such as high-gain beam patterns, frequency agility, and precise multi-target tracking capabilities. Innovations like frequency diverse array (FDA) radar further optimize beam patterns dynamically across range and angle, adapting to environmental conditions for enhanced performance in complex scenarios [15]. At the forefront of radar technology are cognitive radar (CR) systems, which integrate adaptive waveform techniques and machine learning to autonomously optimize radar operations based on real-time data and mission objectives, thereby pushing the boundaries of radar capability and application [16].

There are two primary categories of radars based on the number of antennas, i.e., single antenna radars and multiple antenna radars [17; 18]. Single antenna radars traditionally employ mechanical rotations to scan the surveillance region in all directions. Later advancements introduced electrical beam steering in phased array radars (PAR), which were initially developed at Lincoln Laboratory in 1958 [19]. This marked the beginning of utilizing multiple antenna elements in radar systems, enabling precise control over the radar beam direction without mechanical movement.

Phased array radars, comprising an array of antenna elements, exploit relative phase variations among these elements to direct the radiation pattern towards desired directions while mitigating undesired ones [14; 20; 21]. The Figure 2.1 show a PAR system based on a ULA with N antennas. These PAR systems offer high-gain beam patterns that are computationally efficient, providing enhanced frequency agility, the capability to generate multiple beams, and improved accuracy in tracking multiple targets [14]. These attributes make phased arrays pivotal in modern radar applications. Despite their advantages, PAR systems typically employ electronic phase shifters, which are significantly more expensive than traditional reflector antennas used in surveillance. Moreover, conventional phased array beam steering remains fixed in angle across all range cells, independent of target range, limiting performance in applications reliant on range-specific operations such as interference suppression, ambiguity

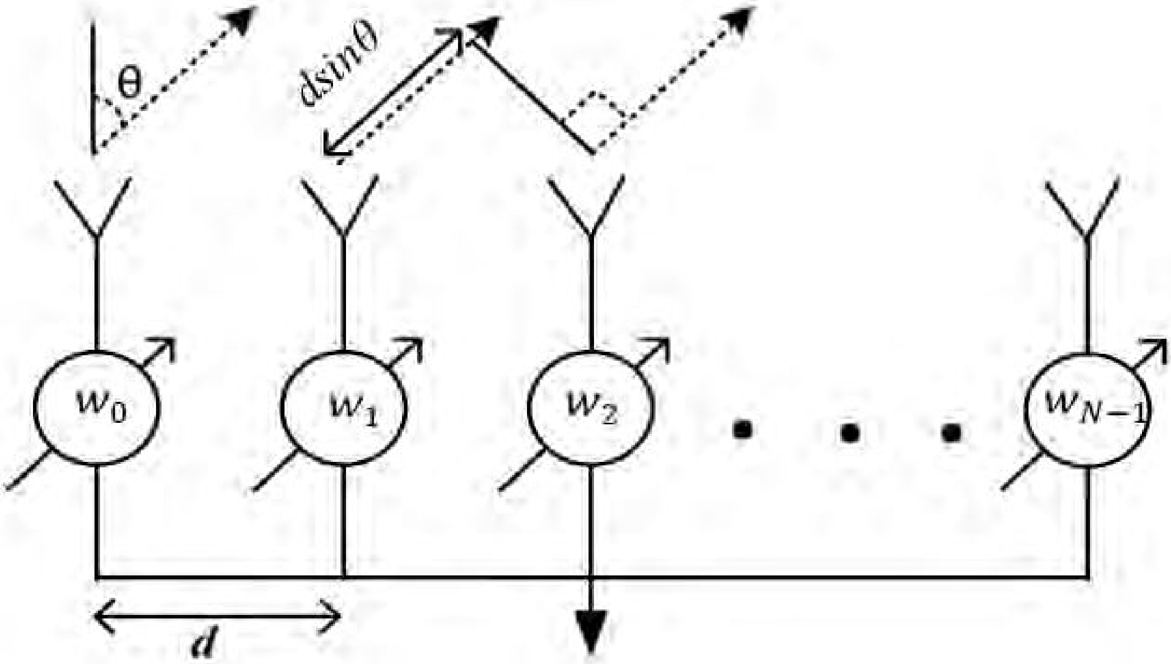

Figure 2.1: Uniform linear array based PAR system with N antennas [1]

resolution, and directional communications [22].

To address these limitations of PAR economically and effectively, researchers have developed frequency diverse array (FDA) radars [23–25]. These systems implement range-angle dependent electronic beam steering using successive frequency offsets across array elements. The Figure 2.2 show a PAR system based on a ULA with *N* antennas. By varying frequencies, FDAs can dynamically adjust beam patterns in response to range and angle changes, facilitating adaptive responses to range-dependent interferences [26; 27]. Unlike PAR systems, FDA radar beam patterns exhibit periodicity in range, angle, and time, periodically illuminating specific range-angle pairs of object positions.

In addition to traditional phased arrays and FDAs, multiple-input multiple-output (MIMO) radar systems represent another advancement in radar technology [2; 28]. The Figure 2.3 show an *N* antenna MIMO system, transmitter and receiver. MIMO radars utilize multiple transmit and receive antennas to exploit spatial diversity, enhancing target detection, localization accuracy, and ro-

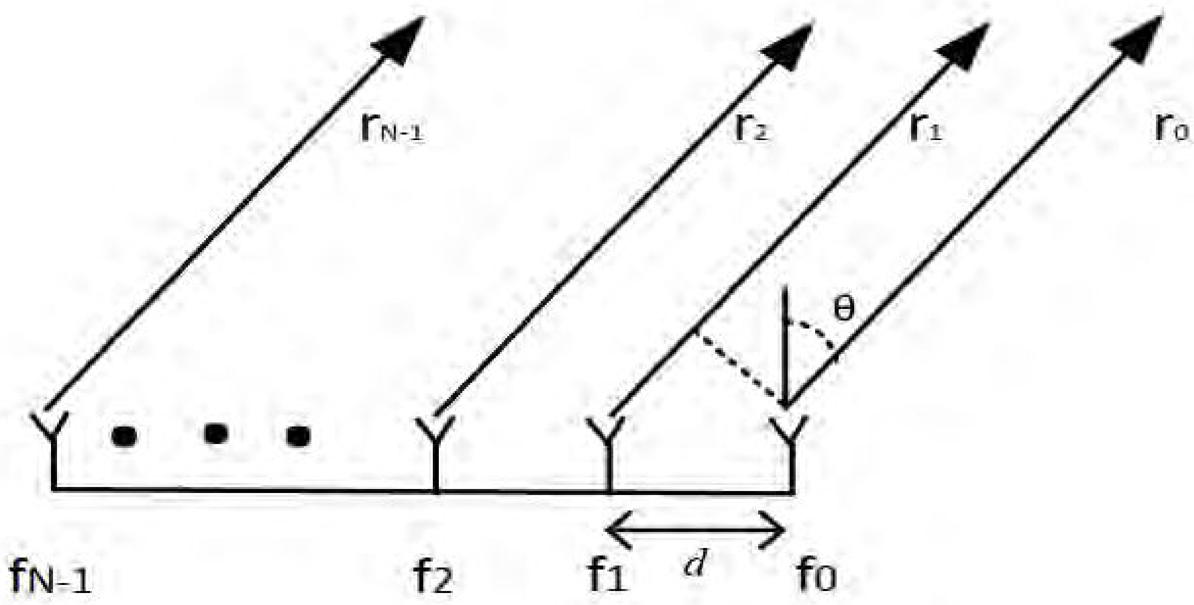

Figure 2.2: Uniform linear array based FDA system with N antennas [1]

bustness against interference [29]. MIMO configurations enable simultaneous transmission of multiple waveforms and reception of complex signals, leveraging spatial processing techniques to achieve superior performance in diverse radar scenarios [30].

2.1.2 Communication

Communication systems, integral to modern society, encompass a rich history of technological advancements and evolving applications [31–33]. Originating from fundamental telegraphy and telephony systems of the 19th and early 20th centuries, modern communication technologies have transformed global connectivity and information exchange. Today's communication systems span a wide spectrum, from traditional wired telephony to advanced wireless networks and satellite communications.

The term 'communication' broadly refers to the transmission and reception of information between entities, enabling real-time interaction, data exchange,

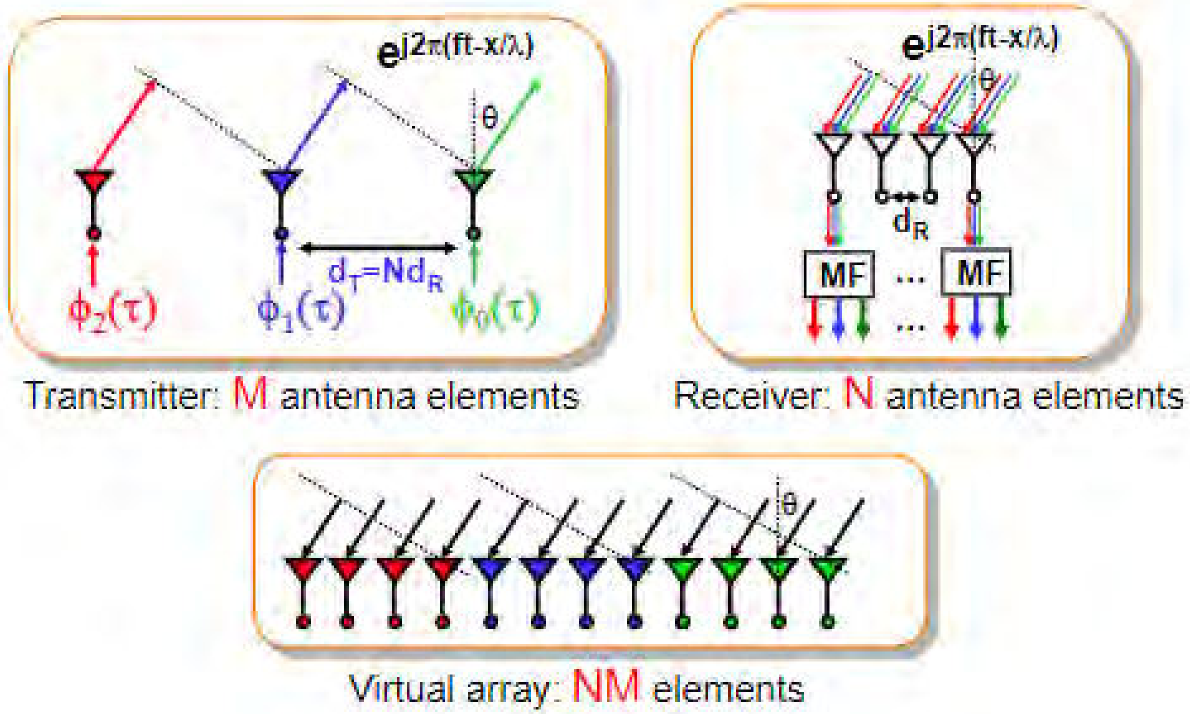

Figure 2.3: MIMO transmitter and receiver with virtual array concept [2]

and collaboration across vast distances. Early communication technologies such as the telegraph, invented in the early 19th century, revolutionized long-distance messaging by transmitting coded electrical signals over wires [34]. This innovation laid the groundwork for subsequent developments in telecommunications, leading to the invention of the telephone by Alexander Graham Bell in 1876, which enabled voice communication over long distances [35].

In the 20th century, rapid advancements in communication technologies accelerated the evolution of global networks. The development of radio communication and wireless telegrahhy, pioneered by figures like Guglielmo Marconi, facilitated wireless transmission of signals over long distances, transforming maritime communication, broadcasting, and eventually, mobile communications [36; 37]. The mid-20th century saw the advent of digital communication technologies, beginning with the invention of the transistor and the subsequent development of digital signal processing techniques.

Recent decades have witnessed a paradigm shift in communication systems driven by digitalization, convergence, and the proliferation of mobile and broadband technologies [38–40]. The emergence of the internet in the late 20th century revolutionized communication by enabling global data transmission through interconnected networks. The integration of voice, data, and multimedia services over IP-based networks has ushered in the era of converged communication systems, where traditional boundaries between telecommunication, broadcasting, and computing continue to blur.

Today, communication systems encompass a diverse range of technologies including fiber-optic networks, satellite communications, cellular networks, and emerging technologies such as 5G and beyond. These systems enable high-speed data transmission, multimedia streaming, real-time collaboration, and IoT connectivity on a global scale. The evolution towards more intelligent, adaptive, and secure communication systems continues to drive innovation in areas such as artificial intelligence, machine learning, and quantum communication.

2.1.3 Joint Radar-Communication

DFRC systems represent a convergence of radar and communication technologies, aimed at maximizing spectrum utilization and operational efficiency [8–10]. Historically, radar and communication systems have evolved independently, serving distinct purposes in navigation, surveillance, and information exchange. However, the integration of these technologies into unified systems promises enhanced capabilities for both civilian and military applications. Figure (2.4) shows different scenarios of joint radar-communication for autonomous vehicles.

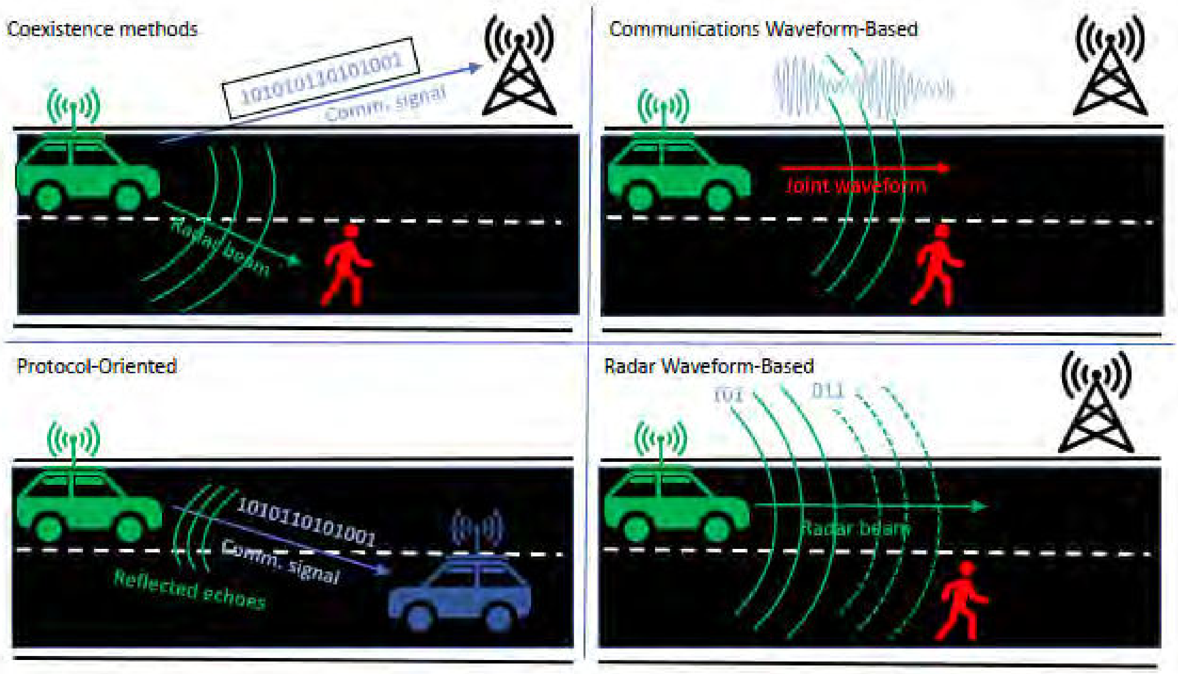

Figure 2.4: Different joint radar-communication scenarios for autonomous vehicles [3]

The term 'joint radar-communication' refers to systems that combine radar functionalities, such as object detection and tracking, with communication capabilities for data exchange or control signaling. This integration enables dual-functionality within a single platform, reducing equipment footprint, power consumption, and operational costs while enhancing mission flexibility and situational awareness.

Early developments in DFRC systems date back to experimental efforts during the mid-20th century, where radar systems were adapted to carry out rudimentary communication tasks and vice versa [6]. However, significant advancements have been made in recent decades, driven by advances in signal processing, antenna technology, and system integration.

Modern DFRC systems leverage sophisticated waveform design techniques to optimize signal transmission and reception in shared frequency bands [41–43]. These systems employ adaptive beamforming and beamsteering technologies to enhance spatial resolution, minimize interference, and improve communication reliability. By dynamically allocating resources between radar and communication functions, DFRC systems maximize spectrum efficiency while maintaining operational effectiveness.

Recent developments in DFRC systems include the integration of cognitive capabilities, where systems autonomously adapt their operation based on environmental conditions and mission objectives [44–46]. Cognitive radar-communication systems utilize machine learning algorithms to analyze and optimize waveform characteristics, adapt to changing electromagnetic environments, and mitigate interference [47].

The deployment of DFRC systems spans diverse applications, from military surveillance and battlefield communications to civilian use cases such as air traffic control, disaster response, and remote sensing. These systems enable simultaneous operation of radar and communication functions, facilitating real-time data exchange, target tracking, and situational awareness in dynamic and complex environments.

2.2 Waveform Design: Optimizing Signals for Wireless Applications

At the heart of modern telecommunications and radar systems lies the concept of waveform design [41; 42; 48]. A waveform, is a time-varying signal that carries information or serves a specific purpose in a system. It is typically represented by its amplitude and frequency characteristics. It can take various forms — from simple sine waves to complex modulated signals — each tailored to meet specific requirements in communication, radar, or other applications.

In communications, waveforms encode information that can be transmitted over a medium, such as wires, fiber optics, or through the air via radio waves. These signals can be analog or digital, depending on the nature of the information and the transmission medium. In radar systems, waveforms are essential for transmitting and receiving signals that detect and track objects. These waveforms, transmitted as pulses or continuous waves, interact with objects and reflect back to the radar receiver, providing information on the object's range, speed, and other characteristics.

Waveform design plays a crucial role in optimizing the performance and efficiency of communication and radar systems. The design process involves shaping the characteristics of the signal to achieve desired objectives, such as maximizing data transmission rates, improving signal-to-noise ratio (SNR), enhancing spectral efficiency, and ensuring robustness against interference and noise.

Waveforms can be classified in different ways like continuous, pulsed and modulated waveforms. Continuous waveforms have a continuous and unbroken shape over time, such as sine waves and cosine waves. They are commonly used in applications requiring continuous transmission or oscillation, such as in radar for continuous wave (CW) radar systems. Pulsed waveforms consist of discrete bursts of energy separated by periods of little to no transmission. They are widely employed in radar systems for detecting and ranging objects, where the duration and timing of pulses determine the radar's range resolution and maximum detectable range. Modulated waveforms alter one or more properties of a carrier wave to encode information. Common modulation techniques include Amplitude Modulation (AM), Frequency Modulation (FM), Phase Modulation (PM), and more advanced forms such as Quadrature Amplitude Modulation (QAM) used in digital communication systems.

The design of optimal waveforms presents several challenges, particularly in modern, complex systems. Designers must balance conflicting objectives such as bandwidth efficiency versus robustness to noise and interference, which often involves trade-offs. In systems like Multiple-Input Multiple-Output (MIMO) radar and communication, waveform design becomes even more intricate due to the need to optimize multiple signals transmitted and received by multiple antennas simultaneously. Additionally, waveforms should be adaptive to changing environmental conditions, varying channel characteristics, and operational requirements to maintain reliable performance.

Recent advancements in waveform design leverage sophisticated mathematical tools and algorithms to enhance system performance. Optimization techniques, such as genetic algorithms (GA), particle swarm optimization (PSO), and convex optimization, are employed to determine optimal waveform parameters under given constraints. Machine learning approaches, including Deep Learning and Reinforcement Learning, are increasingly applied to automate waveform design, enabling adaptive optimization based on real-time conditions. Additionally, cognitive waveforms utilize cognitive techniques to dynamically adjust parameters based on environmental feedback, thereby improving adaptability and efficiency.

2.2.1 Waveform Design for Radar

The design of radar waveforms has been a topic of significant research interest for several decades [1]. A fundamental question in this field is: what constitutes a good waveform for radar? This question was particularly challenging in the early days of radar technology, as radar waveforms themselves do not inherently carry information; any pulse, pulse train, or continuous wave

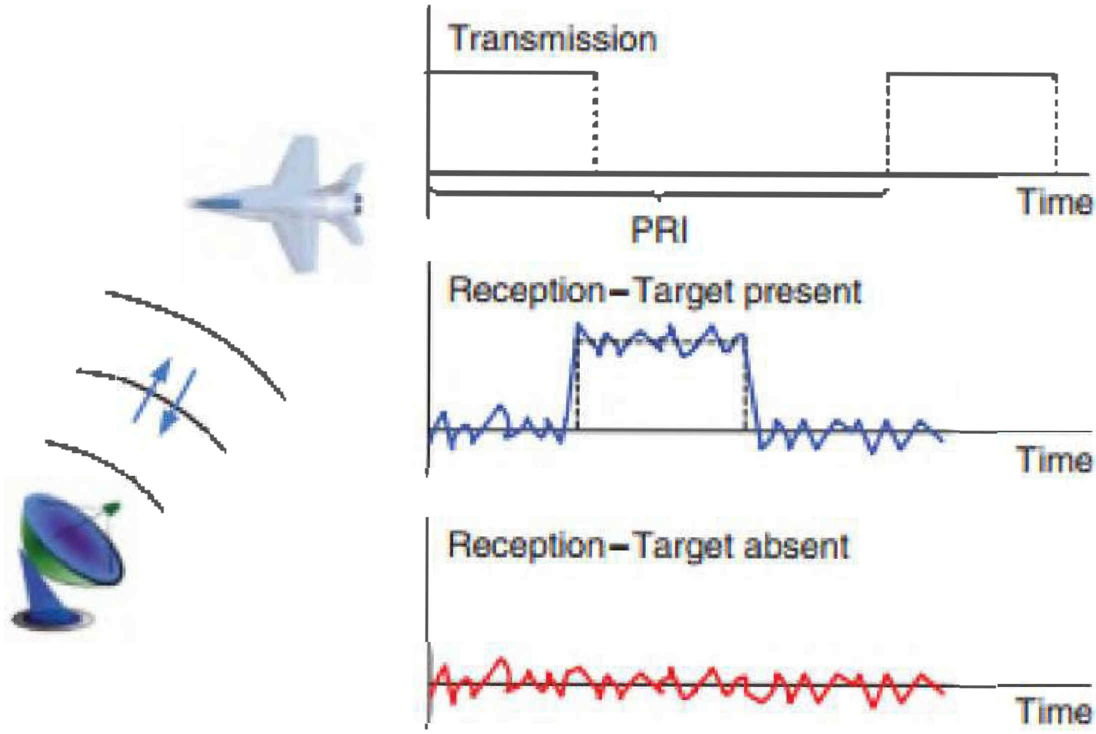

Figure 2.5: Basic operation of pulse radar [4]

can be reflected from metallic targets. However, research has demonstrated that certain properties make some waveforms more suitable for specific radar functions than others. The approach to designing an optimal radar waveform is typically task-dependent. For instance, to detect a particular target, maximizing the output signal-to-noise ratio (SNR) is crucial, and the optimal waveform concentrates all available energy into the target's largest mode. A well-designed transmit waveform not only facilitates accurate parameter estimation but also reduces the computational burden at the receiver, enhancing overall system performance.

Pulse radar systems were developed prior to the extensive progress made during World War II. These early radar systems primarily employed simple pulse waveforms, which involved transmitting short bursts of electromagnetic energy into the environment. The reflections of these pulses were analyzed to determine the presence and distance of objects. In waveform design, pulse radar systems transmit bursts separated by periods of silence, during which the radar listens for echoes. The basic principle of a pulse radar is shown in Figure (2.5). The time delay between the transmission and reception of a pulse is used to calculate the distance to the target. Valued for their straightforward and reliable design, pulse radar waveforms provide crucial range information and enable the detection of various objects, such as aircraft and ships.

World War II served as a transformative period for radar technology, accelerating its development in significant ways. The maturation of several pivotal radar techniques in the late 1940s and early 1950s—including pulse Doppler, also known as moving target identifier (MTI), monopulse (simultaneous lobing), phased array, and synthetic aperture—marked crucial milestones in waveform design for radar systems. These advancements underscored the importance of tailored waveforms to meet specific operational challenges and enhance performance across various radar applications.

- **Pulse Doppler radar (MTI):** Introduced to distinguish moving targets amidst clutter, pulse Doppler radar systems required waveforms optimized for precise Doppler frequency resolution, enabling enhanced target detection capabilities.

- **Monopulse radar:** Essential for accurate target tracking and guidance systems, monopulse radar relied on meticulously designed waveforms to ensure high angular resolution and stability, crucial for maintaining tracking accuracy.

- **Phased array radar:** Phased array radars revolutionized beam steering by electronically adjusting waveforms, necessitating sophisticated designs to maintain beam coherence and accuracy across multiple array elements.

- **Synthetic aperture radar (SAR):** SAR systems demanded waveforms capable of high range resolution and long-term coherence to synthesize large apertures and achieve detailed spatial imaging of target areas.

- **Frequency Diverse Arrays (FDA):** FDA radar systems utilized waveform designs that dynamically adjusted beam patterns based on range and angle, enhancing adaptability and performance in complex environments with varying interferences.

- **Multiple-Input Multiple-Output (MIMO) Radar:** Leveraging spatial diversity with multiple antennas, MIMO radar systems required waveform designs capable of simultaneous transmission and reception of multiple signals, optimizing target detection, localization accuracy, and interference mitigation.

Table 2.1 highlights significant milestones in the evolution of radar waveform design.

2.2.2 Waveform Design for Communication

Waveform design in communication systems has evolved significantly over the past centuries, driven by technological advancements and the quest for more efficient and reliable transmission methods. From the early days of Morse code to the era of 5G and beyond, each milestone represents a leap forward in our ability to transmit information over vast distances with increased speed, accuracy, and resilience to noise and interference.

Year	Milestone
1862	Maxwell's equations lay the theoretical foundation for electromagnetic wave propagation and reflection.
1884	Oliver Heaviside simplifies Maxwell's equations, making them more accessible and applicable to practical engineering.
1904	Development of pulse-Doppler radar during World War II, significantly enhancing radar's ability to detect moving targets.
1943	Introduction of matched filter theory, optimizing radar waveform design to maximize signal-to-noise ratio (SNR) and detection performance.
1950s	Introduction of continuous wave (CW) radar and frequency-modulated continuous wave (FMCW) radar, improving range resolution and measurement accuracy.
1958	Development of phased array radar (PAR) at Lincoln Laboratory, enabling electronic beam steering and multi-target tracking.
1970s	Development of chirp radar and linear frequency modulation (LFM) waveforms, which offer improved range resolution and Doppler tolerance
1980s	Advancements in synthetic aperture radar (SAR) and inverse synthetic aperture radar (ISAR) using sophisticated waveform design for high-resolution imaging.
1990s	Introduction of adaptive radar waveforms, utilizing real-time environmental feedback to optimize performance.
2000s	Emergence of multiple-input multiple-output (MIMO) radar, leveraging spatial diversity and advanced waveforms for enhanced detection and resolution.
2010s	Development of cognitive radar systems, incorporating machine learning and adaptive waveforms to optimize radar operations dynamically
2020s	Exploration of quantum radar technologies, potentially revolutionizing radar waveform design with principles of quantum mechanics for superior performance

Table 2.1: Important Milestones in Radar Waveform Design

2.2.2.1 Early Telegraph and Telephone Era

The journey of waveform design can be traced back to the 19th century, when Samuel Morse's demonstration of the telegraph system in 1838 marked a pivotal moment in communication history. Morse code, using simple on-off keying waveforms, allowed messages to be transmitted over electric wires by encoding text characters as sequences of dots and dashes. This method laid the foundation for subsequent advancements in telecommunication.

In 1876, Alexander Graham Bell patented the telephone, revolutionizing communication with analog waveforms that transmitted voice signals over wires.

The analog signals varied in amplitude (for voice) and frequency (for tones), enabling real-time voice communication across distances previously unimaginable.

2.2.2.2 Radio Broadcasting and Modulation Techniques

The advent of radio broadcasting in the early 20th century introduced new challenges and opportunities in waveform design. Amplitude modulation (AM), widely adopted in the 1920s, enabled the transmission of audio signals over radio waves by varying the amplitude of the carrier signal in proportion to the amplitude of the input signal. This breakthrough allowed for widespread dissemination of news, entertainment, and cultural programming.

In 1933, Edwin Armstrong's invention of frequency modulation (FM) offered improved audio quality and greater resistance to noise compared to AM. FM works by varying the frequency of the carrier wave in response to the audio signal, reducing interference and static, thus enhancing the clarity of broadcasted sound.

2.2.2.3 The Digital Revolution and Modern Modulation Schemes

The digital revolution in communication began in earnest in the mid-20th century with the development of digital modulation techniques. Pulse code modulation (PCM), introduced in the 1950s, revolutionized voice communication by converting analog signals into digital form for transmission over digital networks. PCM paved the way for digital communication systems, offering higher fidelity and reliability compared to analog counterparts.

During the 1960s, phase-shift keying (PSK) and frequency-shift keying (FSK) emerged as early digital modulation schemes. PSK modulates the phase of the carrier signal to represent digital data, while FSK uses different frequencies to represent different binary states. These techniques laid the groundwork for more sophisticated digital communication systems capable of transmitting data with improved efficiency and reliability.

2.2.2.4 Advancements in Modulation Complexity

By the 1970s, quadrature amplitude modulation (QAM) emerged as a breakthrough modulation scheme, combining amplitude and phase modulation to achieve higher data rates and spectral efficiency. QAM variants such as 16-QAM and 64-QAM became integral to digital communication standards, enabling higher-speed data transmission over existing communication channels.

In the 1980s, orthogonal frequency-division multiplexing (OFDM) emerged as a pivotal modulation technique. OFDM divides the transmission bandwidth into multiple orthogonal subcarriers, each carrying a part of the data stream. This approach improves spectral efficiency, mitigates multipath interference, and enhances robustness in challenging transmission environments, making it ideal for broadband communication systems.

2.2.2.5 Digital Security and Spread Spectrum Techniques

The 1990s witnessed significant advancements in digital security and robustness with the introduction of spread spectrum techniques. Direct sequence spread spectrum (DSSS) and frequency-hopping spread spectrum (FHSS) techniques were developed to enhance communication security and resistance to interference. DSSS spreads the signal over a wide frequency band using a pseudo-random sequence, while FHSS rapidly switches frequencies during transmission to minimize the impact of interference.

2.2.2.6 Emergence of MIMO and Cognitive Radio

In the 2000s, multiple-input multiple-output (MIMO) technology revolutionized wireless communication by using multiple antennas to transmit and receive multiple data streams simultaneously. MIMO systems leverage spatial diversity to improve spectral efficiency, increase data throughput, and enhance link reliability in both stationary and mobile communication environments.

The concept of cognitive radio emerged as a promising approach in the 2010s, enabling intelligent and adaptive use of radio spectrum. Cognitive radio systems employ dynamic spectrum access and advanced waveform adaptation techniques to optimize spectrum utilization in real-time based on environmental conditions and user requirements. This approach maximizes spectral efficiency and enhances the flexibility of communication networks, paving the way for future 5G and beyond technologies.

2.2.2.7 Cellular Netwroks - Towards 5G and Beyond

In the 2020s, the focus has shifted towards millimeter-wave (mmWave) communication and 5G technologies. These advancements leverage advanced waveform designs and massive MIMO (multiple-input multiple-output) to achieve unprecedented data rates, ultra-low latency, and massive connectivity. mmWave communication utilizes high-frequency bands to transmit large volumes of data, enabling applications such as augmented reality, autonomous vehicles, and industrial automation.

Wireless mobile communication has evolved through several generations, from the introduction of 1G networks in the 1980s enabling basic voice calls to the current 5G networks offering enhanced mobile broadband services and support for IoT devices. Each generation, including 2G for digital voice and

SMS, 3G for mobile internet access, and 4G for high-speed data transmission, has marked significant milestones in improving connectivity and user experience. 5G builds upon these advancements by introducing ultra-reliable low-latency communication (URLLC), massive machine-type communication (mMTC), and enhanced mobile broadband (eMBB), supporting diverse applications with varying requirements. Looking ahead, research and development efforts are underway for 6G networks, envisioned to further enhance capabilities such as terahertz spectrum utilization, AI-driven networks, and ubiquitous connectivity, ushering in a new era of seamless, high-speed wireless communication.

Table 2.2 highlights significant milestones in the progress of waveform design of communication systems.

2.2.3 Waveform Design for Joint Radar-Communication

Waveform design for DFRC systems encompasses several strategic approaches aimed at integrating radar and communication functionalities efficiently. These methods can be categorized into four main classes: separate coordinated signal transmission, communications waveform-based schemes, radar waveform-based techniques, and dedicated dual-function waveforms.

2.2.3.1 Separate Coordinated Signal Transmission

In this approach, distinct signals are employed for radar and communication purposes to mitigate cross-interference between the two functions. This is the scenario where radar and communication systems co-exist on the same frequencies spectrum but do use the same hardware platforms. Techniques such as time and frequency division are commonly used to allocate separate resources

Year	Milestone
1838	Samuel Morse demonstrates the first practical telegraph system, using simple on-off keying waveforms (Morse code) for communication.
1876	Alexander Graham Bell patents the telephone, which uses analog waveforms to transmit voice signals over wires.
1920s	Introduction of amplitude modulation (AM) for radio broadcasting, enabling audio signals to be transmitted over long distances.
1933	Edwin Armstrong develops frequency modulation (FM), providing improved audio quality and resistance to noise compared to AM.
1948	Claude Shannon publishes his groundbreaking work on information theory, laying the theoretical foundation for digital communication and waveform design.
1950s	Introduction of pulse code modulation (PCM), a method for digitally representing analog signals, leading to the development of digital communication systems.
1960s	Development of phase-shift keying (PSK) and frequency-shift keying (FSK), early digital modulation schemes that improve data transmission efficiency and reliability.
1970s	Emergence of quadrature amplitude modulation (QAM), combining amplitude and phase modulation to achieve higher data rates.
1980s	Introduction of OFDM, which improves spectral efficiency and robustness to multipath interference, becoming the basis for many modern communication standards.
1990s	Development of spread spectrum techniques, such as direct sequence spread spectrum (DSSS) and frequency-hopping spread spectrum (FHSS), enhancing security and resistance to interference.
2000s	Implementation of MIMO technology, utilizing multiple antennas and sophisticated waveforms to significantly increase data throughput and link reliability.
2010s	Advancements in cognitive radio, leveraging dynamic spectrum access and adaptive waveforms to optimize communication in real-time based on environmental conditions.
2020s	Exploration of millimeter-wave (mmWave) communications and 5G technologies, utilizing advanced waveforms and massive MIMO to achieve unprecedented data rates and low latency.

Table 2.2: Important Milestones in Communication Waveform Design

for each waveform. For instance, different time slots or frequency bands are assigned to radar and communication signals, ensuring minimal interference and optimizing system resources [17]. Fixed and non-overlapping frequency allocation strategies have been explored in various studies [18], while others have introduced randomized antenna allocation to enhance communication rates and radar angular resolution [19]. Spatial beamforming with multiple antennas is also utilized to reduce interference by directing radar waveforms away from communication receivers' channels [21]. Despite the computational demands of optimal resource allocation, simpler fixed allocation schemes are often implemented to balance performance and complexity.

2.2.3.2 Communications Waveform-Based Schemes

This approach involves using standard communication waveforms for radar probing, leveraging their efficiency and adaptability. Orthogonal Frequency Division Multiplexing (OFDM) is widely adopted in communication-centric JRC designs due to its spectral efficiency and robustness against inter-symbol interference (ISI) [23]. OFDM waveforms are adapted for radar applications by adjusting sub-carrier spacing to accommodate radar range and velocity requirements [24], [25]. However, processing OFDM waveforms for radar purposes can lead to high sidelobes, a challenge addressed by dividing subcarriers into symbol-specific groups [22].

2.2.3.3 Radar Waveform-Based Techniques

Radar-centric JRC strategies embed communication functionalities within radar waveforms or use index modulation (IM) techniques. Modified radar waveforms, such as frequency modulated continuous wave (FMCW) with embedded phase-modulated symbols, offer simplicity and power efficiency but may limit data rates due to waveform constraints [26], [27]. IM techniques exploit radar parameters like antenna allocation or carrier frequency indices to transmit communication data without altering the radar waveform itself. IM-based systems, including those utilizing Frequency Agile Radar (FAR) principles, enhance spectral efficiency by adapting radar waveforms dynamically across multiple carrier frequencies [30], [31], [33].

Year	Reference	Description
1963	[6]	The first DFRC scheme is proposed, the radar pulses are used to embed communication data
1996	[7]	The AMRFC program by the Office of Naval Research (ONR) of the US to develop integrated RF systems that could simultaneously perform multiple RF functions
2003	[49]	An investigation of radar and communications utilizing LFM waveforms is presented
2006	[50]	An integration system of radar and communication based on DSSS is proposed
2006	[51]	Application of MIMO radar-centric OFDM waveforms for communication application is proposed
2007	[52]	The designed, simulated, fabricated, and tested of UWB multifunctional communication-radar system is presented
2011	[42]	OFDM based DFRC signaling scheme is proposed
2014	[53]	The first information-theoretical analysis for DFRC systems
2016	[54]	The first signaling scheme for MIMO DFRC systemis in proposed where communication data is embedded into the sidelob of a MIMO radar beampattern
2020	[55]	First instance of RIS-assisted joint radar-communication
2022	[56]	First instance of application of beamspace to JRC applications

Table 2.3: Important Milestones in Joint Radar-Communication Waveform Design

2.2.3.4 Dedicated Dual-Function Waveforms

The evolution towards dedicated dual-function waveforms aims to optimize performance trade-offs between radar and communication functions. These waveforms are specifically designed to fulfill both radar detection requirements and communication data transmission needs simultaneously. Unlike traditional waveform extensions, dedicated dual-function waveforms are tailored to achieve specific radar beam patterns while maintaining communication integrity [36]–[38]. Optimization techniques such as joint precoding and beamforming ensure that radar performance meets desired criteria while minimizing interference and maximizing communication reliability [37], [38].

Table 2.3 highlights significant achievements in the field of DFRC systems.

2.3 Beamspace Processing and Beamspace Transformation Matrix Design

Beamspace (BS) signal processing is a spatial signal processing technique that uses beam output data to perform various operations, such as beamforming, direction-of-arrival (DOA) estimation, and interference mitigation. In BS processing, the array output is first processed by a beamformer to form a set of beams, and then the beam outputs are used for further processing instead of the element outputs.

Some key applications of BS signal processing in joint radar-communications include the following.

- **Waveform design:** BS processing can be used to design waveforms for dual-function radar-communication (DFRC) systems. For example, Saleem *et al.* have designed constant modulus waveforms for MIMO-based DFRC systems using BS techniques.

- **DoA Estimation:** BS processing can improve DOA estimation performance at low computational cost compared to element-space processing. Qi *et al.* have proposed a method for DOA estimation of coherent signals using BS matrix reconstruction.

- **Interference mitigation:** By restricting beams to a sector of interest, BS processing can attenuate signals or interferences outside that sector, reducing their impact on the desired signal.

- **Reduced computational complexity:** BS processing has lower dimensionality than element-space processing, requiring fewer samples for covariance matrix estimation and reducing computational load.

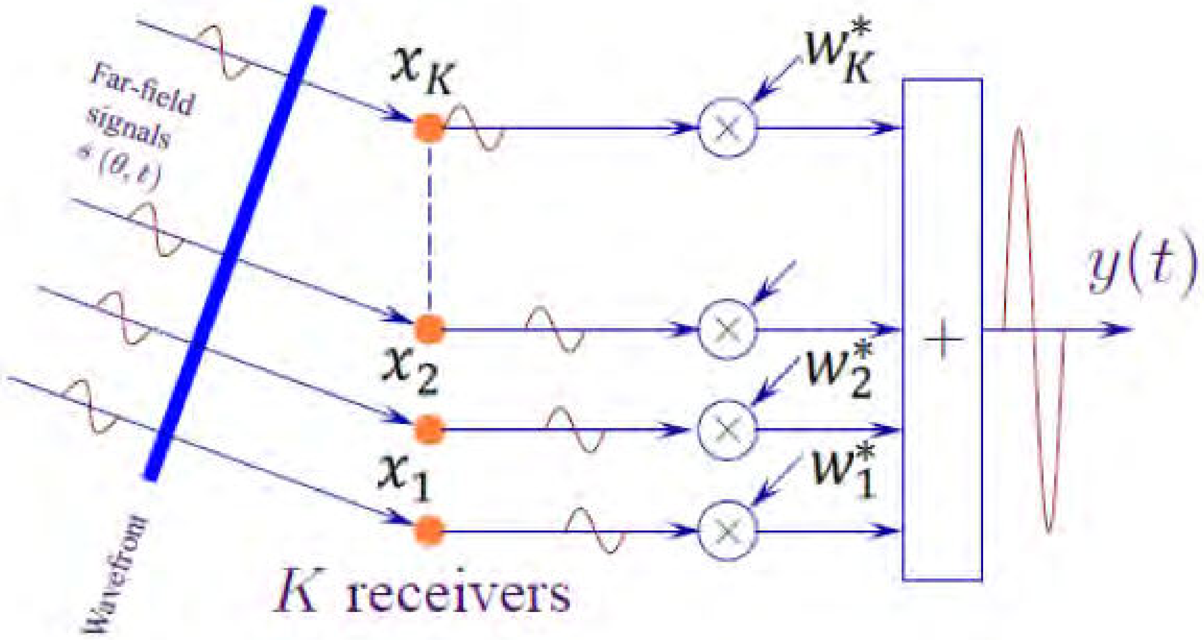

Figure 2.6: Beamforming in element-space [5]

- **Improved detection threshold:** The averaging procedure in BS beamforming can lower the detection signal-to-noise ratio (SNR) threshold compared to element-space processing.

- **Robustness to noise and wavefront distortions:** BS processing can reduce the sensitivity of high-resolution methods to noise distribution and wavefront distortions.

Beamspace processing can be contrasted with the so-called element-space processing. In element-space processing, the input data consists of the raw signals from each individual antenna element, while in beamspace processing, the input data is the output of a beamformer that combines the signals from multiple elements into a set of beams. The space spanned by output of the beamformers is called beamspace, and processing using this output is called beamspace processing. Figures 2.6 and 2.7 show the comparison of a beamformer in element-space and beamspace, respectively. Beamspace processing has lower dimen-

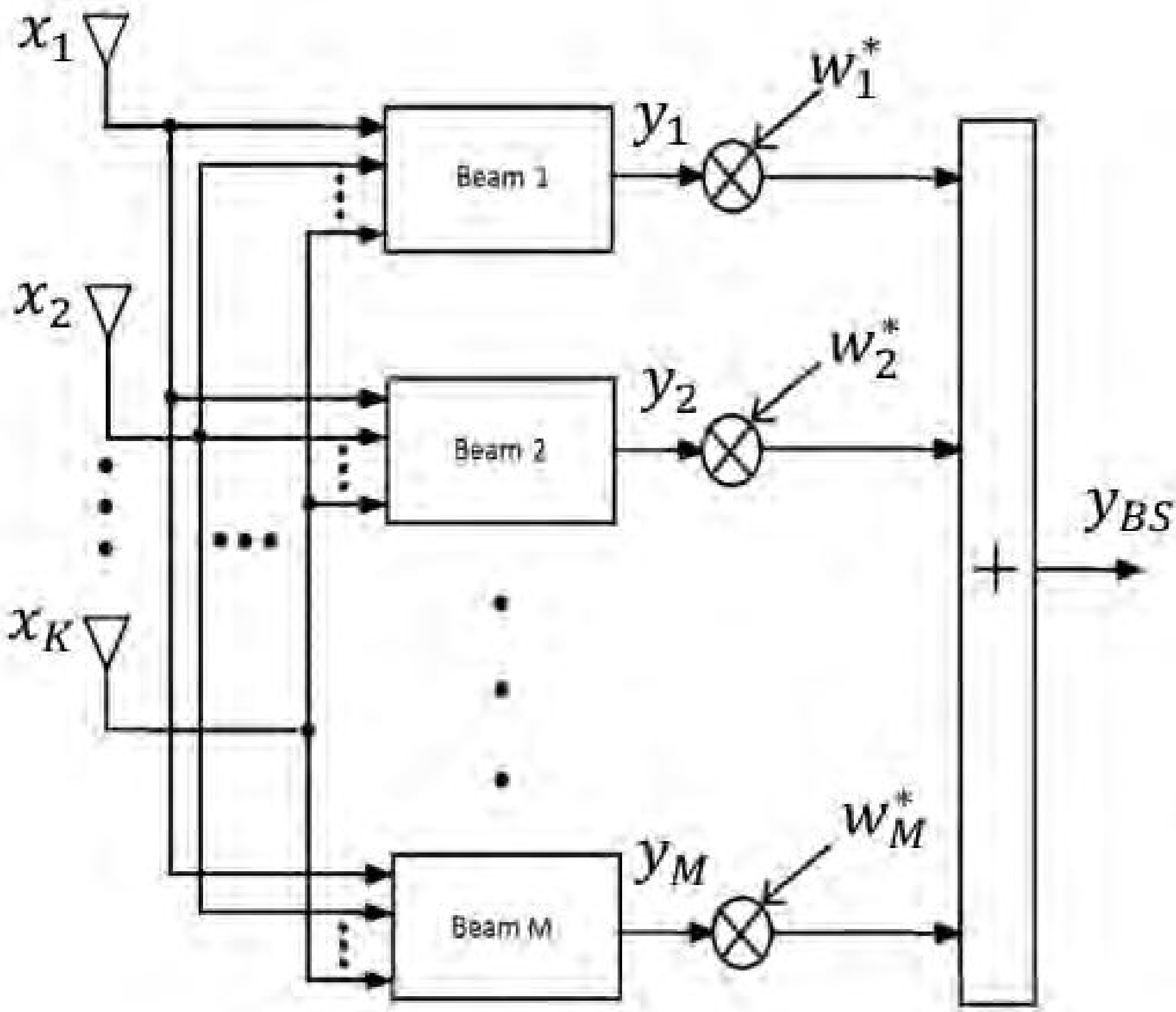

Figure 2.7: Beamforming in beamspace [5]

sionality than element-space processing, as the number of beams is typically much smaller than the number of antenna elements, leading to reduced computational complexity. It also offers improved interference mitigation by restricting beams to the sector of interest and attenuating signals outside that sector, a capability not present in element-space processing. Furthermore, beamspace processing can enhance direction-of-arrival (DOA) estimation performance at a lower computational cost, though element-space processing provides higher resolution. Beamspace processing also reduces sensitivity to noise distribution and wavefront distortions, making it more robust compared to element-space processing, which is more susceptible to these effects. However, element-space processing is more compatible with existing radar systems that use individual antenna elements, whereas beamspace processing requires additional beamforming hardware and software.

2.3.1 Beamspace Technology: State-of-the-Art

Beamspace technology has gained significant attention in various wireless communication and radar applications due to its ability to enhance spatial resolution and improve spectral efficiency. Recent literature highlights its efficacy in millimeter wave (mmWave) systems, where it enables precise beamforming and spatial multiplexing, crucial for high-speed data transmission and robust radar imaging [57–59]. Moreover, advancements in hybrid beamforming and the integration of reconfigurable intelligent surfaces (RIS) further underscore its potential in overcoming propagation challenges and optimizing system performance [60–62]. Sun *et al.* proposed a joint user grouping and beam selection algorithm for lens antenna arrays in beamspace millimeter-wave multi-user massive MIMO (B-MIMO), which significantly enhanced energy efficiency without a substantial loss in spectral efficiency [63]. Wei *et al.* proposed an efficient alternating optimization algorithm based on the techniques of weighted minimum mean square error, Lagrange multiplier, and majorization-minimization to enhance system performance and validate the effectiveness of double-RIS in improving system performance [64]. Cheng *et al.* proposed an expectation maximization (EM) based algorithm for learning the parameters in the formulation of channel estimation, integrating it into the framework of sparse signal recovery [65]. Pal et al introduced a novel beam selection algorithm for downlink mmWave multi-user MIMO systems, selecting K beams for users and demonstrating superior performance compared to existing methods [66]. Sarker *et al.* proposed a hybrid beam selection (HBS) scheme for beamspace MIMO-NOMA systems, enabling efficient multiple beam group selection to enhance spectral performance and solve power allocation challenges through an iterative beam power maximization algorithm [67].

2.4 Alternating Direction Method of Multipliers

The Alternating Direction Method of Multipliers (ADMM) is a powerful algorithm designed to solve convex optimization problems efficiently by decomposing them into smaller, more manageable pieces. This decomposition-coordination approach allows for the solutions to local subproblems to be coordinated to find an optimal solution to a larger, more complex global problem.

ADMM can be viewed as a strategic blend of dual decomposition and augmented Lagrangian methods. Dual decomposition breaks down a problem into smaller subproblems that can be solved in parallel, while the augmented Lagrangian method introduces penalty terms to enforce constraints more effectively. By combining these two approaches, ADMM leverages the strengths of both, achieving efficient and robust solutions to constrained optimization problems.

ADMM is closely related to several other well-known algorithms in the optimization landscape. These include:

- **Douglas-Rachford Splitting:** An iterative method for finding zeroes of the sum of two maximal monotone operators.

- **Spingarn's Method of Partial Inverses:** A technique for solving convex optimization problems by iteratively applying partial inverses.

- **Dykstra's Alternating Projections Method:** An algorithm for finding the intersection of convex sets by iteratively projecting onto each set.
- **Bregman Iterative Algorithms:** Methods that use Bregman distances to solve various optimization problems.

2.4.1 ADMM - Applications in Radar-Communication

The versatility of ADMM has led to its application across a wide range of fields, including machine learning, signal processing, and control systems. Following are some of the applications of ADMM in radar signal processing.

- **Waveform Design:** Optimizing radar waveforms for improved target detection and classification can be formulated as a constrained optimization problem. ADMM helps in designing waveforms that meet specific criteria, such as maximizing the signal-to-noise ratio (SNR) while adhering to power and bandwidth constraints.
- **Sparse Signal Recovery:** Radar systems often need to recover sparse signals from noisy measurements, such as in target detection and imaging. ADMM is well-suited for solving sparse optimization problems, enabling the accurate reconstruction of signals with minimal computational resources.
- **Beamforming:** In radar beamforming, the goal is to direct the radar beam in specific directions to enhance target detection. ADMM is used to optimize the weights of the antenna array elements, ensuring that the beam is accurately steered towards the desired direction while minimizing interference.

Following of some applications of ADMM in signal processing for communication.

- **MIMO Systems:** Multiple-input multiple-output (MIMO) systems use multiple antennas at both the transmitter and receiver to improve communication performance. ADMM is employed to solve optimization problems related to channel estimation, beamforming, and power allocation, enhancing the system's capacity and reliability.

- **Network Optimization:** In communication networks, optimizing resource allocation, such as bandwidth and power, is essential for maintaining high-quality service. ADMM is used to solve distributed optimization problems, allowing network resources to be allocated efficiently across multiple nodes while meeting quality-of-service (QoS) constraints.

- **Signal Detection and Estimation:** Accurate detection and estimation of transmitted signals in the presence of noise and interference are critical for reliable communications. ADMM is applied to various signal processing tasks, including equalization, channel estimation, and error correction, improving the overall performance of communication systems.

2.4.2 ADMM - Recent Literature

There has been significant recent research on the applications of ADMM to optimization problems in radar, communication, and joint radar-communication systems. Cheng et al authors propose a decentralized algorithm using ADMM and decomposition theory to co-design radar waveforms and communication transmit weights for collocated MIMO radar and MISO communication systems sharing the same frequency band, minimizing DOA estimation errors while satisfying SINR and energy constraints [68]. Cheng *et al.* proposed a method using alternating minimization and ADMM for transmit sequence design in DFRC systems with one-bit DACs, aiming to minimize symbol mean-square error while ensuring radar target localization, and also present a computationally efficient beamforming design using an accelerated primal gradient method [69]. Xu *et al.* proposed using Rate-Splitting Multiple Access (RSMA) in multi-antenna Dual-Functional Radar-Communication (DFRC) systems to jointly optimize communication and radar performance using ADMM, and claimed enhanced system efficiency, and simplified architecture [70]. Liu *et al.* investigated RIS-assisted DFRC systems optimizing transmit waveform using ADMM and RIS passive beamforming using majorization-minimization methods to enhance radar sensing and communication [71]. Yu *et al.* The paper introduces a spatio-spectral modulation strategy for integrated waveform design in a dual-function MIMO system, aiming to optimize radar beampattern and multi-user communication by minimizing ISL and shaping ESD, using an SBE framework with ADMM to ensure convergence and effectiveness [72]. Wei *et al.* introduced a DFRC system with multiple intelligent reflecting surfaces (IRSs) to improve detection of non-line-of-sight targets through joint design of frequency-dependent beamforming and phase shifts, via ADMM-based maximin optimization [73]. Cheng et al. explored transmit hybrid beamforming and DOA estimation in multi-carrier DFRC systems, integrating communication symbols into radar pulses and optimizing beamforming with consensus-ADMM for QoS while ensuring orthogonality and power constraints [74].

Here are some of the most recent references from the relevant literature, i.e., past and current year. Murtada *et al.* proposed a method to accelerate the convergence of ADMM formulations for distributed radar imaging, which can enhance radar imaging performance by capturing diverse spatial scattering properties [75]. Zhao *et al.* proposed RIS-assisted ISAC systems with optimized transceiver designs integrating communication metrics and non-convex radar constraints, utilizing ADMM, based on manifold optimization theory [76]. Yao *et al.* addressed mutual interference in radar-aided mmWave vehicle-to-infrastructure (V2I) communication, in spectrally crowded environments, using joint MIMO waveform and filter bank design, optimizing SINR via ADMM, enhancing location accuracy and lowering V2I beam training overhead [77]. Chalise *et al.* proposed a generalized likelihood ratio test-based constant false alarm detector for distributed radar networks using ADMM, achieving robust performance via distributed average consensus-based estimation and demonstrating effectiveness across varying communication conditions and modulation techniques [78]. Chen *et al.* presented an ADMM-based algorithm for optimizing ISAC waveform precoding, balancing communication interference and radar waveform fidelity under PAPR constraints, and introduced a new criteria for ideal radar waveform design to enhance sensing performance, validated through numerical simulations [79]. This paper introduces a comprehensive MIMO-radar-MIMO-communications framework addressing spectral sharing challenges between the two systems using ADMM-based design of radar codes and precoders [80]. Zhang *et al.* highlighted the use of multipath exploitation in RIS-assisted ISAC systems for fluctuating target detection, emphasizing the benefits of spatial diversity gain, and proposed to use an ADMM-based optimization algorithm to jointly design transmit and RIS reflection beamforming in ISAC systems, enhancing target detection and communication quality by exploiting multipath propagation [81]. Li *et al.* proposed a novel symbol-level precoding-based waveform design for MIMO-OFDM ISAC systems, minimizing range-Doppler sidelobes using the ADMM method [82]. Lee *et al.* proposed designing constant modulus waveforms for dual-function radar-communication systems using ADMM and majorization-minimization algorithms for joint optimization of radar sensing and communication [83].

2.5 Summary

This chapter explored the historical development and advancements in radar and communication technologies, followed by an examination of DFRC systems and recent trends in these fields. Radar technology evolved from early 20th-century ship detection methods to sophisticated systems with enhanced signal processing and beamforming capabilities. Communication technologies similarly progressed, incorporating complex modulation schemes and data transmission techniques. The convergence of these fields led to DFRC systems, which efficiently integrated radar and communication functionalities, utilizing shared waveforms and hardware for improved spectrum utilization. The review also covered advanced optimization techniques, such as the alternating direction method of multipliers (ADMM), highlighting their role in enhancing the performance and efficiency of modern radar, communication, and DFRC systems. The chapter concluded with a discussion of current trends, reflecting ongoing innovations and emerging applications in these interconnected domains.

Chapter 3

ADMM based Waveform Design for Dual-Function Radar-Communication

This chapter introduces two methods for designing waveforms for MIMO dual-function radar-communication (DFRC) systems, focusing on constant modulus and constant power waveforms. The constant modulus waveform design formulates the problem as an optimization problem with constraints on waveform synthesis and constant modulus, and solves the problem iteratively using the ADMM framework. This approach produces waveforms that approximate a desired beampattern with high-gain radar and communication beams, maintaining low sidelobe levels, and ensuring improved detection probability and bit error rate (BER). Similarly, the constant power waveform design aims to minimize power radiation in undesirable locations while adhering to constraints on waveform similarity and power constancy, also utilizing an ADMM-based algorithm. A novel method for selecting penalty parameters enhances this process, resulting in waveforms that achieve high radar and communication mainbeams with low sidelobes and effectively approximate the desired waveforms at the receiver end. Both methods are validated through simulation results, demonstrating their effectiveness in enhancing the performance of dual-function radar-communication systems. This research makes significant contributions to waveform design in DFRC systems, offering robust solutions to the inherent complexities of such systems and advancing the field's development.

3.1 Constant Modulus Waveform Design for DFRC

In this section, we investigate a constant modulus waveforms design to approximate a desired beampattern for dual-function radar-communication based on a MIMO system. Note that the desired beampattern consists of a high-gain radar main beam with a slightly high gain communication beam while maintaining the desired low sidelobe levels. First, we formulate the waveform design problem as an optimization problem. Because the constant modulus constraint makes the problem non-convex and NP-hard, traditional methods cannot be applied to solve the problem. Therefore, we use a well-known alternating direction method of multipliers (ADMM) algorithm to obtain an iterative solution to the problem. The ADMM blends the idea of the augmented Lagrangian method (ALM) with the dual decomposition method [54,55] to achieve an improved performance. The designed waveforms ensure an improved detection probability and bit error rate (BER) for radar and communications parts, respectively. Finally, the simulation results validate the efficiency of the proposed design in terms of convergence, approximation of the desired waveform, and beampattern synthesis

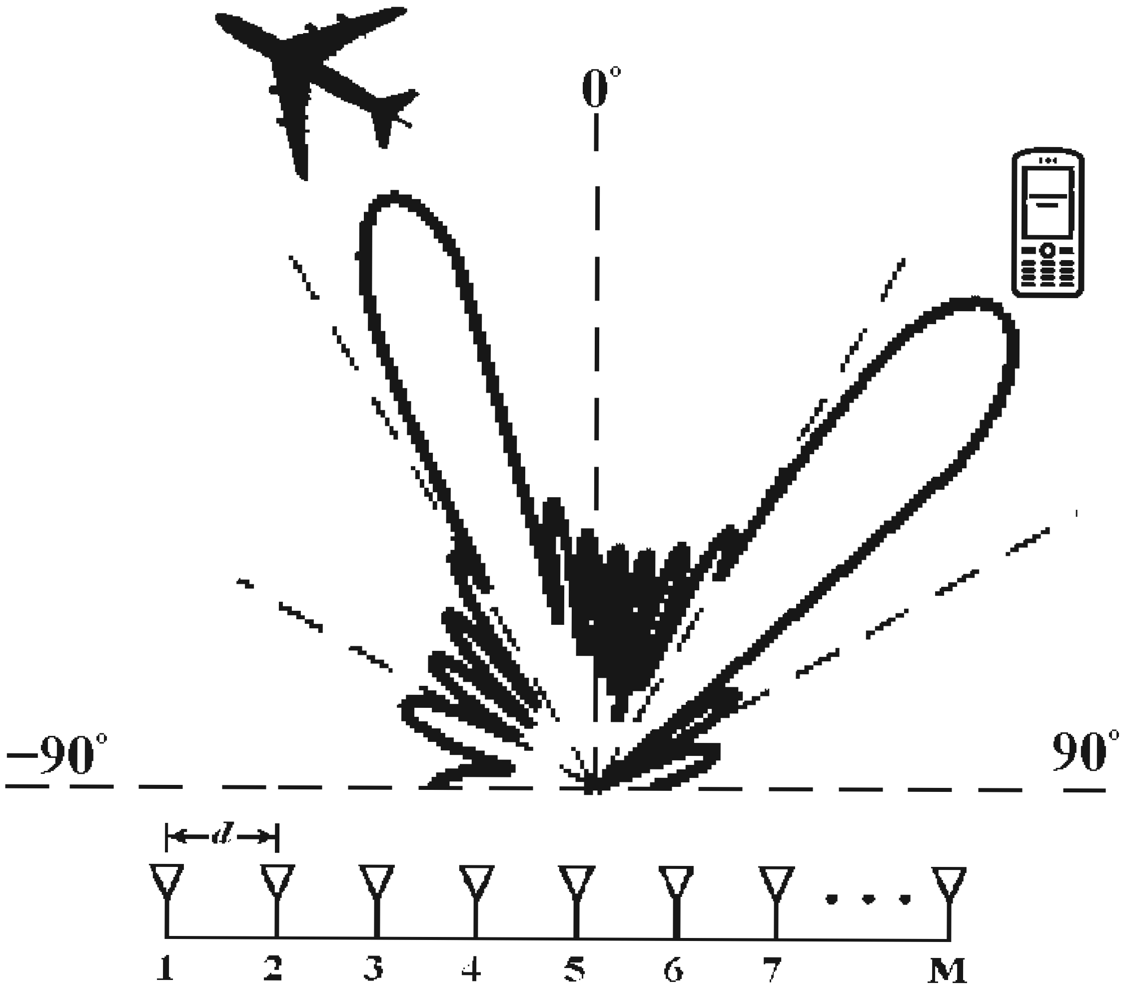

Figure 3.1: System model

3.1.1 Signal Model

Consider a multi-input, multi-output joint radar-communication system, which is equipped with a uniform linear array (ULA), consisting of M transmit antenna sensors, as shown in Figure 3.1. Also, the radar and communication receivers consist of M transmit antenna elements. The antenna array transmits an integrated waveform for radar target detection that is also decoded at the communication end for the detecting encoded information.

Let $s_m(n) \in \mathbb{C}$ denote the nth sample of a discrete waveform, consisting of N samples, emitted by the mth antenna, where $m = 1, ..., M$ and $n = 1, ..., N$. Let $\mathbf{s}(n)$ denote a vector that collects the nth samples of the waveforms transmitted by all antennas, i.e. $\mathbf{s}(n) = [s_1(n), ..., s_M(n)]^T$. Then the far-field waveform in the direction θ is given by

$$x(n;\theta) = \mathbf{a}^H(\theta)\mathbf{s}(n) \tag{3.1}$$

where

$$a(\theta) = [1, e^{-j2\pi dsin(\theta)/\lambda}, ..., e^{-j2\pi(M-1)dsin(\theta)/\lambda}]^T \tag{3.2}$$

is the transmit steering vector, with λ being the wavelength and d the inter-element spacing between the individual antenna elements. Let $\mathbf{S} = [s_1, ..., s_N]$ is the $M \times N$ space-time transmit waveform matrix.

Let $\mathbf{x}_R = [x_R(0), ..., x_R(N-1)]^T$ be the desired radar waveform and $\mathbf{x}_C = [x_C(0), ..., x_C(N-1)]^T$ be the desired communication waveform. The transmit waveform matrix $\mathbf{S}$ is designed such that the $\mathbf{x}_R$ is synthesized in radar direction θ_R and $\mathbf{x}_C$ in communication direction θ_C,respectively, where $\theta_R \neq \theta_C$, i.e.,

$$\mathbf{a}(\theta_R)\mathbf{S} = \mathbf{x}_R^T \tag{3.3}$$

and

$$\mathbf{a}(\theta_C)\mathbf{S} = \mathbf{x}_C^T. \tag{3.4}$$

Equations (3.3) and (3.4) can be combined as

$$\mathbf{A}^H(\Theta)\mathbf{S} = \mathbf{X}, \tag{3.5}$$

where $\mathbf{A}(\Theta) = [\mathbf{a}(\theta_R), \mathbf{a}(\theta_C)]$ and $\mathbf{X} = [\mathbf{x}(\theta_R), \mathbf{x}(\theta_C)]^T$.

3.1.2 Problem Formulation

The problem under consideration is to design a transmit waveform matrix $\mathbf{S}$ so that the power radiation in the sidelobe region can be minimized. Moreover, there are two constraints. The first constraint is the waveform synthesis (WS) constraint i.e., the transmit waveform matrix $\mathbf{S}$ synthesizes the desired radar waveform $\mathbf{x}_R$ and the desired communication waveform $\mathbf{x}_C$ in the direction of radar target and communication users, respectively, as given by Eq. (3.5). The second constraint is the constant modulus constraint which prevents the non-linear signal distortion in the amplifiers to increase the efficiency of the transmitter. The constant modulus constraint constraint is expressed as

$$|\mathbf{S}(m,n)| = 1, 0 \leq m \leq M-1; 0 \leq n \leq N. \tag{3.6}$$

The problem can be formulated as an optimization problem given by

$$\begin{aligned} \underset{\mathbf{S}}{\text{minimize}} \quad & \| \mathbf{A}^H \left(\widetilde{\Theta}\right) \mathbf{S} \|_F^2 \\ \text{subject to} \quad & \mathbf{A}^H (\Theta) \mathbf{S} = \mathbf{X} \\ & |\mathbf{S}(m,n)| = 1, 0 \leq m \leq M-1; 0 \leq n \leq N, \end{aligned} \tag{3.7}$$

where $\Theta = [\theta_R, \theta_C]$ is the collection of radar and communication direction angles while $\widetilde{\Theta} = [\theta_1, \theta_2, \cdots, \theta_K]$ is the collection of angles of K side lobes.

The CM constraint Equations (3.6) renders the optimization problem (3.7) as non-convex. Being NP-hard, this problem is difficult to solve using any convex optimization methods. The problem (3.7) can be re-formulated for ease of analysis, in two steps: the vectorization step and the realization step.

3.1.2.1 Vectorization

In the vectorization step, the matrices $\mathbf{S}$ and $\mathbf{X}$ are vectorized by stacking all of their respective columns vectors into a single columns vector. Correspondingly, matrices $\mathbf{A}(\Theta)$ and $\mathbf{A}\left(\widetilde{\Theta}\right)$ are also updated. This is given by

$$\begin{aligned}
\bar{\mathbf{s}} &= \mathrm{vec}(\mathbf{S}) \\
\bar{\mathbf{x}} &= \mathrm{vec}(\mathbf{X}) \\
\overline{\mathbf{A}}(\Theta) &= \mathbf{I}_N \otimes \mathbf{A}(\Theta) \\
\overline{\mathbf{A}}\left(\widetilde{\Theta}\right) &= \mathbf{I}_N \otimes \mathbf{A}\left(\widetilde{\Theta}\right).
\end{aligned} \tag{3.8}$$

The CM constraint is given in terms of $\bar{\mathbf{s}}$ as

$$|\bar{\mathbf{s}}(i)| = 1, i = 1, 2, \cdots, MN \tag{3.9}$$

which is, equivalently, given by

$$\bar{\mathbf{s}}^T \mathbf{E}_i \bar{\mathbf{s}} = 1, i = 1, 2, \cdots, MN \tag{3.10}$$

where

$$\mathbf{E}_i(m,n) = \begin{cases} 1, & m = n = i \\ 0, & otherwise \end{cases} \tag{3.11}$$

where $0 \le m, n, i \le MN$. At the end of the vectorization step, the problem Eq. (3.7) can be express as

$$\begin{aligned}
\underset{\bar{\mathbf{s}}}{\text{minimize}} \quad & \bar{\mathbf{s}}^H \overline{\mathbf{A}}\left(\widetilde{\Theta}\right) \overline{\mathbf{A}}^H\left(\widetilde{\Theta}\right) \bar{\mathbf{s}} \\
\text{subject to} \quad & \overline{\mathbf{A}}^H(\Theta)\bar{\mathbf{s}} = \bar{\mathbf{x}} \\
& \bar{\mathbf{s}}^T \mathbf{E}_i \bar{\mathbf{s}} = 1, i = 1, 2, \cdots, MN.
\end{aligned} \tag{3.12}$$

3.1.2.2 Realization

In the realization step, the complex-valued variables are converted to the real-valued version. For example, the realization of $\bar{\mathbf{s}}$ takes the real part of $\bar{\mathbf{s}}$ in one column vector and the complex part in another vector and then stacks the columns vectors together to give $\bar{\mathbf{s}}_r$. The realization of $\bar{\mathbf{s}}_r$, $\bar{\mathbf{x}}_r$, $\overline{\mathbf{A}}_r(\Theta)$ and $\overline{\mathbf{A}}_r\left(\widetilde{\Theta}\right)$ is given as

$$
\begin{aligned}
\bar{\mathbf{s}}_r &= \begin{bmatrix} \Re\{\bar{\mathbf{s}}\} \\ \Im\{\bar{\mathbf{s}}\} \end{bmatrix} \\
\bar{\mathbf{x}}_r &= \begin{bmatrix} \Re\{\bar{\mathbf{x}}\} \\ \Im\{\bar{\mathbf{x}}\} \end{bmatrix} \\
\overline{\mathbf{A}}_r(\Theta) &= \begin{bmatrix} \Re\{\overline{\mathbf{A}}(\Theta)\} & -\Im\{\overline{\mathbf{A}}(\Theta)\} \\ \Im\{\overline{\mathbf{A}}(\Theta)\} & \Re\{\overline{\mathbf{A}}(\Theta)\} \end{bmatrix} \\
\overline{\mathbf{A}}_r\left(\widetilde{\Theta}\right) &= \begin{bmatrix} \Re\{\overline{\mathbf{A}}\left(\widetilde{\Theta}\right)\} & -\Im\{\overline{\mathbf{A}}\left(\widetilde{\Theta}\right)\} \\ \Im\{\overline{\mathbf{A}}\left(\widetilde{\Theta}\right)\} & \Re\{\overline{\mathbf{A}}\left(\widetilde{\Theta}\right)\} \end{bmatrix}
\end{aligned}
\tag{3.13}
$$

In terms of vectorized real-valued variables, the CM constraint is given by

$$\bar{\mathbf{s}}_r^T \mathbf{E}_i \bar{\mathbf{s}}_r = 1, i = 1, 2, \cdots, 2MN \tag{3.14}$$

where

$$\mathbf{E}_i(m,n) = \begin{cases} 1 & : m = n = i \\ 1 & : m = n = i + MN \\ 0 & : otherwise \end{cases} \tag{3.15}$$

and $0 \leq m,n,i \leq 2MN$. At the end of the realization step, the problem Eq. (3.12) can be expressed as

$$\begin{aligned} \underset{\overline{\mathbf{s}}_r}{\text{minimize}} \quad & \overline{\mathbf{s}}_r^T \overline{\mathbf{A}}_r \left(\widetilde{\Theta}\right) \overline{\mathbf{A}}_r^T \left(\widetilde{\Theta}\right) \mathbf{s}_r \\ \text{subject to} \quad & \overline{\mathbf{A}}_r^T (\Theta) \overline{\mathbf{s}}_r = \overline{\mathbf{x}}_r \\ & \overline{\mathbf{s}}_r^T \mathbf{E}_i \overline{\mathbf{s}}_r = 1, i = 1, 2, \cdots, MN. \end{aligned} \tag{3.16}$$

The optimization problem in Eq. (3.16) can be solved to get $\overline{\mathbf{s}}_{r-opt}$, which is the vectorized and real-valued version of $\mathbf{S}_{opt}$. So the reverse operation i.e.,

$$\mathbf{S}_{opt} = mtx\left(\overline{\mathbf{s}}_{r1-opt} + i \cdot \overline{\mathbf{s}}_{r2-opt}\right) \tag{3.17}$$

can be performed to get $\mathbf{S}_{opt}$, where $\overline{\mathbf{s}}_{r1-opt}$ contains the first MN elements, the real part, and $\overline{\mathbf{s}}_{r2-opt}$ contains the other MN elements, the imaginary part.

3.1.3 ADMM Formulation and Solution

The optimization problem Equation (3.16), like Equation (3.7), is non-convex and NP-hard. Analytical solutions to problems like this are challenging to get and alternatives like numerical or heuristic techniques are employed instead to get approximate solutions. Even using heuristic techniques, like genetic algorithm (GA), it may be difficult to formulate the CM constraint. Therefore, we use the ADMM based iterative technique to approximate a solution to this problem.

An auxiliary variable $\overline{\mathbf{r}}_r$ is introduced in Eq. (3.16) and the following equivalent version is obtained

$$\begin{aligned}
\underset{\bar{\mathbf{r}}_r,\bar{\mathbf{s}}_r}{\text{minimize}} \quad & \bar{\mathbf{r}}_r^T \mathbf{A}_r\left(\widetilde{\Theta}\right)\mathbf{A}_r^T\left(\widetilde{\Theta}\right)\bar{\mathbf{s}}_r \\
\text{subject to} \quad & \mathbf{A}_r^T(\Theta)\,\bar{\mathbf{r}}_r + \mathbf{A}_r^T(\Theta)\,\bar{\mathbf{s}}_r = 2\bar{\mathbf{x}}_r \\
& \mathbf{T}(\bar{\mathbf{r}}_r)\,\bar{\mathbf{s}}_r - \mathbf{1} = \mathbf{0} \\
& \bar{\mathbf{r}} = \bar{\mathbf{s}}.
\end{aligned} \tag{3.18}$$

It can be observed that the WS constraint in Equation (3.16), $\bar{\mathbf{s}}_r$ is expressed as two times $\bar{\mathbf{s}}_r$ and one of them is replaced by $\bar{\mathbf{r}}_r$ in Equation (3.18). Also, the CM constraint, consisting of MN equations in Equation (3.16), is expressed in its compact form in Equation 3.18 as

$$\mathbf{G}(\bar{\mathbf{r}}_r,\bar{\mathbf{s}}_r) = \mathbf{G}(\bar{\mathbf{s}}_r,\bar{\mathbf{r}}_r) = \mathbf{0} \tag{3.19}$$

where $\mathbf{G}(\bar{\mathbf{r}}_r,\bar{\mathbf{s}}_r) \in \mathbb{R}^{2MN\times 2MN}$ is a vector given by

$$\mathbf{G}(\bar{\mathbf{r}}_r,\bar{\mathbf{s}}_r) = \mathbf{T}(\bar{\mathbf{r}}_r)\,\bar{\mathbf{s}}_r - \mathbf{1}, \tag{3.20}$$

where $\mathbf{1}$ and $\mathbf{0}$ are $2MN \times 1$ vectors all 1's and 0's respectively, and

$$\mathbf{T}(\bar{\mathbf{r}}_r) = \left[\bar{\mathbf{r}}_r^T\mathbf{E}_1; \bar{\mathbf{r}}_r^T\mathbf{E}_2; \cdots; \bar{\mathbf{r}}_r^T\mathbf{E}_{MN}\right] \in \mathbb{R}.^{MN\times 2MN} \tag{3.21}$$

The augmented Lagrangian of Eq. (3.18) is given as

$$\begin{aligned}
\mathscr{L}\{\bar{\mathbf{r}}_r,\bar{\mathbf{s}}_r,\mathbf{u},\mathbf{v},\mathbf{w},\} \;=\;& \bar{\mathbf{r}}_r^T\mathbf{A}_r\left(\widetilde{\Theta}\right)\mathbf{A}_r^T\left(\widetilde{\Theta}\right)\bar{\mathbf{s}}_r \\
+\;& \tfrac{\rho_1}{2}\left\|\mathbf{A}_r^T(\Theta)\,\bar{\mathbf{r}}_r + \mathbf{A}_r^T(\Theta)\,\bar{\mathbf{s}}_r - 2\bar{\mathbf{x}}_r + \mathbf{u}\right\|_2^2 \\
+\;& \tfrac{\rho_2}{2}\left\|\mathbf{T}(\bar{\mathbf{r}}_r)\,\bar{\mathbf{s}}_r - \mathbf{1} + \mathbf{v}\right\|_2^2 \\
+\;& \tfrac{\rho_3}{2}\left\|\bar{\mathbf{r}}_r - \bar{\mathbf{s}}_r + \mathbf{w}\right\|_2^2
\end{aligned} \tag{3.22}$$

where $\mathbf{u} \in \mathbb{R}^{4N\times 1}, \mathbf{v} \in \mathbb{R}^{MN\times 1}$ and $\mathbf{w} \in \mathbb{R}^{2MN\times 1}$ are the dual variables and

$\rho_1, \rho_2, \rho_3 > 0$ are the adjustable penalty parameters.

The $(m+1)$th iteration of the algorithm, in terms of the different variables, is given as following

$$\bar{\mathbf{r}}_r^{m+1} := \arg\min_{\bar{\mathbf{r}}_r} \mathscr{L}\left(\bar{\mathbf{r}}_r, \bar{\mathbf{s}}_r^m, \mathbf{u}^m, \mathbf{v}^m, \mathbf{w}^m\right) \tag{3.23a}$$

$$\bar{\mathbf{s}}_r^{m+1} := \arg\min_{\bar{\mathbf{s}}_r} \mathscr{L}\left(\bar{\mathbf{r}}_r^{m+1}, \bar{\mathbf{s}}_r, \mathbf{u}^m, \mathbf{v}^m, \mathbf{w}^m\right) \tag{3.23b}$$

$$\mathbf{u}^{m+1} := \mathbf{u}^m + \mathbf{A}_r^T \bar{\mathbf{r}}_r^{m+1} + \mathbf{A}_r^T \bar{\mathbf{s}}_r^{m+1} - 2\mathbf{x}_r \tag{3.23c}$$

$$\mathbf{v}^{m+1} := \mathbf{v}^m + \mathbf{T}\left(\bar{\mathbf{r}}_r^{m+1}\right) \bar{\mathbf{s}}_r^{m+1} - \mathbf{1} \tag{3.23d}$$

$$\mathbf{w}^{m+1} := \mathbf{w}^m + \bar{\mathbf{r}}_r^{m+1} - \bar{\mathbf{s}}_r^{m+1}. \tag{3.23e}$$

As can be seen from Equation (3.23), the update Equations (3.23c), (3.23d) and (3.23e) are straight-forward. The sub-equations Equation (3.23a) and Equation (3.23b) are convex and give closed-form solutions. The details of the updates of variables $\bar{\mathbf{r}}_r$ and $\bar{\mathbf{s}}_r$ is presented next.

3.1.3.1 Update of $\bar{\mathbf{r}}_r$

To get the $(m+1)$th update of $\bar{\mathbf{r}}_r$, we take the gradient of Equation (3.23a) with respect to $\bar{\mathbf{r}}_r$ and equate the result with 0, *i.e.*,

$$\nabla_{\bar{\mathbf{r}}_r} \mathscr{L}\left(\bar{\mathbf{r}}_r, \bar{\mathbf{s}}_r^m, \mathbf{u}^m, \mathbf{v}^m, \mathbf{w}^m\right) = \mathbf{0}. \tag{3.24}$$

The solution to Equation (3.24) is given by

$$\bar{\mathbf{r}}_r^{m+1} = \Xi_1^{-1} \xi_1 \tag{3.25}$$

where

$$\Xi_1 = \rho_1 \mathbf{A}_r(\Theta)\mathbf{A}_r^T(\Theta) + \rho_2 \mathbf{T}^T(\overline{\mathbf{s}}_r)\mathbf{T}(\overline{\mathbf{s}}_r) + \rho_3 \mathbf{I} \tag{3.26}$$

and

$$\begin{aligned} \xi_1 =_C & M\rho_1 \mathbf{A}_r(\Theta)\left(2\mathbf{x}_r - \mathbf{u} - \mathbf{A}_r^T(\Theta)\overline{\mathbf{s}}_r\right) \\ & \rho_2 \mathbf{T}^T(\overline{\mathbf{s}}_r)(\mathbf{1} - \mathbf{v})\rho_3(\overline{\mathbf{s}}_r - \mathbf{w}) \\ & - \mathbf{A}_r\left(\widetilde{\Theta}\right)\mathbf{A}_r^T\left(\widetilde{\Theta}\right)\overline{\mathbf{s}}_r. \end{aligned} \tag{3.27}$$

3.1.3.2 Update of $\overline{\mathbf{s}}_r$

Similar to the $\overline{\mathbf{r}}_r$ update, in $\overline{\mathbf{s}}_r$ update, we take the gradient of Equation (3.23b) with respect to $\overline{\mathbf{s}}_r$ and equate the result with 0, *i.e.*,

$$\nabla_{\overline{\mathbf{s}}_r}\mathscr{L}\left(\overline{\mathbf{r}}_r^{m+1}, \overline{\mathbf{s}}_r, \mathbf{u}^m, \mathbf{v}^m, \mathbf{w}^m\right) = \mathbf{0}. \tag{3.28}$$

The solution to Equation (3.28) is given by

$$\overline{\mathbf{s}}_r^{m+1} = \Xi_2^{-1}\xi_2 \tag{3.29}$$

where

$$\Xi_2 = \rho_1 \mathbf{A}_r(\Theta)\mathbf{A}_r^T(\Theta) + \rho_2 \mathbf{T}^T(\overline{\mathbf{r}}_r)\mathbf{T}(\overline{\mathbf{r}}_r) + \rho_3 \mathbf{I} \tag{3.30}$$

and

$$\begin{aligned} \xi_2 = & \rho_1 \mathbf{A}_r(\Theta)\left(2\mathbf{x}_r - \mathbf{u} - \mathbf{A}_r^T(\Theta)\overline{\mathbf{r}}_r\right) \\ & + \rho_2 \mathbf{T}^T(\overline{\mathbf{r}}_r)(\mathbf{1} - \mathbf{v}) + \rho_3(\overline{\mathbf{r}}_r + \mathbf{w}) \\ & - \mathbf{A}_r\left(\widetilde{\Theta}\right)\mathbf{A}_r^T\left(\widetilde{\Theta}\right)\overline{\mathbf{r}}_r. \end{aligned} \tag{3.31}$$

3.1.3.3 Termination Criteria of the Algorithm

Let the primal residuals at iteration $m+1$ be defined as

$$d_{pr1}^{m+1} = \mathbf{A}_r^T \mathbf{r}_r^{m+1} + \mathbf{A}_r^T \mathbf{s}_r^{m+1} - 2\mathbf{x}_r \tag{3.32a}$$

$$d_{pr2}^{m+1} = \mathbf{T}\left(\mathbf{r}_r^{m+1}\right)\mathbf{s}_r^{m+1} - \mathbf{1} \tag{3.32b}$$

$$d_{pr3}^{m+1} = \mathbf{r}_r^{m+1} - \mathbf{s}_r^{m+1} \tag{3.32c}$$

and the dual residuals be defined as

$$d_{rs1}^{m+1} = \mathbf{r}_r^{m+1} - \mathbf{r}_r^{m} \tag{3.33a}$$

$$d_{rs2}^{m+1} = \mathbf{s}_r^{m+1} - \mathbf{s}_r^{m}. \tag{3.33b}$$

Then, as suggested by [84], reasonable termination criteria are

$$\| d_{pr1}^{m+1} \|_2^2 \leq \ \varepsilon_1^{pri}, \tag{3.34a}$$

$$\| d_{pr2}^{m+1} \|_2^2 \leq \ \varepsilon_2^{pri}, \tag{3.34b}$$

$$\| d_{pr3}^{m+1} \|_2^2 \leq \ \varepsilon_3^{pri}, \tag{3.34c}$$

$$\| d_{dr1}^{m+1} \|_2^2 \leq \ \varepsilon^{dual}, \tag{3.34d}$$

$$\| d_{dr2}^{m+1} \|_2^2 \leq \ \varepsilon^{dual}. \tag{3.34e}$$

where ε_1^{pri}, ε_2^{pri}, ε_3^{pri} are the tolerances for the primal residual and ε_1^{dual} is the tolerance for dual residuals. These tolerances, in accordance with [84], are defined as

$$\varepsilon_1^{pri} = \sqrt{4N}\varepsilon^{abs} + \varepsilon^{rel}\max\left\{\| \mathbf{A}_r^T \mathbf{r}_r^{m+1} \|_2, \| \mathbf{A}_r^T \mathbf{s}_r^{m+1} \|_2, \| 2\mathbf{x}_r \|_2\right\} \tag{3.35a}$$

$$\varepsilon_2^{pri} = \sqrt{MN}\varepsilon^{abs} + \varepsilon^{rel}\max\left\{\| \mathbf{T}\left(\mathbf{r}_r^{m+1}\right)\mathbf{s}_r^{m+1} \|_2, \| \mathbf{1} \|_2\right\} \tag{3.35b}$$

$$\varepsilon_3^{pri} = \sqrt{2MN}\varepsilon^{abs} + \varepsilon^{rel}\max\left\{\| \mathbf{r}_r^{m+1} \|_2, \| \mathbf{s}_r^{m+1} \|_2\right\} \tag{3.35c}$$

$$\varepsilon^{dual} = \sqrt{2MN}\varepsilon^{abs} + \varepsilon^{rel} \| \rho_1\mathbf{w} \|_2 \tag{3.35d}$$

Table 3.1 summarizes the steps of the algorithm.

Summary of the proposed algorithm
Input: Step 1) **Initialize:** $\mathbf{r}_r^0, \mathbf{s}_r^0, \mathbf{u}^0, \mathbf{v}^0, \mathbf{w}^0, \rho_1, \rho_2, \rho_3$, ε_1^{pri}, ε_2^{pri}, ε_2^{pri}, ε^{dual}, $m = 1$ Step 2) **While** the termination criteria, Eq. 3.34, are not satisfied, do Step 3) Update $\mathbf{r}_r^{m+1}$ using Eq. 3.25 Step 4) Update $\mathbf{s}_r^{m+1}$ using Eq. 3.29 Step 5) Update $\mathbf{u}^{m+1}$ using Eq. 3.23c Step 6) Update $\mathbf{v}^{m+1}$ using Eq. 3.23d Step 7) Update $\mathbf{w}^{m+1}$ using Eq. 3.23e Step 8) $m = m + 1$ Step 9) **End while** **Output:**

Table 3.1: Summary of the proposed algorithm

For clarity, a list of symbols, their dimensions and description is provided in Table 3.2.

3.1.3.4 Penalty Parameter Selection

Choosing the penalty parameters properly is very important in ADMM. The values of penalty parameters are decreased or increased depending on the values of some predefined tolerances. Different methods can be used choose the penalty parameters like hit-and-trial etc. Another method is to related the values of the penalty parameters to iteration numbers so that the values of penalty parameters increased or decreased (from initially defined value) in steps. One standard method is to relate the values of the residual norms with the tolerances by using the concept of 'residual balancing' as given by Eq. (3.36).

Symbol	Dimension	Description
M	1×1	Number of antennas
N	1×1	Number of samples
K	1×1	Number of side lobes
d	1×1	Antenna inter-element spacing
$\mathbf{I}_N$	$N\times N$	Identity matrix
λ	1×1	Wavelength
$s_m(n)$	1×1	nth sample of a discrete waveform
$\mathbf{s}(n)$	$M\times 1$	nth samples of the waveforms transmitted by all antennas
$\mathbf{S}$	$M\times N$	Space-time transmit waveform matrix
$\bar{\mathbf{s}}$	$MN\times 1$	Vector version of $\mathbf{s}$
$\bar{\mathbf{s}}_r$	$2MN\times 1$	Real-valued version of $\bar{\mathbf{s}}$
$\mathbf{x}_R$	$N\times 1$	Desired radar waveform
$\mathbf{x}_C$	$N\times 1$	Desired communication waveform
$\mathbf{X}$	$2\times N$	Combination of desired communication waveform as a matrix
$\bar{\mathbf{x}}$	$2N\times 1$	Vector version of $\mathbf{X}$
$\bar{\mathbf{x}}_r$	$4N\times 1$	Real-valued version of $\bar{\mathbf{x}}$
$\mathbf{a}(\theta_R)$	$M\times 1$	Steering vector in radar direction
$\mathbf{a}(\theta_C)$	$M\times 1$	Steering vector in communication direction
$\mathbf{A}(\Theta)$	$M\times 2$	Combination of $\mathbf{a}(\theta_R$ and $\mathbf{a}(\theta_C$
$\overline{\mathbf{A}}(\Theta)$	$MN\times 2N$	Vector version of $\mathbf{A}(\Theta)$
$\overline{\mathbf{A}}_r(\Theta)$	$2MN\times 4N$	Real-valued version of $\overline{\mathbf{A}}(\Theta)$
$\mathbf{A}\left(\widetilde{\Theta}\right)$	$M\times K$	Combination of side lobe steering vectors
$\overline{\mathbf{A}}\left(\widetilde{\Theta}\right)$	$MN\times KN$	Vector version of $\mathbf{A}\left(\widetilde{\Theta}\right)$
$\overline{\mathbf{A}}_r\left(\widetilde{\Theta}\right)$	$2MN\times 2KN$	Real-valued version of $\overline{\mathbf{A}}\left(\widetilde{\Theta}\right)$
$\mathbf{u}$	$4N\times 1$	Dual variable
$\mathbf{v}$	$MN\times 1$	Dual variable
$\mathbf{w}$	$2MN\times 1$	Dual variable
η, μ	1×1	Positive constants
ρ_1, ρ_2, ρ_3	1×1	Penalty parameters

Table 3.2: List of symbols

$$\rho_{k+1}=\begin{cases}\eta\rho_k & \text{if} \quad d_{pr1}^{m+1}>\mu\varepsilon_1^{pri}\\ \rho_k/\eta & \text{if} \quad \varepsilon_1^{pri}>\mu d_{pr1}^{m+1}\\ \rho_k & otherwise\end{cases} \tag{3.36}$$

where ρ_k is the penalty parameter, and $\mu>1$ and $\eta>1$ are constants, d_{pr1}^{m+1} is the primary residual and ε_1^{pri} is the tolerance.

Note: A a novel method for penalty parameter optimization was proposed in another work, also discussed later in this chapter. That method is not discussed in this section.

3.1.4 Simulation Results and Analysis

In this section, the performance analysis of the algorithm is discussed and the results of some numerical examples are presented to evaluate the performance of the proposed waveform design method. A ULA consisting of $M = 32$ antenna elements having half wavelength enter-element spacing has been considered at the transmitter and receiver sides. The radar target is located at $\theta_R = 0^\circ$ and the communication user at $\theta_C = 45^\circ$. The desired radar waveform is based on linear frequency modulation (LFM). Similarly, the desired communication waveform uses the QPSK modulation scheme. We have considered $N_s = 1$ symbols and $N_b = 2$ bits per symbol. Thus each waveform carries 2 bits of information per pulse repetition interval (PRI).

Different experiments are performed to evaluate the performance in different scenarios. Since both radar and communication receivers expect some desired waveforms, coherent detection can be used to match the received signal waveform with the desired waveform. Monte-Carlo simulations are done to evaluate the performance of communication for different values of signal-to-noise ratio (SNR).

The proposed method is compared with far-field radiated emission design (FFRED) [85], iterative optimization technique (using directly normalized waveforms) [86], and the theoretical values. In FFRED method, 0%, 10% and 40% of the total power is allocated to the orthogonal complement waveform, of which the FFRED-40% has the best performance. Authors of [86] proposed several waveform design methods. One method designed non-constant modulus waveforms, had closed-form solution to the waveform design problem. They also proposed an iterative method for constant modulus waveforms. However, being computationally complex, they used the results of the first method using non-constant modulus waveforms and used iterative optimization for further refining those waveforms. They defined this method as "directly normalized" in their simulations.

3.1.4.1 Computational Complexity Analysis

The computational complexity analysis helps estimate the computational resources, like time and memory, needed to execute an algorithm. It provides insight into how the algorithm scales with the input size. This information is useful for optimizing the algorithm or considering alternative approaches if the complexity is too high.

To determine the computational complexity of the proposed algorithm, each section of the code was examined to count the number of operations or iterations relative to the input size. The main loop in the code runs 'iter' times. Within each iteration, there are multiple operations, including matrix multiplications, norm calculations, and variable updates. The complexity of each of these operations was analyzed and combined to obtain an overall complexity estimate. Input size-dependent variables, such as M and L, and their influence on complexity were also considered.

The proposed algorithm has high computational complexity, approximately cubic. This is mainly due to a matrix inversion operation. After matrix inversion, other significant time-consuming operations include matrix multiplications.

For $\mathbf{r}$ updates, the calculation of Ξ_1 takes $O(KM^2L^2)$, calculation of γ takes

$O(M^2L^2)$, therefore the complexity of the update of $\mathbf{r}$ using Eq (3.25) is $O(KM^2L^2 + M^2L^2 + M^3L^3)$. Overall, the computational complexity of the algorithm is $O(2(KM^2L^2 + M^2L^2 + M^3L^3))$ at each iteration.

3.1.4.2 Data Rate Performance

The communication data rate is

$$R = N_b \times N_s \times f_{PRF}, \tag{3.37}$$

where N_b is the number of bits per symbol, N_s is the number of symbols in one pulse and f_{PRF} is the pulse repetition frequency.

3.1.4.3 ADMM Convergence Analysis

Plots of the norms of primal and dual residuals d_{pr1}, d_{pr2}, d_{pr3}, d_{dr2}, d_{dr2}, and the stopping criteria limits ε_1^{pri}, ε_2^{pri}, ε_2^{pri}, ε^{dual} against the iteration numbers are shown in Figure 3.2 and 3.3. The plots show that the stopping conditions are met within 20 iterations.

Figure 3.4 shows a plot of the objective function values. The objective function is the first line of Equation (3.18). As obvious in the figure, the objective function settles within 10 iterations. This is in accordance with the settling down of the primary and dual residuals, Figure 3.2 and 3.3, and the constant modulus requirement, Figure 3.4.

3.1.4.4 Beampattern Analysis

Figure 3.5 shows the transmit beampattern formed by the waveform matrix **S** designed through the propose ADMM based approach for a DFRC system with 32 antenna elements.

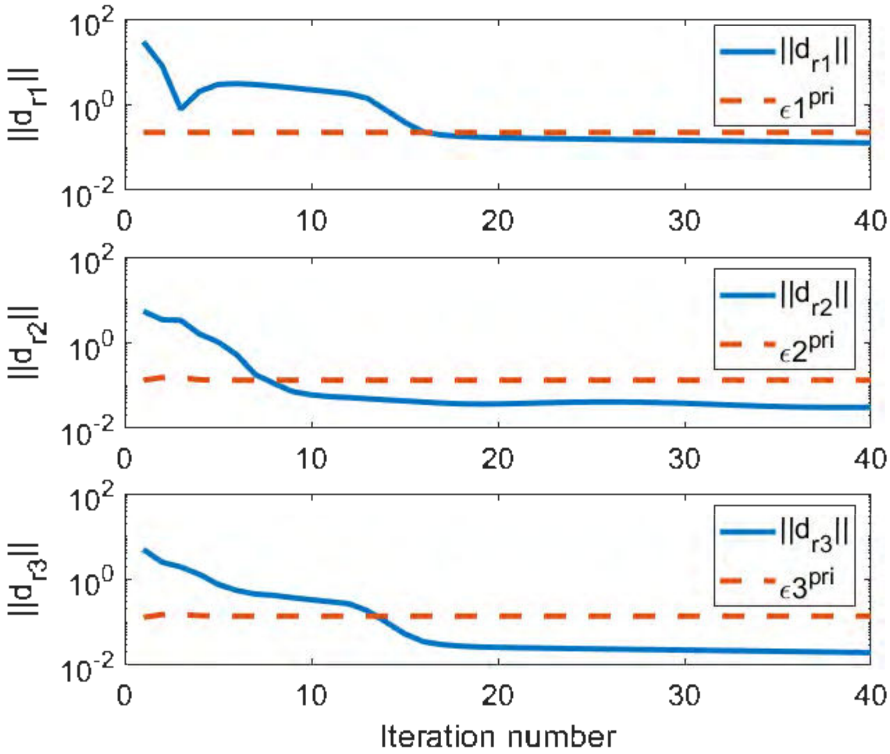

Figure 3.2: Norms of primary residuals per iteration

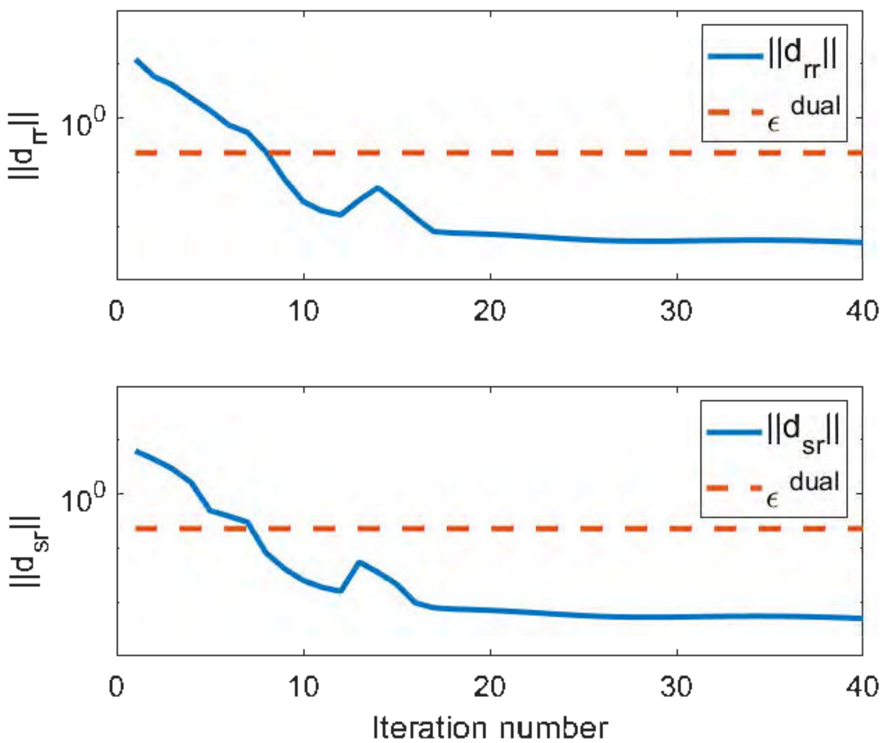

Figure 3.3: Norms of dual residuals per iteration

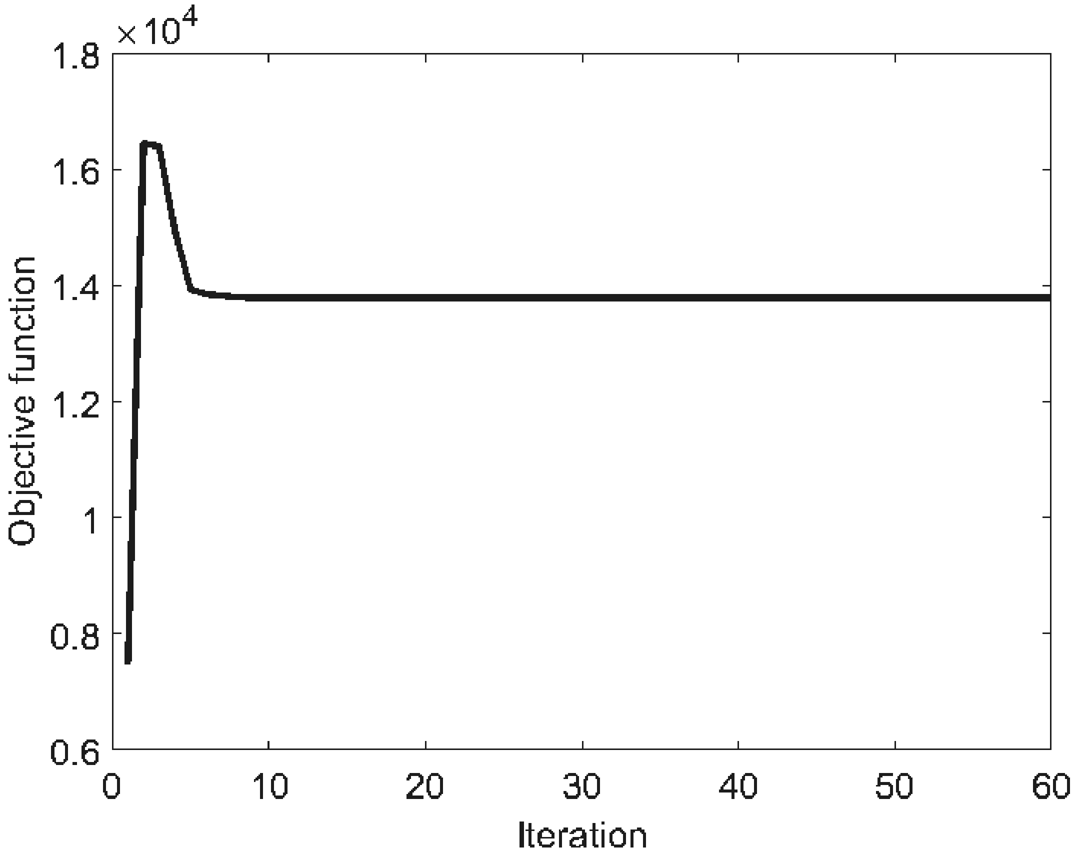

Figure 3.4: Convergence of the objective function Eq. (3.18)

Figure 3.6 shows the transmit beampatterns as synthesized by the waveform matrix $\mathbf{S}$ designed through the propose ADMM based approach and that of iterative optimization with amplitude weighting (IO-AW) as reported in [87]. In both cases, the systems have 16 antenna elements, the radar target is located at $\theta_R = 0°$ and the communication user at $\theta_C = 45°$. Also, in both cases, the power of the desired radar waveform is designed to be 10 dB more than that of the communication waveform. As it can be seen in the figure the IO-AW method leaks power at $-45°$ or, in other words, makes a mirror lobe towards a direction where there is no communication user. Otherwise, the sidelobe levels of the two beampatterns are almost the same. Thus, the beampattern formed through the proposed method outperforms the beampattern formed through IO-AW.

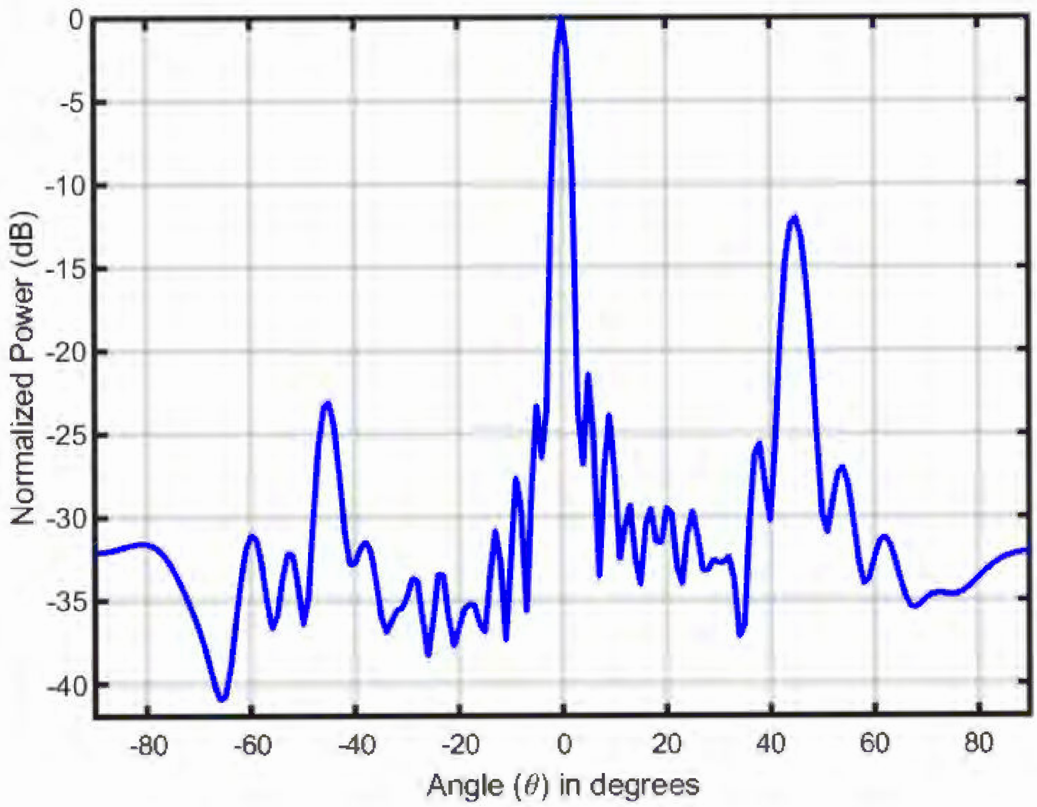

Figure 3.5: The transmit beampattern formed by the DFRC system with 32 antenna elements

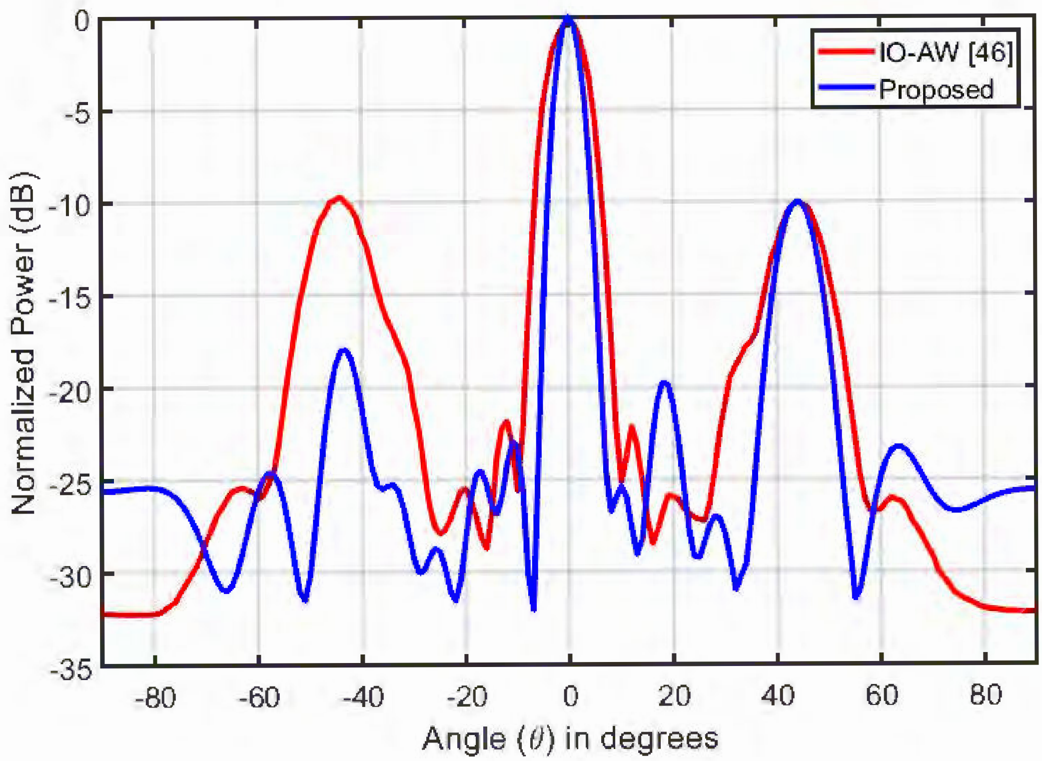

Figure 3.6: The transmit beampattern formed by the systems

3.1.4.5 Waveform Error Analysis

Normalized waveform error is a performance metric that can be used to describe how closely the desired waveforms match the synthesized waveforms. Moreover, it can also give convergence performance, as the faster it decreases with the increasing number of iterations, the better the performance of the algorithm. Mathematically, this metric, denoted here as η_i, is defined as

$$\eta_i = \frac{||\mathbf{X}_i||_F^2}{||\mathbf{X}||_F^2} \tag{3.38}$$

where

$$\mathbf{X}_i = \mathbf{A}^H(\Theta)\mathbf{S}_i. \tag{3.39}$$

Figure 3.7 shows the normalized waveform error in decibels (dB) plotted against the iterations. Since this is a normalized metric, it typically does not have specific units.

Table 3.3 provides a comparison of different methods for normalized waveform error.

Method	Waveform modulus	Normalized waveform error/dB
FFRED-0%	Non-constant	-320.08
FFRED-10%	Constant	-34.08
FFRED-40%	Constant	-113.56
MNO	Non-constant	-312.06
IO	Constant	-39.40
IO-AW	Constant	-40.90
ADMM-based (Proposed)	Constant	-35

Table 3.3: Comparison of different methods for normalized waveform error

Figure 3.8 shows how the CM constraint is met. The plots in the figure show the maximum and the minimum modulus samples of $\mathbf{S}$, and the desired uni-modulus samples, at each iteration. As can be seen in the plots, the maximum

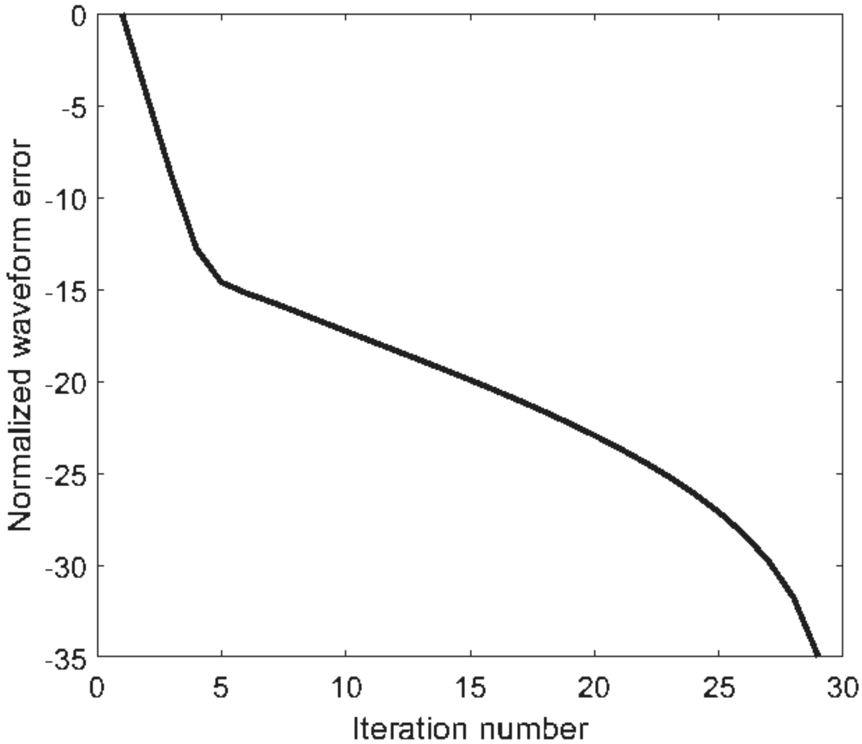

Figure 3.7: Normalized waveform error

and the minimum values settle at 1 at about the 10th iteration.

3.1.4.6 Radar Performance Analysis

The radar performance evaluation is provided in two figures: the first figure compares the desired LFM waveform for radar and the far-field synthesized waveform, whereas the second gives the detection probability (pD) versus SNR.

The waveform synthesized in the radar direction is shown in Figure 3.9. As shown in Figure 3.9(a), the synthesized radar waveform and the desired radar waveform seem almost identical, which validates the efficiency of the proposed scheme. However, there are small differences between the waveforms, shown in Figure 3.9(b). These differences or sample errors are defined as

$$\mathbf{e}_R = \mathbf{x}_R - \mathbf{a}(\theta_R)\mathbf{S}. \tag{3.40}$$

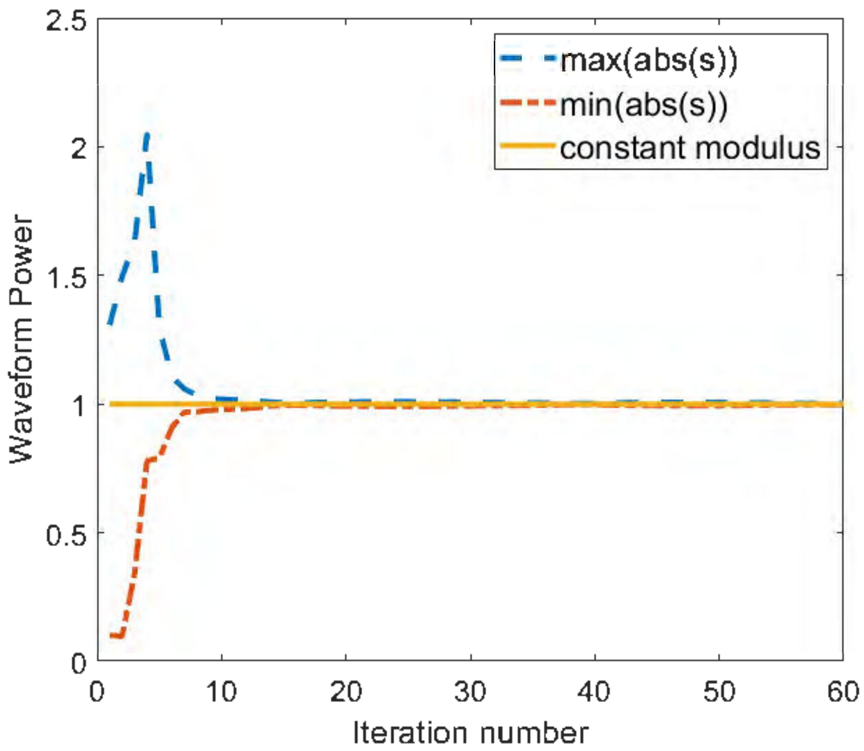

Figure 3.8: The waveform modulus per iteration showing the constant modulus constraint is satisfied.

Figure 3.10 shows the graph of detection probability plotted against SNR. The probability of false alarm is set as 10^{-4}. For comparison, pD versus SNR graphs of other methods are also provided. As the figure shows, FFRED-40% [85] has the best pD, which is almost the same as that of the desired LFM. However, the graph of the proposed method is so close that the difference becomes visible on zooming-in the plots. At the same time, the proposed method provides better pD than that of directly normalized method [86].

3.1.4.7 Communication Performance Analysis

Like radar performance, communication performance, too, is evaluated by two figures: the first figure gives a comparison of the desired communication waveform and the far-field synthesized waveform, whereas the second figure gives the SER versus SNR.

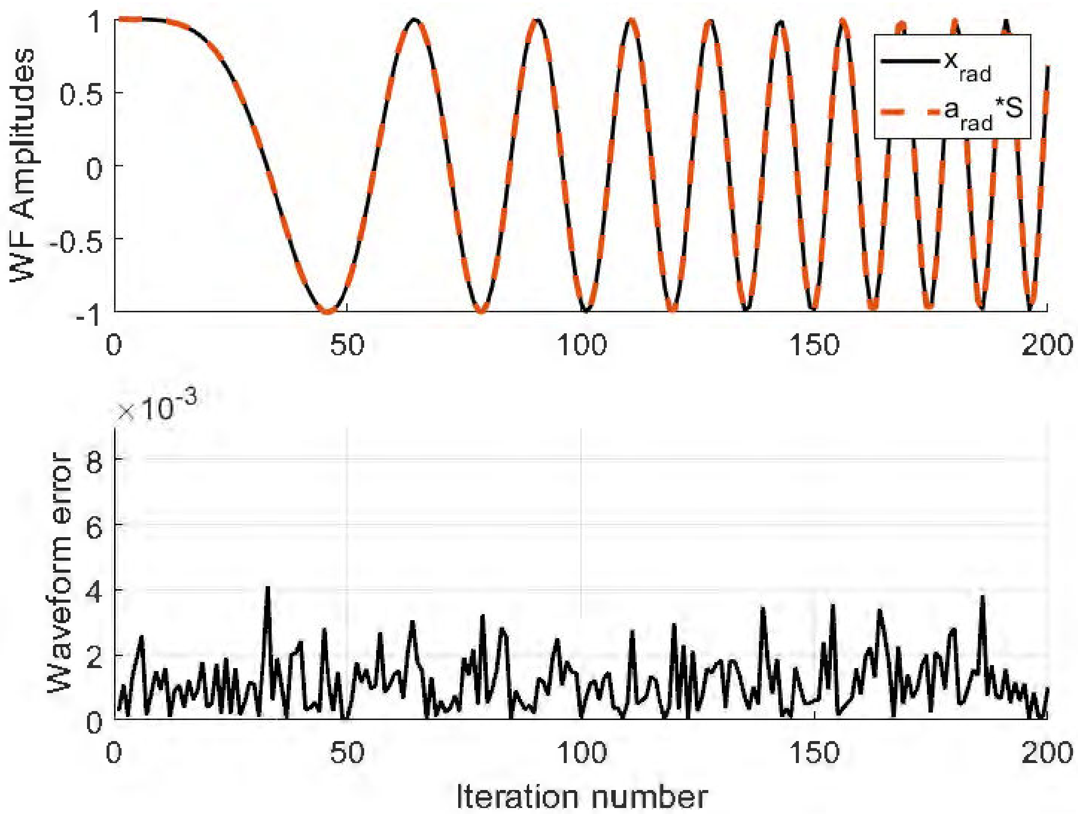

Figure 3.9: Synthesized radar waveform, (a) Desired waveform vs far-field synthesized waveform, (b) Difference between the desired waveform vs far-field synthesized waveform.

The waveform synthesized in the communication direction is shown in Figure 3.11. As with radar waveforms, the synthesized and the desired communication waveforms seem almost exact. The sample errors in this case, Figure 3.11(b), are defined as

$$\mathbf{e}_C = \mathbf{x}_C - \mathbf{a}(\theta_C)\mathbf{S}. \tag{3.41}$$

Figure 3.12 shows SER plotted against SNR. Again, for comparison, SER versus SNR graphs of other methods are provided. The '2 bits per symbol' graph represents the theoretical values. Again, the graphs of FFRED-40% [85] and the proposed ADMM method are very close, although FFRED-40% has a relatively better performance. Both methods outperform the directly normalized waveform method [86].

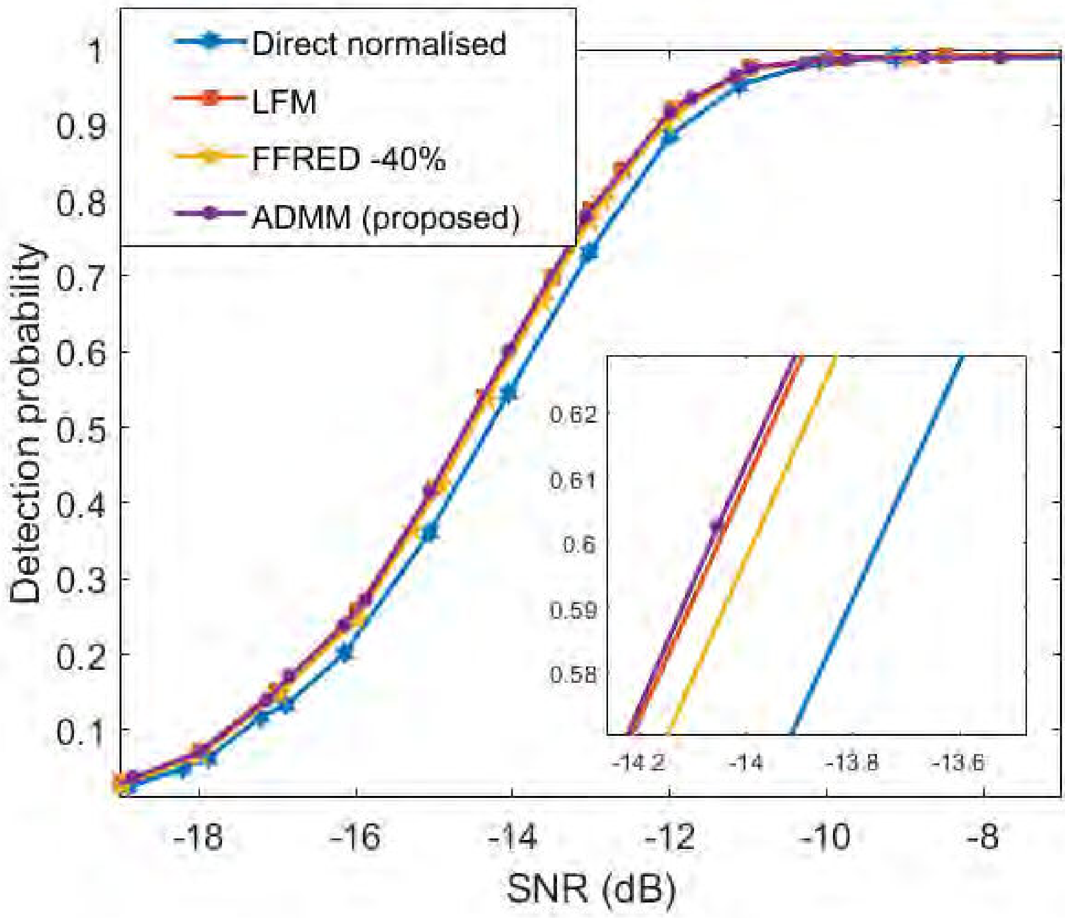

Figure 3.10: Comparison of different methods: detection probability vs SNR

3.2 Constant Power Waveform Design for MIMO based DFRC Systems

In this work, we present a waveform design strategy for MIMO-based joint radar-communication systems, addressing the challenge of constant power waveforms. At first, the optimization problem focuses on minimizing power radiation in the undesired locations while adhering to constraints like waveform similarity and constant power. Next, we utilize the ADMM algorithm as the computational framework for addressing the problem. Importantly, we introduce a novel approach for selecting penalty parameters for achieving an optimized waveforms to successfully approximate the desired beampattern, achieving high radar and communication main-beams in the desired directions, while

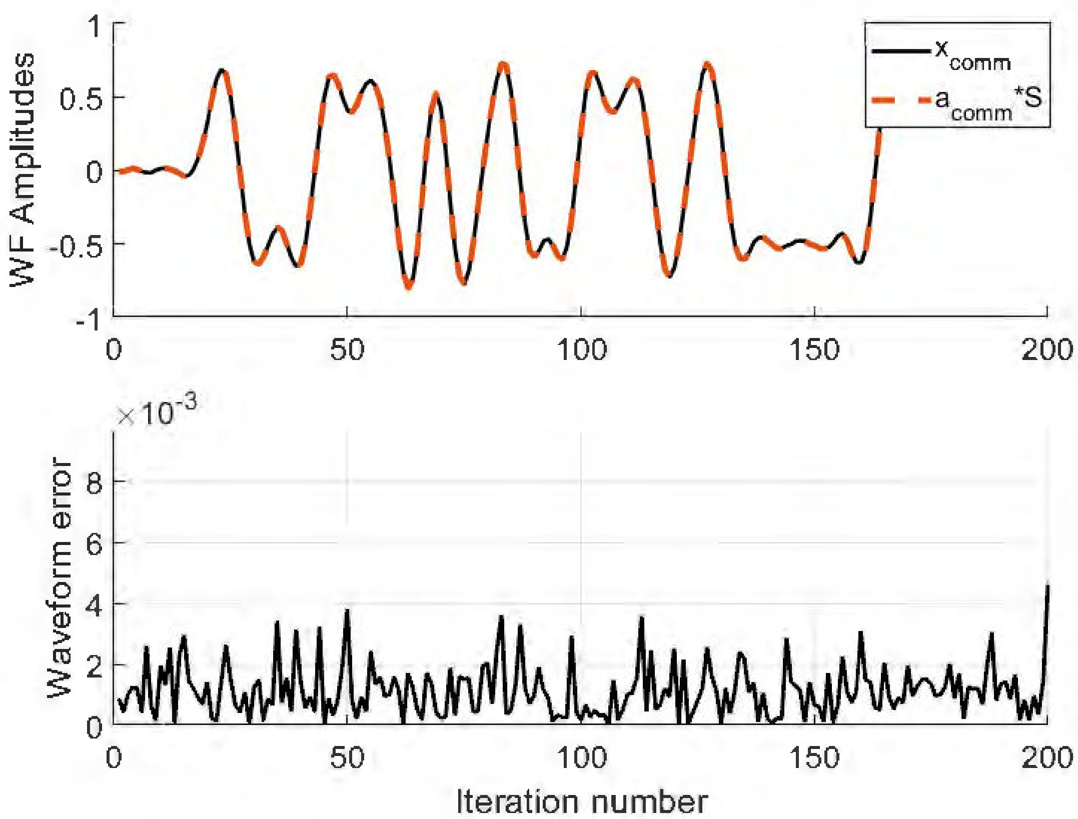

Figure 3.11: Synthesized communication waveform, (a) Desired waveform vs far-field synthesized waveform, (b) Difference between the desired waveform vs far-field synthesized waveform.

generating low sidelobes elsewhere. Moreover, these waveforms effectively generate the intended radar and communication signals within the far-field of the antenna array. Ultimately, the simulation outcomes substantiate the efficacy of this devised methodology, offering a prospective solution for dual-function radar-communication within MIMO setups.

3.2.1 System Model

An integrated system with MIMO DFRC architecture is considered. The setup comprises a uniform linear array (ULA) with M transmit-receive antenna elements. In the far-field of the system reside the radar and communication receivers, each composed of M antenna elements. The DFRC system send out an

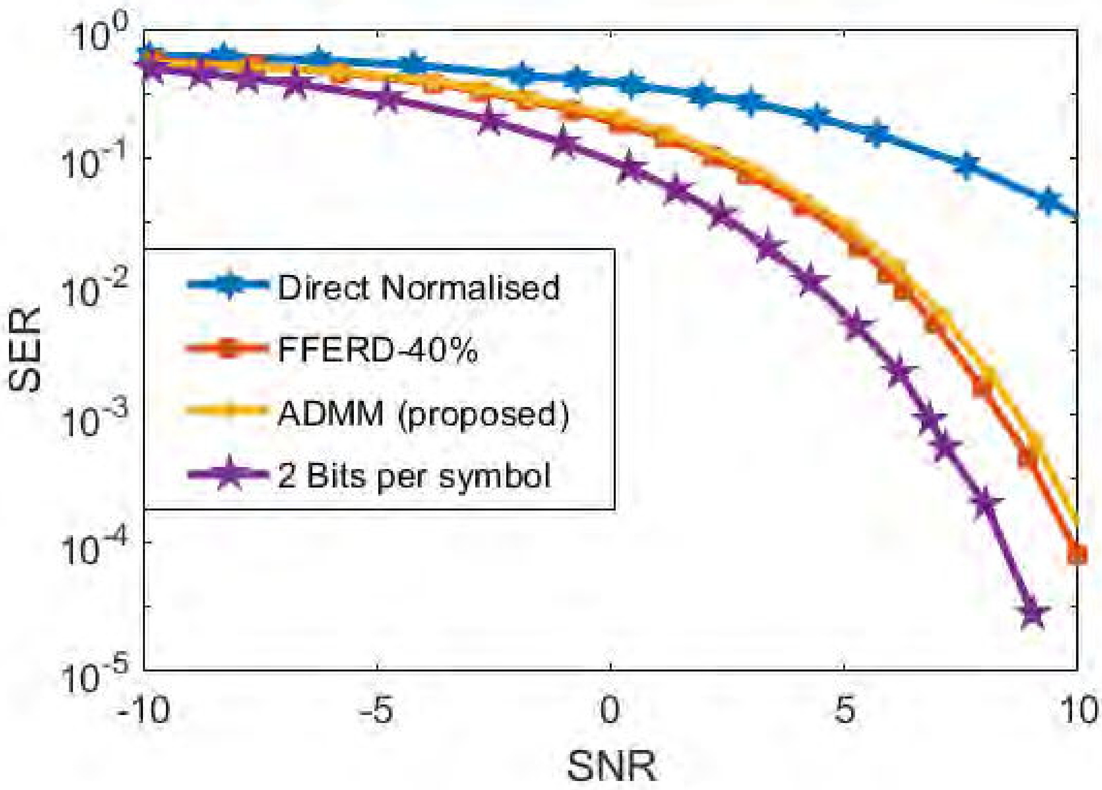

Figure 3.12: Comparison of different methods: SER vs SNR

integrated waveform, utilized both for encoding information in communication and for radar functionality, processing echoes reflected from potential targets. The system is the same as shown in Figure 3.1.

Consider $s_m(l) \in \mathbb{C}$ be the l-th sample, $l = 1,\ldots,L$, of the desired joint waveform, transmitted by the m-th antenna, $m = 1,\ldots,M$ and $l = 1,\ldots,L$, of the ULA.

Similarly, let $\mathbf{s}_l = [s_1(l), s_2(l), \ldots, s_M(l)]^T \in \mathbb{C}^{M\times 1}$ denote the l-th samples of the waveforms transmitted from all the M antennas. The synthesised waveform in the direction θ is given by

$$x(l;\theta) = \mathbf{a}^H(\theta)\mathbf{s}_l \tag{3.42}$$

where $a(\theta)$ is steering vector, given by

$$a(\theta) = [1, e^{-j2\pi d sin(\theta)/\lambda}, \ldots, e^{-j2\pi(M-1)d sin(\theta)/\lambda}]^T \in \mathbb{C}^{M\times 1} \tag{3.43}$$

with d being the distance between the adjacent antenna elements and λ the wavelength. Also let the collection $\mathbf{s} = [\mathbf{s}_1^T, \mathbf{s}_2^T, \ldots, \mathbf{s}_L^T]^T \in \mathbb{C}^{LM\times 1}$ be the space-time transmit waveform vector.

Let $\mathbf{x}_R = [x_R(0), \ldots, x_R(L-1)]^T \in \mathbb{C}^{L\times 1}$ denote the desired radar waveform. Similarly let $\mathbf{x}_C = [x_C(0), \ldots, x_C(L-1)]^T \in \mathbb{C}^{L\times 1}$ denote the desired communication waveform. The $LM \times 1$ transmit waveform vector $\mathbf{s}$ is required to be designed such that it synthesises $\mathbf{x}_R$ in the radar direction θ_R and $\mathbf{x}_C$ in communication direction θ_C, where $\theta_R \neq \theta_C$, i.e.,

$$\mathbf{a}^H(\theta_R)\mathbf{s}_l = x_{R,l} \tag{3.44}$$

and

$$\mathbf{A}^H(\theta_R)\mathbf{s} = \mathbf{x}_R \tag{3.45}$$

where $\mathbf{A}(\theta_R) = \mathbf{I}_L \otimes \mathbf{a}(\theta_R) \in \mathbb{C}^{LM\times L}$. Similarly

$$\mathbf{a}^H(\theta_C)\mathbf{s}_l = x_{C,l} \tag{3.46}$$

and

$$\mathbf{A}^H(\theta_C)\mathbf{s} = \mathbf{x}_C \tag{3.47}$$

where $\mathbf{A}(\theta_C) = \mathbf{I}_L \otimes \mathbf{a}(\theta_C) \in \mathbb{C}^{LM\times L}$. For ease of computation, a combination of Equations (3.45) and (3.47) can be formulated as

$$\mathbf{A}^H(\Theta)\,\mathbf{s} = \mathbf{x}, \tag{3.48}$$

where $\mathbf{A}(\Theta) = [\mathbf{A}(\theta_R) \;\; \mathbf{A}(\theta_C)] \in \mathbb{C}^{LM \times 2L}$ and $\mathbf{x} = [\mathbf{x}^T \;\; \mathbf{x}^T]^T \in \mathbb{C}^{2L \times 1}$.

3.2.2 Problem Formulation

The main objective involves the design of waveform $\mathbf{s}$ to minimize transmitted power within the sidelobes while maintaining unchanged transmission in the radar and communication directions. Additionally, two specific constraints are imposed: the first constraint necessitates that the transmitted waveform $\mathbf{s}$ produces the waveform $\mathbf{x}_R$, which is the required radar waveform, towards the target, and the waveform $\mathbf{x}_C$, which the required communication waveform, in the communication user's direction. This represents the waveform synthesis (WS) constraint, formulated mathematically in Equation (3.48). The other constraint is guarantee that the same amount of power is radiated in each transmission instance. This is the constant power constraint, as gives by Equation (3.48)

$$\mathbf{s}^T\mathbf{s} = P_{max} \tag{3.49}$$

This problem, the objective and constraints, is framed as an optimization problem as

$$\begin{aligned} \underset{\mathbf{s}}{\text{minimize}} \quad & \| \mathbf{A}^H \left(\widetilde{\Theta}\right) \mathbf{s} \|_2^2 \\ \text{subject to} \quad & \mathbf{A}^H (\Theta) \mathbf{s} = \mathbf{x} \\ & \mathbf{s}^T\mathbf{s} = P_{max}, \end{aligned} \tag{3.50}$$

where $\Theta = [\theta_R \;\; \theta_C]$ is the representation of radar and communication angles in combined form, and $\widetilde{\Theta} = [\theta_1 \;\; \theta_2 \;\; \cdots \;\; \theta_K]$ is the set of K undesired directions..

To make the computation easy, the variables are converted into their real-valued versions by stacking together their real and imaginary parts. In the end, the real and imaginary parts can be combined again. For example, the real part of the $ML \times 1$ complex-valued $\mathbf{s}$, the waveform vector, is stored in one vector and the complex part in another vectore and the two are stacked together to give another $2ML \times 1$ real-valued vector $\mathbf{s}_r$.

This procedure is applied to $\mathbf{s}$, $\mathbf{x}$, $\mathbf{A}(\Theta)$, and $\mathbf{A}\left(\widetilde{\Theta}\right)$ as

$$
\begin{aligned}
\mathbf{s}_r &= \begin{bmatrix} \Re\{\mathbf{s}\} \\ \Im\{\mathbf{s}\} \end{bmatrix} \\
\mathbf{x}_r &= \begin{bmatrix} \Re\{\mathbf{x}\} \\ \Im\{\mathbf{x}\} \end{bmatrix} \\
\mathbf{A}_r(\Theta) &= \begin{bmatrix} \Re\,\mathbf{A}(\Theta)\} & -\Im\{\mathbf{A}(\Theta)\} \\ \Im\{\mathbf{A}(\Theta)\} & \Re\{\mathbf{A}(\Theta)\} \end{bmatrix} \\
\mathbf{A}_r\left(\widetilde{\Theta}\right) &= \begin{bmatrix} \Re\{\mathbf{A}\left(\widetilde{\Theta}\right)\} & -\Im\{\mathbf{A}\left(\widetilde{\Theta}\right)\} \\ \Im\{\mathbf{A}\left(\widetilde{\Theta}\right)\} & \Re\{\mathbf{A}\left(\widetilde{\Theta}\right)\} \end{bmatrix}
\end{aligned} \tag{3.51}
$$

In terms of these new variables, the constant power constraint is given by

$$
\mathbf{s}_r^T \mathbf{s}_r = P_{max}. \tag{3.52}
$$

Similarly, the problem Equation (3.50) is changed as

$$
\begin{aligned}
\underset{\mathbf{s}_r}{\text{minimize}} \quad & \mathbf{s}_r^T \mathbf{A}_r\left(\widetilde{\Theta}\right) \mathbf{A}_r^T\left(\widetilde{\Theta}\right) \mathbf{s}_r \\
\text{subject to} \quad & \mathbf{A}_r^T(\Theta)\,\mathbf{s}_r = \mathbf{x}_r \\
& \mathbf{s}_r^T \mathbf{s}_r = P_{max}.
\end{aligned} \tag{3.53}
$$

Different methods, numerical or others, can be used to approach the waveform design problem, Equation (3.53), and obtain the solution, i.e., the real-valued version, $\mathbf{s}_{r-opt}$, of the required transmit waveform $\mathbf{s}_{opt}$. The required transmit waveform is obtained as

$$\mathbf{s}_{opt} = \mathbf{s}_{r1,opt} + i \cdot \mathbf{s}_{r2,opt} \tag{3.54}$$

where $\mathbf{s}_{r1,opt}$ has the first ML elements and $\mathbf{s}_{r2,opt}$ contains the other ML elements, the real and imaginary imaginary parts of $\mathbf{s}_{opt}$. In this work, ADMM is used to solved the considered problem.

3.2.3 ADMM based Problem Formulation and Solution

Let Equation (3.53) be rewritten as

$$\begin{aligned}
\underset{\mathbf{r}_r,\mathbf{s}_r}{\text{minimize}} \quad & \mathbf{r}_r^T \mathbf{A}_r\left(\widetilde{\Theta}\right)\mathbf{A}_r^T\left(\widetilde{\Theta}\right)\mathbf{s}_r \\
\text{subject to} \quad & \mathbf{A}_r^T(\Theta)\,\mathbf{r}_r + \mathbf{A}_r^T(\Theta)\,\mathbf{s}_r - 2\mathbf{x}_r = \mathbf{0} \\
& \mathbf{r}_r^T\mathbf{s}_r - P_{max} = \mathbf{0} \\
& \mathbf{r}_r = \mathbf{s}_r.
\end{aligned} \tag{3.55}$$

where $\mathbf{r}_r$ is an auxilliary variable. Then, augmented Lagrangian of Equation (3.55) is represented as

$$\begin{aligned}
\mathscr{L}\{\mathbf{r}_r, \mathbf{s}_r, \mathbf{u}, v, \mathbf{w}\} \;=\;& \mathbf{r}_r^T \mathbf{A}_r\left(\widetilde{\Theta}\right)\mathbf{A}_r^T\left(\widetilde{\Theta}\right)\mathbf{s}_r \\
+\;& \tfrac{\rho_1}{2}\left\|\mathbf{A}_r^T(\Theta)\,\mathbf{r}_r + \mathbf{A}_r^T(\Theta)\,\mathbf{s}_r - 2\mathbf{x}_r + \mathbf{u}\right\|_2^2 \\
+\;& \tfrac{\rho_2}{2}\left\|\mathbf{r}_r^T\mathbf{s}_r - P_{max} + v\right\|_2^2 \\
+\;& \tfrac{\rho_3}{2}\left\|\mathbf{r}_r - \mathbf{s}_r + \mathbf{w}\right\|_2^2
\end{aligned} \tag{3.56}$$

where $\mathbf{u} \in \mathbb{R}^{4L\times 1}$, $v \in \mathbb{R}^{1\times 1}$, and $\mathbf{w} \in \mathbb{R}^{2ML\times 1}$ are the dual variables, and $\rho_1, \rho_2, \rho_3 > 0$ are the penalty parameters. The augmented Lagrangian is dependent on the variables $\mathbf{r}_r, \mathbf{s}_r, \mathbf{u}, v$, and $\mathbf{w}$. The solution for these variables can be achieved individually by partitioning the problem into multiple sub-problems. The solutions for these individual sub-problems can be acquired as

$$\mathbf{r}_r^{m+1} := \arg\min_{\mathbf{r}_r} \mathscr{L}\left(\mathbf{r}_r, \mathbf{s}_r^m, \mathbf{u}^m, \nu^m, \mathbf{w}^m\right) \tag{3.57a}$$

$$\mathbf{s}_r^{m+1} := \arg\min_{\mathbf{s}_r} \mathscr{L}\left(\mathbf{r}_r^{m+1}, \mathbf{s}_r, \mathbf{u}^m, \nu^m, \mathbf{w}^m\right) \tag{3.57b}$$

$$\mathbf{u}^{m+1} := \mathbf{u}^m + \mathbf{A}_r^T \mathbf{r}_r^{m+1} + \mathbf{A}_r^T \mathbf{s}_r^{m+1} - 2\mathbf{x}_r \tag{3.57c}$$

$$\nu^{m+1} := \nu^m + \left(\mathbf{r}_r^{m+1}\right)^T \mathbf{s}_r^{m+1} - P_{max} \tag{3.57d}$$

$$\mathbf{w}^{m+1} := \mathbf{w}^m + \mathbf{r}_r^{m+1} - \mathbf{s}_r^{m+1}. \tag{3.57e}$$

Solutions of the Equations (3.57c)–(3.57e) are straightforward. The subequations (3.57a) and (3.57b) yeild closed-form solutions and their details are provided in the following sub-sections.

3.2.3.1 Update of $\mathbf{r}_r$

Take the derivative of subequation (3.57a) with respect to $\mathbf{r}_r$ and make the resulting expression equal to 0 to obtain the $(m+1)$-th update of the solution of $\mathbf{r}_r$, , i.e.,

$$\nabla_{\mathbf{r}_r} \mathscr{L}\left(\mathbf{r}_r, \mathbf{s}_r^m, \mathbf{u}^m, \nu^m, \mathbf{w}^m\right) = \mathbf{0}. \tag{3.58}$$

The solution of Equation (3.58) is expressed as

$$\mathbf{r}_r^{m+1} = \Xi_1^{-1} \xi_1 \tag{3.59}$$

where

$$\Xi_1 = \rho_1 \mathbf{A}_r(\Theta) \mathbf{A}_r^T(\Theta) + \rho_2 \mathbf{s}_r \mathbf{s}_r^T + \rho_3 \mathbf{I} \tag{3.60}$$

and

$$\begin{aligned}\xi_1 &= \rho_1 \mathbf{A}_r(\Theta)\left(2\mathbf{x}_r - \mathbf{u} - \mathbf{A}_r^T(\Theta)\overline{\mathbf{s}}_r\right)\\ &+ \rho_2(P_{max} - v)\mathbf{s}_r - \rho_3(\mathbf{s}_r - \mathbf{w})\\ &- \mathbf{A}_r\left(\widetilde{\Theta}\right)\mathbf{A}_r^T\left(\widetilde{\Theta}\right)\mathbf{s}_r.\end{aligned} \tag{3.61}$$

3.2.3.2 Update of $\mathbf{s}_r$

As in the update for $\mathbf{r}_r$, here too, the derivative of subequation (3.57b) with respect to $\mathbf{s}_r$ is computed, and the resulting expression is set equal to zero. Mathematically denoted as

$$\nabla_{\mathbf{s}_r}\mathscr{L}\left(\mathbf{r}_r^{m+1}, \mathbf{s}_r, \mathbf{u}^m, v^m, \mathbf{w}^m\right) = \mathbf{0}. \tag{3.62}$$

The solution of Equation (3.62) is expressed as

$$\mathbf{s}_r^{m+1} = \Xi_2^{-1}\xi_2 \tag{3.63}$$

where

$$\Xi_2 = \rho_1 \mathbf{A}_r(\Theta)\mathbf{A}_r^T(\Theta) + \rho_2 \mathbf{r}\mathbf{r}^T + \rho_3 \mathbf{I} \tag{3.64}$$

and

$$\begin{aligned}\xi_2 &= \rho_1 \mathbf{A}_r(\Theta)\left(2\mathbf{x}_r - \mathbf{u} - \mathbf{A}_r^T(\Theta)\mathbf{r}_r\right)\\ &+ \rho_2(P_{max} - v) + \rho_3(\mathbf{r}_r + \mathbf{w})\\ &- \mathbf{A}_r\left(\widetilde{\Theta}\right)\mathbf{A}_r^T\left(\widetilde{\Theta}\right)\mathbf{r}_r.\end{aligned} \tag{3.65}$$

3.2.3.3 Termination Criteria of the Algorithm

The primary and dual residuals, which approach zero as the algorithm converges, can be used to define termination measures. Let the primal residuals at

$(m+1)$-th iteration be expressed as

$$d_{pr1}^{m+1} = \mathbf{A}_r^T \mathbf{r}_r^{m+1} + \mathbf{A}_r^T \mathbf{s}_r^{m+1} - 2\mathbf{x}_r \tag{3.66a}$$

$$d_{pr2}^{m+1} = \left(\mathbf{r}_r^{m+1}\right)^T \mathbf{s}_r^{m+1} - P_{max} \tag{3.66b}$$

$$d_{pr3}^{m+1} = \mathbf{r}_r^{m+1} - \mathbf{s}_r^{m+1} \tag{3.66c}$$

Similarly, the dual residuals

$$d_{rs1}^{m+1} = \mathbf{r}_r^{m+1} - \mathbf{r}_r^{m} \tag{3.67a}$$

$$d_{rs2}^{m+1} = \mathbf{s}_r^{m+1} - \mathbf{s}_r^{m}. \tag{3.67b}$$

Then, the following can be considered as reasonable termination criteria [84]

$$\| d_{pr1}^{m+1} \|_2^2 \leq \ \varepsilon_1^{pri}, \tag{3.68a}$$

$$\| d_{pr2}^{m+1} \|_2^2 \leq \ \varepsilon_2^{pri}, \tag{3.68b}$$

$$\| d_{pr3}^{m+1} \|_2^2 \leq \ \varepsilon_3^{pri}, \tag{3.68c}$$

$$\| d_{dr1}^{m+1} \|_2^2 \leq \ \varepsilon^{dual}, \tag{3.68d}$$

$$\| d_{dr2}^{m+1} \|_2^2 \leq \ \varepsilon^{dual}. \tag{3.68e}$$

where ε_1^{pri}, ε_2^{pri}, ε_3^{pri} are tolerances for the primal residuals and ε_1^{dual} is the tolerance for dual residuals, which can be defined as [84]

$$\varepsilon_1^{pri} = \sqrt{4L}\varepsilon^{abs} + \varepsilon^{rel}\max\left\{\| \mathbf{A}_r^T(\Theta)\,\mathbf{r}_r^{m+1} \|_2, \| \mathbf{A}_r^T(\Theta)\,\mathbf{s}_r^{m+1} \|_2, \| 2\mathbf{x}_r \|_2\right\} \tag{3.69a}$$

$$\varepsilon_2^{pri} = \sqrt{MN}\varepsilon^{abs} + \varepsilon^{rel}\max\left\{\| \left(\mathbf{r}_r^{m+1}\right)^T \mathbf{s}_r^{m+1} \|_2 \ , P_{max}\right\} \tag{3.69b}$$

$$\varepsilon_3^{pri} = \sqrt{2MN}\varepsilon^{abs} + \varepsilon^{rel}\max\left\{\| \mathbf{r}_r^{m+1} \|_2, \| \mathbf{s}_r^{m+1} \|_2\right\} \tag{3.69c}$$

$$\varepsilon^{dual} = \sqrt{2MN}\varepsilon^{abs} + \varepsilon^{rel} \| \rho_1 \mathbf{w} \|_2 \tag{3.69d}$$

3.2.3.4 Summary of the algorithm

A summary of the different stages of the suggested methodology is provided as following.

Summary of the proposed algorithm
Input: M, L, K, d, θ_R, θ_C
1: **Initialize:** $\mathbf{r}_r^0, \mathbf{s}_r^0, \mathbf{u}^0, v^0, \mathbf{w}^0, \rho_1, \rho_2, \rho_3$, and ε_1^{pri}, ε_2^{pri}, ε_2^{pri}, ε^{dual}, $m = 1$.
2: **Loop:** Until the termination criteria, Eq. (3.68), are fulfilled, do
3: Update $\mathbf{r}_r^{m+1}$, Eq. (3.59)
4: Update $\mathbf{s}_r^{m+1}$, Eq. (3.63)
5: Update $\mathbf{u}^{m+1}$, Eq. (3.57c)
6: Update v^{m+1}, Eq. (3.57d)
7: Update $\mathbf{w}^{m+1}$, Eq. (3.57e)
8: $m = m + 1$, go to step 2
9: **End loop**
Output: $\mathbf{r}_r^{m+1}$, $\mathbf{s}_r^{m+1}$

To facilitate a clear understanding, a comprehensive list of symbols, along with their associated dimensions and descriptive explanations, is available in Table 3.4.

Table 3.4: List of symbols.

Symbol	Dimension	Description
M	1×1	Antennas elements in the ULA
L	1×1	Waveform samples
K	1×1	Sidelobes
d	1×1	Distance between adjacent antenna elements in the array
$\mathbf{I}_N$	$L \times L$	Identity matrix
λ	1×1	Wavelength
$s_m(n)$	1×1	nth sample of the waveform
$\mathbf{s}_l$	$M \times 1$	l-th waveform samples vector
$\mathbf{s}$	$LM \times 1$	Space-time transmit waveform vector
$\mathbf{s}_r$	$2LM \times 1$	Real-valued equivalent of $\mathbf{s}$
$\mathbf{x}_R$	$L \times 1$	Desired radar waveform
$\mathbf{x}_C$	$L \times 1$	Desired communication waveform
$\mathbf{x}$	$2L \times 1$	$\mathbf{x}_R$ and $\mathbf{x}_C$ combined together in a single vector
$\mathbf{x}_r$	$4L \times 1$	Real-valued equivalent of $\mathbf{x}$
$\mathbf{a}(\theta_R)$	$M \times 1$	Radar steering vector
$\mathbf{a}(\theta_C)$	$M \times 1$	Communication steering vector
$\mathbf{A}(\Theta)$	$M \times 2$	$\mathbf{a}(\theta_R)$ and $\mathbf{a}(\theta_C)$
$\mathbf{A}_r(\Theta)$	$2ML \times 4L$	Real-valued equivalent of $\mathbf{A}(\Theta)$
$\mathbf{A}\left(\widetilde{\Theta}\right)$	$M \times K$	Steering vectors in all undesired directions
$\mathbf{A}_r\left(\widetilde{\Theta}\right)$	$2ML \times 2KL$	Real-valued equivalent of $\mathbf{A}\left(\widetilde{\Theta}\right)$
$\mathbf{u}$	$4L \times 1$	Dual variable
v	1×1	Dual variable
$\mathbf{w}$	$2ML \times 1$	Dual variable
η, μ	1×1	Positive constants
ρ_1, ρ_2, ρ_3	1×1	Penalty parameters

3.2.4 Penalty Parameter Selection

Appropriate penalty parameter selection is crucial for good performance in penalty methods like ADMM because the convergence properties of penalty method are very sensitive to the penalty parameters.

3.2.4.1 Existing Penalty Parameter Selection Methods

There are different methods to choose penalty parameters. The simplest way is to have them fixed. The fixed penalty parameters can be chosen by hit and trial or by intelligent guess. Another option is to increase the penalty parameters with increasing iterations. However, fixed value or monotonically increasing values are not good choices. It is better to have variable penalty parameters that can change adaptively according to the situation. One popular method of adaptive penalty parameters selection is residual balancing [88].

$$\rho_{k+1} = \begin{cases} \eta\rho_k & \text{if} \quad d_{pr1}^{m+1} > \mu\varepsilon_1^{pri} \\ \rho_k/\eta & \text{if} \quad \varepsilon_1^{pri} > \mu d_{pr1}^{m+1} \\ \rho_k & otherwise \end{cases} \tag{3.70}$$

where $\mu > 1$ and $\eta > 1$ are constants, d_{pr1}^{m+1} is the primary residual, and ε_1^{pri} is the tolerance.

3.2.4.2 The Proposed Penalty Parameter Selection Method

The devised approach for selecting penalty parameters ensures an equitable consideration of all constraints during the optimization procedure. In cases where the penalty parameters are not judiciously selected, some of the constraints are optimized well but others remain poorly optimized. During the optimization process, the values of the objective function function (the unconstrained part) and residuals of the constraints get minimized iteratively but they are not equally minimized. To maintain their presence, the values of the comparatively more minimized constraints need to be increased by multiplying them with larger penalty parameters. The proposed methods ensures that the penalty parameters are selected such that all the residuals are minimized equally well.

As an example, re-consider the constrained optimization problem (3.55)

$$\begin{aligned}
\underset{\mathbf{r}_r,\mathbf{s}_r}{\text{minimize}} \quad & \mathbf{r}_r^T \mathbf{A}_r\left(\widetilde{\Theta}\right)\mathbf{A}_r^T\left(\widetilde{\Theta}\right)\mathbf{s}_r \\
\text{subject to} \quad & \mathbf{A}_r^T(\Theta)\,\mathbf{r}_r + \mathbf{A}_r^T(\Theta)\,\mathbf{s}_r - 2\mathbf{x}_r = \mathbf{0} \\
& \mathbf{r}_r^T\mathbf{s}_r - P_{max} = \mathbf{0} \\
& \mathbf{r} = \mathbf{s}.
\end{aligned} \tag{3.71}$$

In penalty methods like ADMM, the transformation of a constrained optimization problem into an unconstrained counterpart is a typical approach, aiming for the solution of the unconstrained problem to ideally converge towards the solution of the original problem. The constrained optimization problem (3.55) is turned into an unconstrained as

$$\begin{aligned}
\mathscr{L}\{\mathbf{r}_r,\mathbf{s}_r\} &= \mathbf{r}_r^T \mathbf{A}_r\left(\widetilde{\Theta}\right)\mathbf{A}_r^T\left(\widetilde{\Theta}\right)\mathbf{s}_r \\
&+ \tfrac{\rho_1}{2}\left\|\mathbf{A}_r^T(\Theta)\,\mathbf{r}_r + \mathbf{A}_r^T(\Theta)\,\mathbf{s}_r - 2\mathbf{x}_r\right\|_2^2 \\
&+ \tfrac{\rho_2}{2}\left\|\mathbf{r}_r^T\mathbf{s}_r - P_{max}\right\|_2^2 \\
&+ \tfrac{\rho_3}{2}\left\|\mathbf{r}_r - \mathbf{s}_r\right\|_2^2
\end{aligned} \tag{3.72}$$

Note the difference of Equation (3.72) from Equation (3.56). While quation (3.56) is a specific for linear ADMM, Equation (3.72) is a generic form. We have chosen this because we are more interested in the primary residuals and the fact that the dual variables $\mathbf{u}$, v, and $\mathbf{w}$ vanish over time if the algorithm is correct. We denote the objective functions which is the first line of Equation (3.71) as $\mathbf{z}_o$. Similarly we give new notations to the primary residuals, Equations (3.66a, 3.66b, 3.66c), as $\mathbf{z}_1$, $\mathbf{z}_2$ and $\mathbf{z}_3$, i.e.

$$\mathbf{z}_o = \left|\mathbf{r}_r^T \mathbf{A}_r\left(\widetilde{\Theta}\right)\mathbf{A}_r^T\left(\widetilde{\Theta}\right)\mathbf{s}_r\right| \tag{3.73a}$$

$$\mathbf{z}_1 = \left\| \mathbf{A}_r^T \mathbf{r}_r^{m+1} + \mathbf{A}_r^T \mathbf{s}_r^{m+1} - 2\mathbf{x}_r \right\|_2^2 \tag{3.73b}$$

$$\mathbf{z}_2 = \left\| \left(\mathbf{r}_r^{m+1}\right)^T \mathbf{s}_r^{m+1} - P_{max} \right\|_2^2 \tag{3.73c}$$

$$\mathbf{z}_3 = \left\| \mathbf{r}_r^{m+1} - \mathbf{s}_r^{m+1} \right\|_2^2 \tag{3.73d}$$

Then for simplicity, we can rewrite Equation (3.72) as

$$\mathscr{J}\left\{\mathbf{r}_r, \mathbf{s}_r\right\} = \mathbf{z}_o + \rho_1 \mathbf{z}_1 + \rho_2 \mathbf{z}_2 + \rho_3 \mathbf{z}_3. \tag{3.74}$$

Then we can choose the penalty parameters as

$$\rho_1 = \mathbf{z}_o / \mathbf{z}_1 \tag{3.75a}$$

$$\rho_2 = \mathbf{z}_o / \mathbf{z}_2 \tag{3.75b}$$

$$\rho_3 = \mathbf{z}_o / \mathbf{z}_3 \tag{3.75c}$$

In Equation (3.75), it can be seen that the residuals $\mathbf{z}_1$, $\mathbf{z}_2$, and $\mathbf{z}_3$ are in denominator. When the values of these residuals start approaching zero, the values of the penalty parameters ρ_1, ρ_2, and ρ_3 get very large. So it is better to impose some upper limit ρ_{max} which should not be exceeded. Therefore, Equation (3.75) can better formulated as

$$\rho_1 = \min\left(\mathbf{z}_o / \mathbf{z}_1, \rho_{max}\right) \tag{3.76a}$$

$$\rho_2 = \min\left(\mathbf{z}_o / \mathbf{z}_2, \rho_{max}\right) \tag{3.76b}$$

$$\rho_3 = \min\left(\mathbf{z}_o / \mathbf{z}_3, \rho_{max}\right). \tag{3.76c}$$

3.2.5 Simulation Results and Analysis

This section delves into evaluating the algorithm's performance through numerical examples. The examination involves a ULA comprising 32 antenna elements at both the transmitter and receiver ends. The enter-element spacing in the ULA is $\lambda/2$. The radar target is supposed to be situated at direction $\theta_R = 0°$ while the communication system is situated at $\theta_C = 45°$. The required waveform of the radar is as an up-chirp LFM signal, while the communication waveform uses the QPSK modulation scheme. To simplify, the scenario considers $N_s = 1$ symbol per pulse repetition interval (PRI) and $N_b = 2$ bits per symbol. Therefore, every waveform conveys 2 bits of information within each PRI. Additional simulation parameters are summarized in Table 4.2.

Table 3.5: A tabulation of the simulation parameters used in the algorithm

Parameter	Value	Description
M	16, 32	Number of antennas elements in the ULA
d	$\lambda/2$	Enter-elements distance in the ULA
$\mathbf{u}$	Random	Dual variable associated with ρ_1
v	Random	Dual variable associated with ρ_2
$\mathbf{w}$	Random	Dual variable associated with ρ_3
η	1.5	Positive constant 1
μ	1.5	Positive constant 2
ρ_1	1, $1e^{12}$	Penalty parameter 1
ρ_2	1, $1e^{12}$	Penalty parameter 2
ρ_3	1, $1e^{12}$	Penalty parameter 3

Numerous experiments were conducted to analyze performance across various scenarios. Given the pre-defined desired waveforms expected by both the communication and radar receivers, coherent detection is employed to match the received signal with the required waveforms at both the radar and communication sides, respectively. Communication performance is examined using Monte-Carlo simulations across different values of signal-to-noise ratio (SNR).

The presented methodology is juxtaposed against the Far Field Radiated

Emission Design (FFRED) approach [85], an iterative optimization technique employing normalized waveforms directly, , i.e., "direct normalization" [86], and theoretical benchmarks. Within the FFRED method, power allocation comprises 0%, 10% and 40% to orthogonal complementary waveforms, with FFRED-40% demonstrating superior performance. In contrast, the authors of [86] have introduced a variety of waveform design methodologies. One such approach involves the development of non-constant mode waveforms, featuring closed-loop solutions to waveform design quandaries. Additionally, they have proposed an iterative process for creating constant mode waveforms. Given the intricate nature of the computations, they have harnessed the outcomes of the initial non-constant modulus waveform method, subsequently subjecting them to iterative optimization for further enhancement. In their simulation endeavors, this strategy is denominated as "direct normalization".

3.2.5.1 Computational Complexity Analysis

To compute the complexity of the proposed algorithm, each code segment is examined for the number of operations based on input size. The algorithm runs 'iter' times, performing tasks like matrix multiplications, norm calculations, and variable updates. The complexity of each operation is summed up, factoring in variables like M and L.

The proposed algorithm has high complexity, primarily cubic, due to matrix inversion and subsequent matrix multiplication operations. The overall complexity of the algorithm is dominated by matrix operations. Matrix multiplication of size $2ML \times 2ML$ contributes $O(M^3L^3)$, while vector operations and additions contribute lower-order terms like $O(M^2L^2)$. The most computationally expensive part is the matrix inversion, which also has complexity $O(M^3L^3)$.

Hence, the overall complexity is $O(M^3L^3)$.

3.2.5.2 Communication Performance in Terms of Data Rate

The data rate can be expressed as

$$R = N_b \times N_s \times f_{PRF}, \tag{3.77}$$

where N_b represents the number of bits per symbol, N_s denotes the number of symbols in one pulse, and f_{PRF} stands for the pulse repetition frequency.

3.2.5.3 ADMM Convergence Analysis

The algorithm's convergence is validated by the gradual decrease of the primal and dual variables. Convergence is confirmed once these variables drop below predefined termination thresholds, following standard practices in optimization and numerical analysis. In Figures 3.13 and 3.14, the graphical representations depict the evolution of the norm values of primal residuals d_{pr1}, d_{pr2}, d_{pr3} and dual residuals d_{dr2}, d_{dr2}, on the y-axis of the corresponding figures, in conjunction with the predefined stopping criteria thresholds ε_1^{pri}, ε_2^{pri}, ε_2^{pri}, ε^{dual} over the course of iterative progress on x-axis. The residuals on the y-axis are unitless abstract values.

The plots clearly demonstrate that the stopping conditions are consistently satisfied within the first 20 iterations. Notably, in Figure 3.13, the primal residual d_{pr2} drops sharply and quickly stabilizes. This sharp decrease is likely due to the relatively high value of the associated penalty parameter ρ_2, which is significantly larger than the other parameters, as shown in Figure 3.17.

Figure 3.15 shows a graphical depiction of the values corresponding to the objective function, defined in the first line of Equation (3.53). The plot clearly

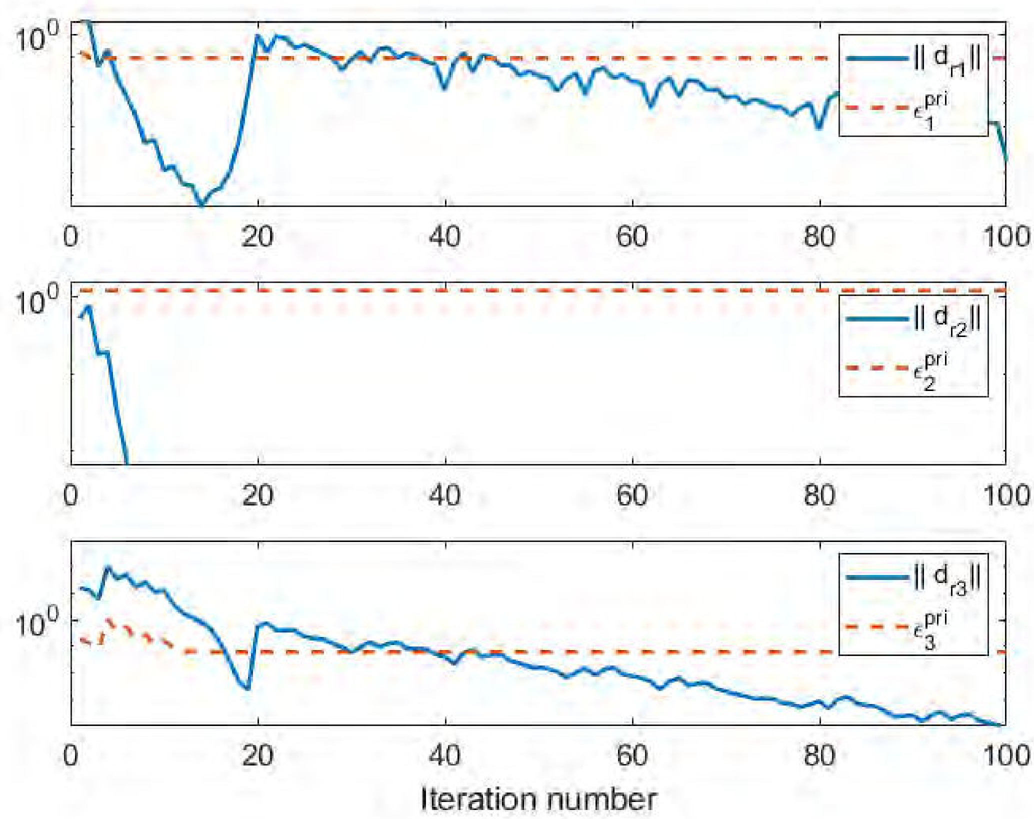

Figure 3.13: Primary residual norms per iteration

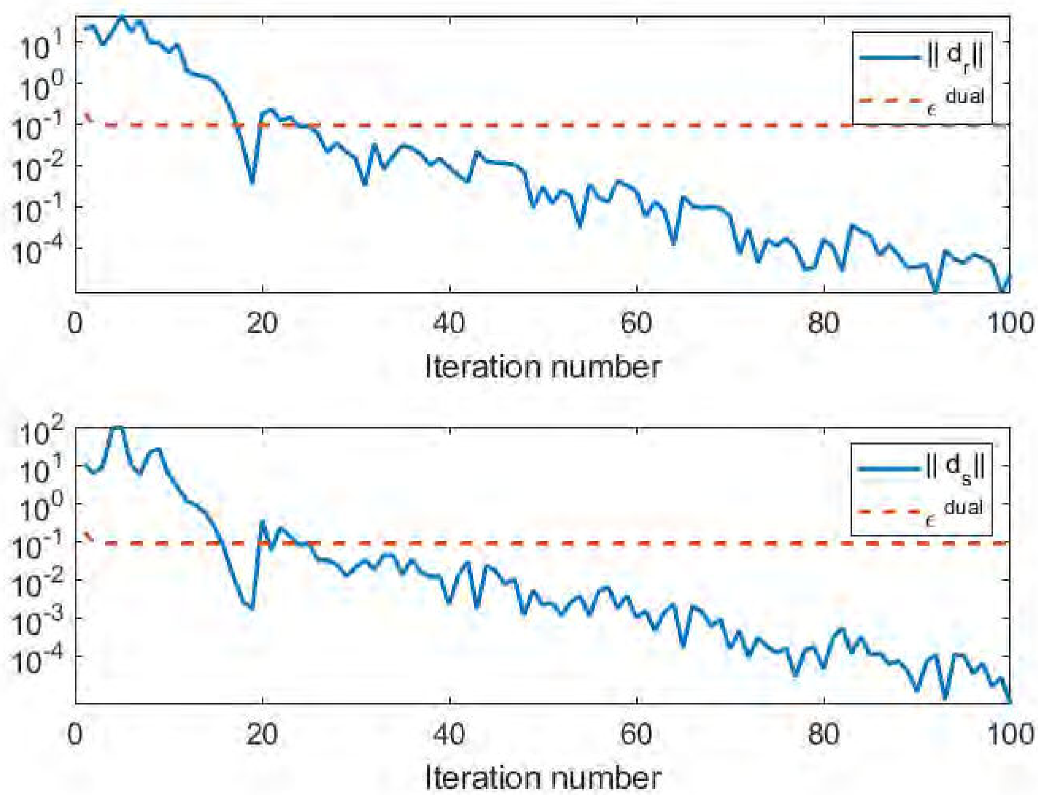

Figure 3.14: Dual residual norms per iteration

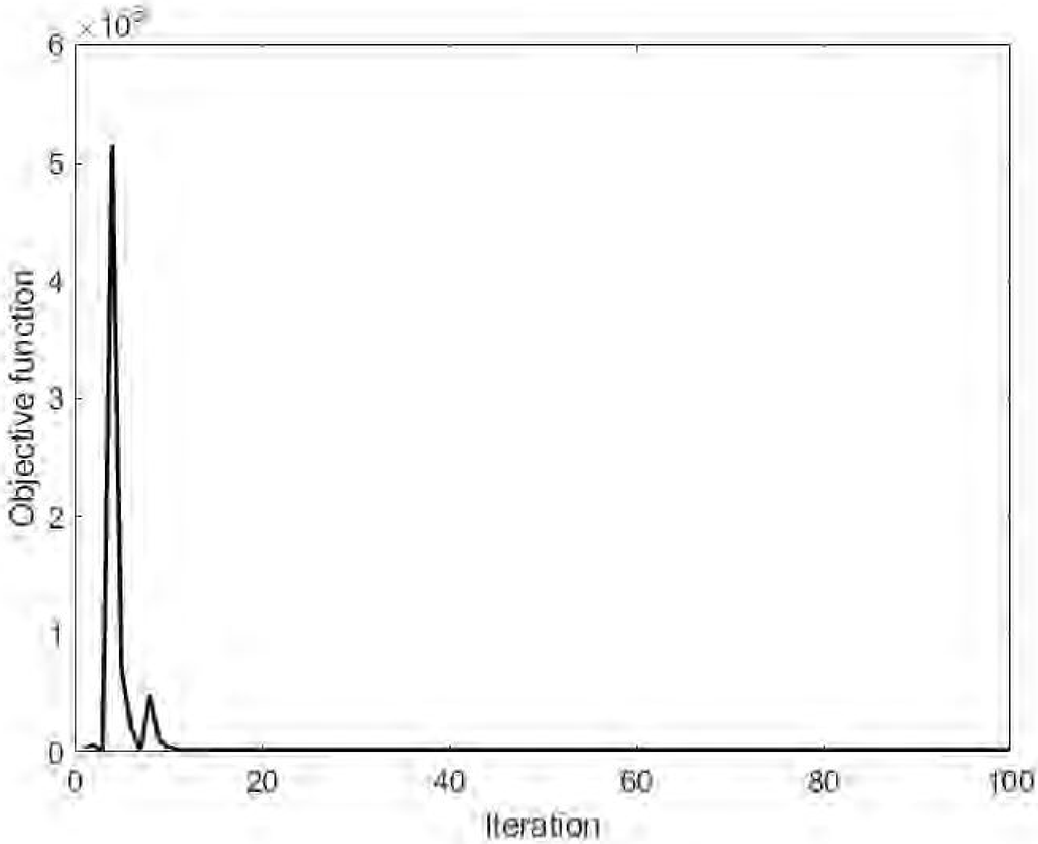

Figure 3.15: Objective function, Eq. (3.74), per iteration

indicates that the objective function converges well within just 10 iterations.

The convergence behavior of the objective function matches the trends observed in both the primary and dual residuals. This is evident in Figures 3.13 and 3.14. Additionally, it adheres to the constant power criterion, as demonstrated in Figure 3.19. These consistent observations point to a unified and coherent convergence pattern throughout the optimization process.

Figures 3.16 and 3.17 display the trajectories of how the penalty parameters vary over the iterations. These figures compare the penalty parameters generated by the proposed selection method with those from the residual balancing method. The comparison highlights the superior performance of the proposed method. It shows that the penalty parameters converge to more optimal values as the iterations progress, validating the method's effectiveness. Figure 3.16

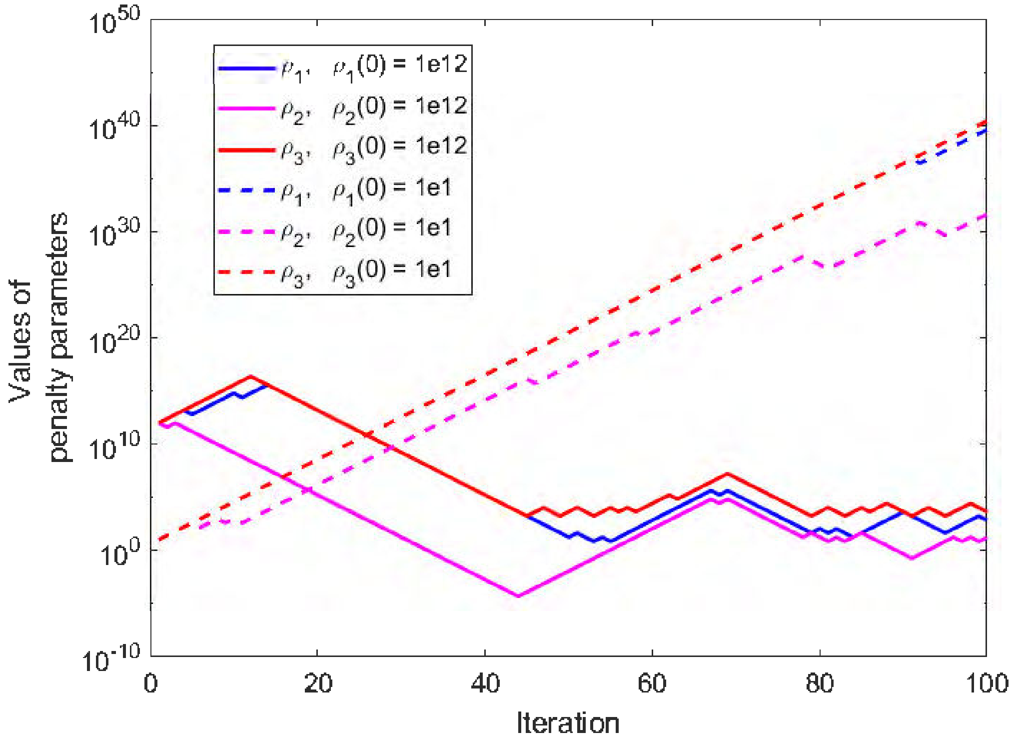

Figure 3.16: The changing values of the penalty parameters with iterations (using residual balancing method)

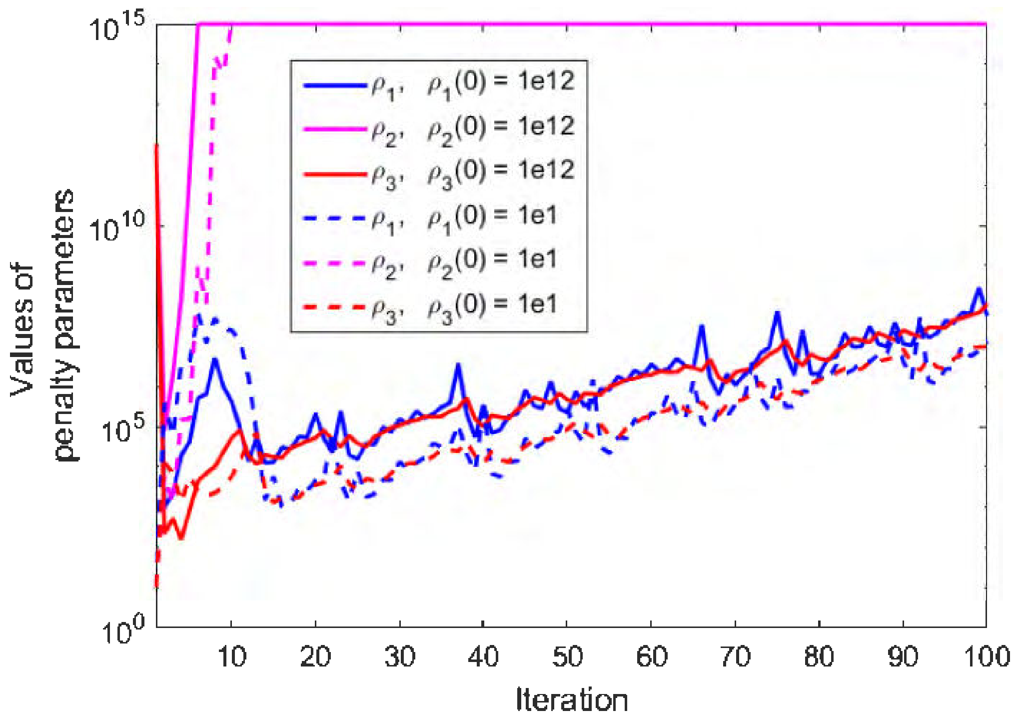

Figure 3.17: The changing values of the penalty parameters with iterations (using the proposed penalty parameters selection method)

shows the values of ρ_1, ρ_2, and ρ_3 over iterations when their respective initial values were 1e1 i.e. 10 each in one experiment and 1e12 in another experiment with the same setting. The trajectories of the parameters follow diverging paths in the two experiments. The same experiments were done using the proposed methods and Figure 3.17 shows the $\rho_i, i = 1,2,3$ with initial values 1e1 approach the values of $\rho_i, i = 1,2,3$ with initial values 1e12.

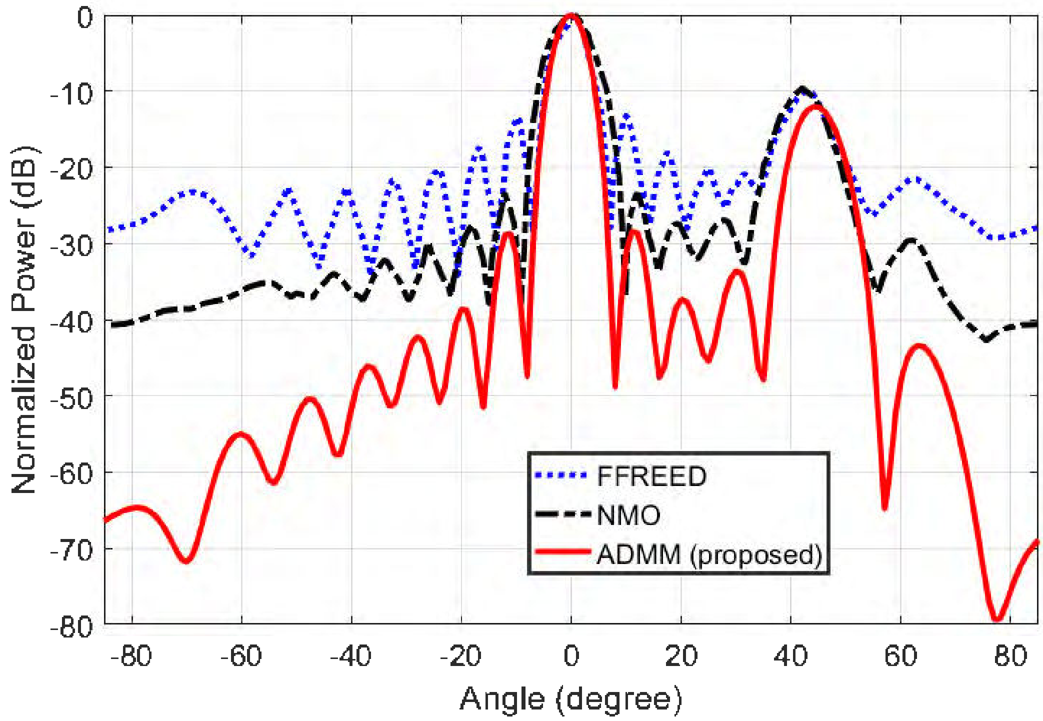

Figure 3.18: The transmit beampattern

3.2.5.4 Beampattern Analysis

Figure 3.18 shows the beampattern generated using $\mathbf{s}$ via the proposed ADMM technique for a 16-antenna DFRC system, compared with the Minimum Norm Optimization (MNO) method [87] and FFRED [85]. In all cases, the systems have 16 antenna elements, the radar target is located at $\theta_R = 0^\circ$ and the communication user at $\theta_C = 45^\circ$. Results show that the beampattern formed through the proposed method outperforms the beampatterns formed through MNO and

FFRED methods. The beampattern achieved through the proposed method has narrower main than the other methods. Also the beampattern achieved through the proposed method has lower sidelobes. When compared with each other, the beampattern of MNO method has better performance than FFRED method in terms of lower sidelobes but FFRED's beampattern has narrower beampattern. But both are outperformed in both cased by the proposed method.

3.2.5.5 Waveform Error Analysis

Figure 3.19 illustrates the fulfillment of the constant power constraint. The graphs show the power of the the designed waveform, $\mathbf{s}$, and its convergence towards the targeted power level throughout each iteration. It is discernible from these plots that the desired power level is effectively approximated for the designed waveform within the first ten iterations. This observation underscores the efficiency of the convergence process in meeting the prescribed constant power constraint.

3.2.5.6 Radar Performance Analysis

The evaluation of radar system performance is presented through two graphical representations. The first figure (Figure 3.20), makes a comparison between the required linear frequency modulation (LFM) waveform designed for radar applications and the synthesized waveform in the far-field. The other figure (Figure 3.21) illustrates the relationship between the detection probability (pD) and the SNR.

Figure 3.20 displays the waveform synthesized in the direction of the radar target. As depicted in Figure 3.20(a), a striking resemblance between the synthesized radar waveform and the required radar waveform is evident, substan-

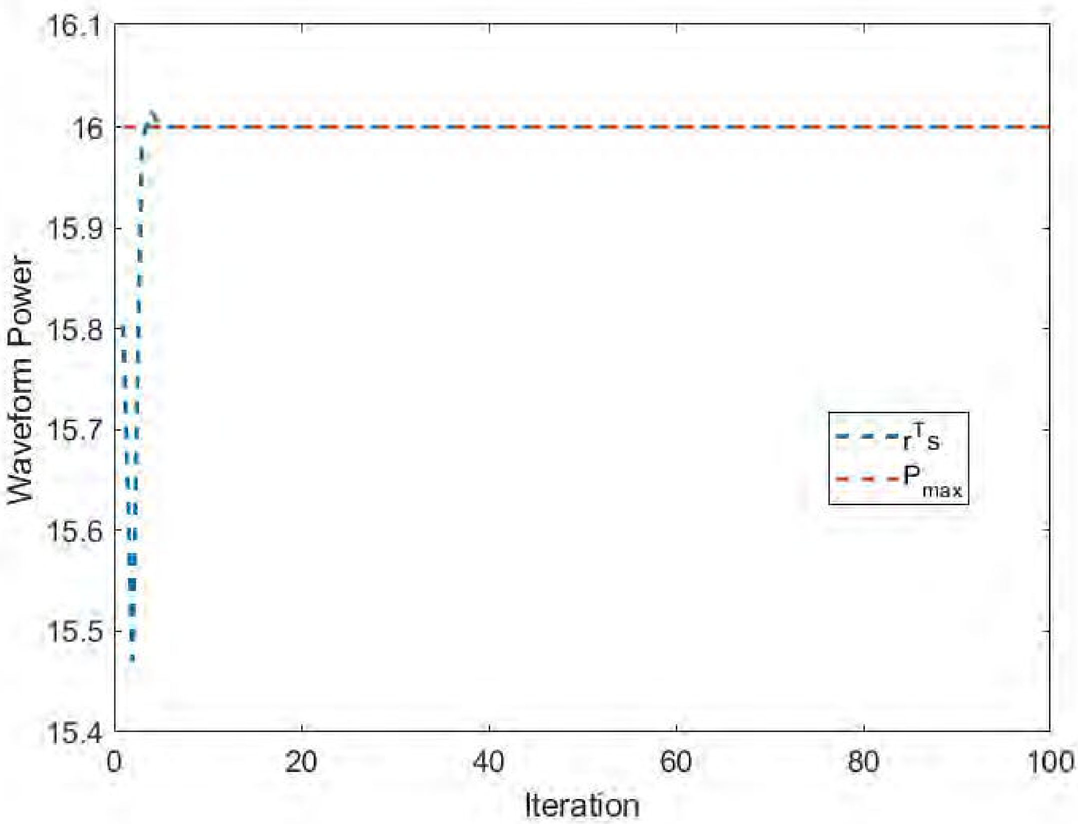

Figure 3.19: Waveform power per iteration depicting how the constant power requirement is met

tiating the efficacy of the proposed methodology. Nonetheless, Figure 3.20(b) exposes subtle disparities between the waveforms, given by the equation

$$\mathbf{e}_R = \mathbf{x}_R - \mathbf{A}(\theta_R)\mathbf{s}. \tag{3.78}$$

In Figure 3.21, a graph representing the detection probability in relation to the SNR is presented. The probability of a false alarm is set at a level of 10^{-4}. Additionally, comparative pD versus SNR curves for alternative methodologies are provided for reference. Notably, the FFRED-40% method [85], exhibits the most favorable pD, closely resembling that of the desired LFM waveform. However, upon closer examination, the proposed method's graph reveals a slight distinction. Simultaneously, it is noteworthy that the proposed

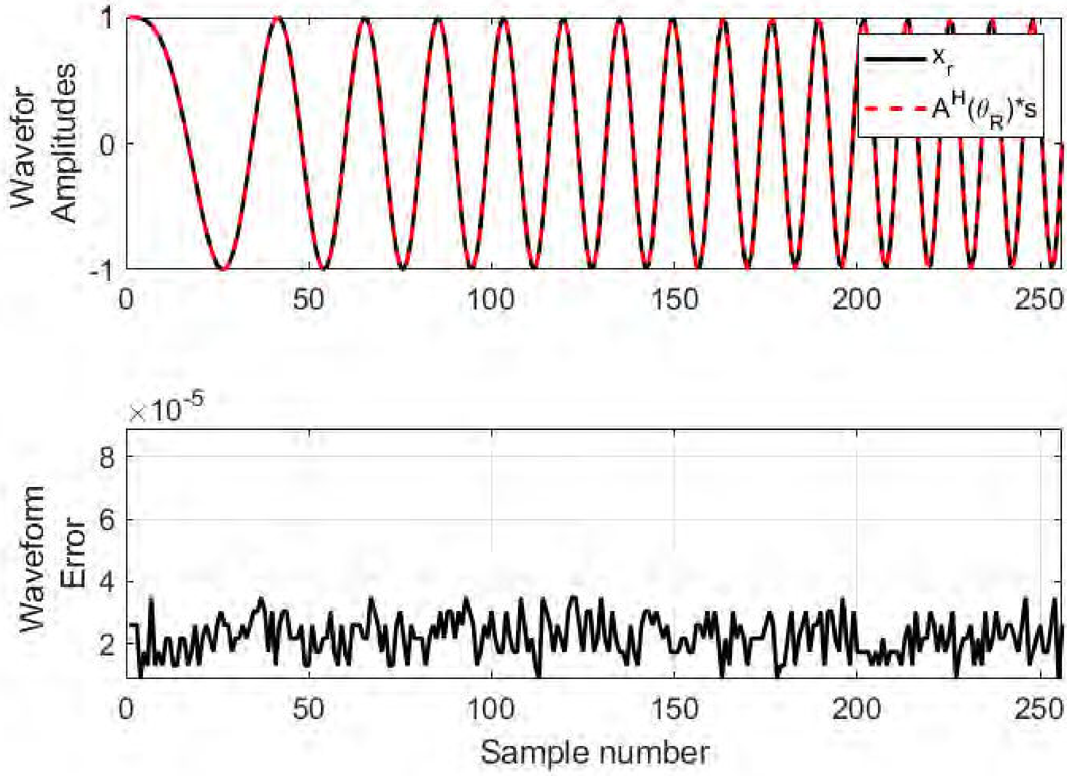

Figure 3.20: Radar waveform, (a) Desired radar waveform x_R vs synthesized far-field waveform $\mathbf{A}(\theta_R)\mathbf{s}$, (b) Waveform error

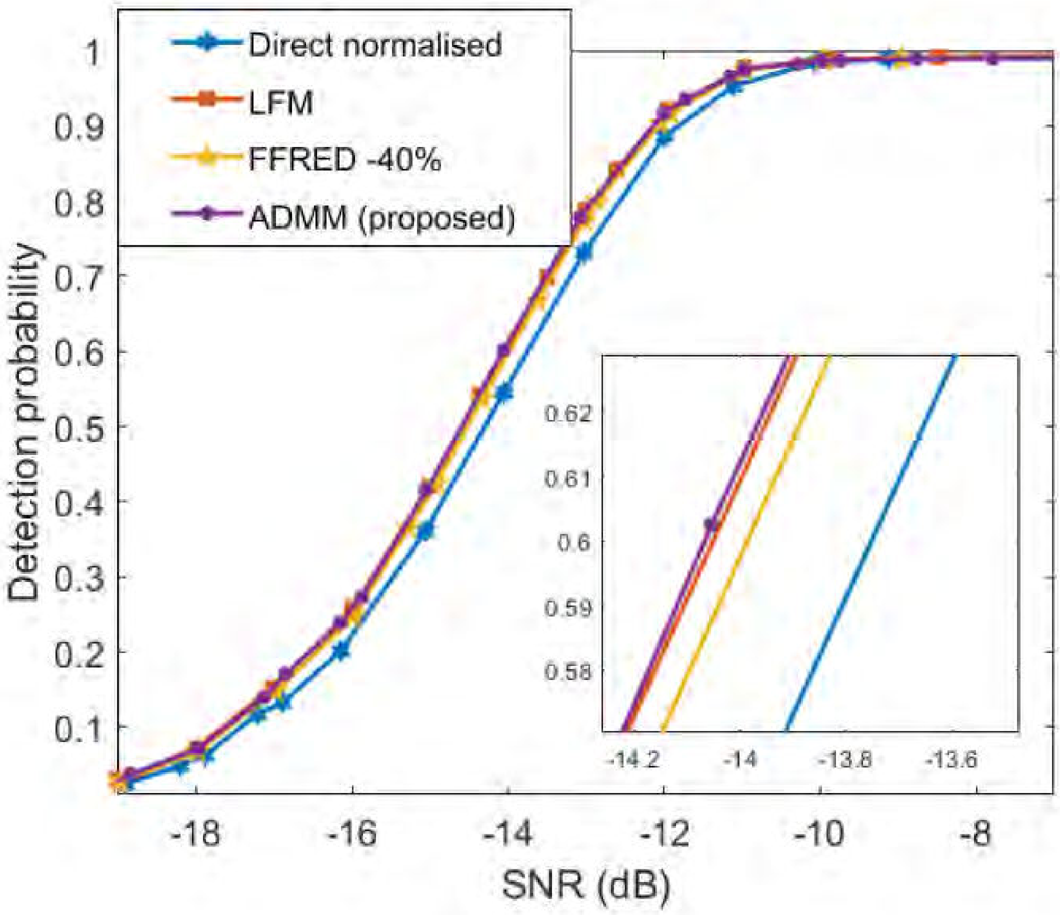

Figure 3.21: Detection probability vs SNR

approach outperforms the directly normalized method detailed in [86] in terms of pD.

3.2.5.7 Communication Performance Analysis

Similar to the assessment of radar system performance, the evaluation of communication system performance also involves two figures. One figure shows a comparison between the required communication waveform and the designed synthesized far-field waveform. While, the other figure assesses the symbol error rate (SER) in relation to the SNR.

Figure 3.22 illustrates the waveform transmitted in the direction θ_C. Analogous to radar waveforms, the resemblance between the synthesized and intended communication waveforms is striking. The sample errors in this context, as depicted in Figure 3.22(b), are characterized by the equation

$$\mathbf{e}_C = \mathbf{x}_C - \mathbf{A}(\theta_C)\mathbf{s}. \tag{3.79}$$

Figure 3.23 presents the SER against SNR for the proposed method. Furthermore, for the purpose of comparison, the SER vs SNR characteristics of alternative methodologies are also provided. Specifically, the graph labeled '2 bits per symbol' corresponds to theoretical values. Moreover, the SER versus SNR plots of FFRED-40% [85] and the proposed methodology exhibit a remarkable degree of proximity. However, FFRED-40% shows slightly superior performance. Both of these methodologies outperform the directly normalized waveform approach [86].

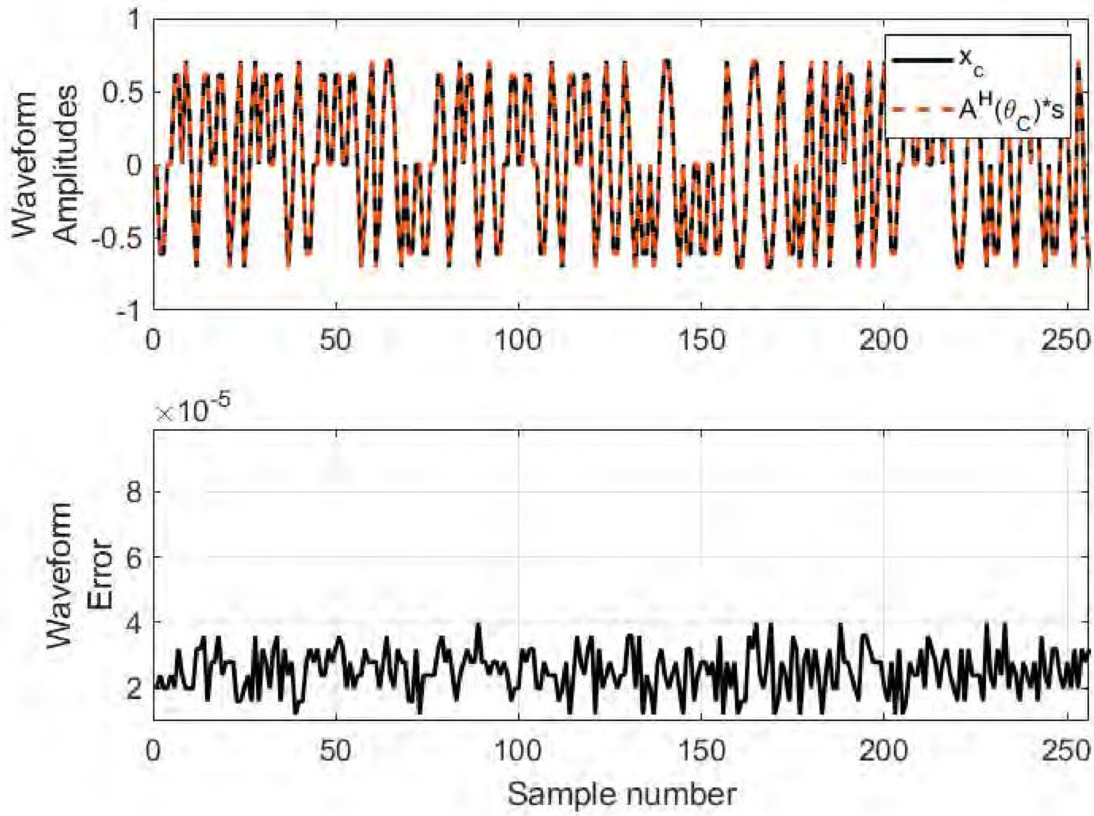

Figure 3.22: Communication waveform, (a) Desired communication waveform x_C vs synthesized far-field waveform $\mathbf{A}(\theta_C)\mathbf{s}$, (b) Waveform error

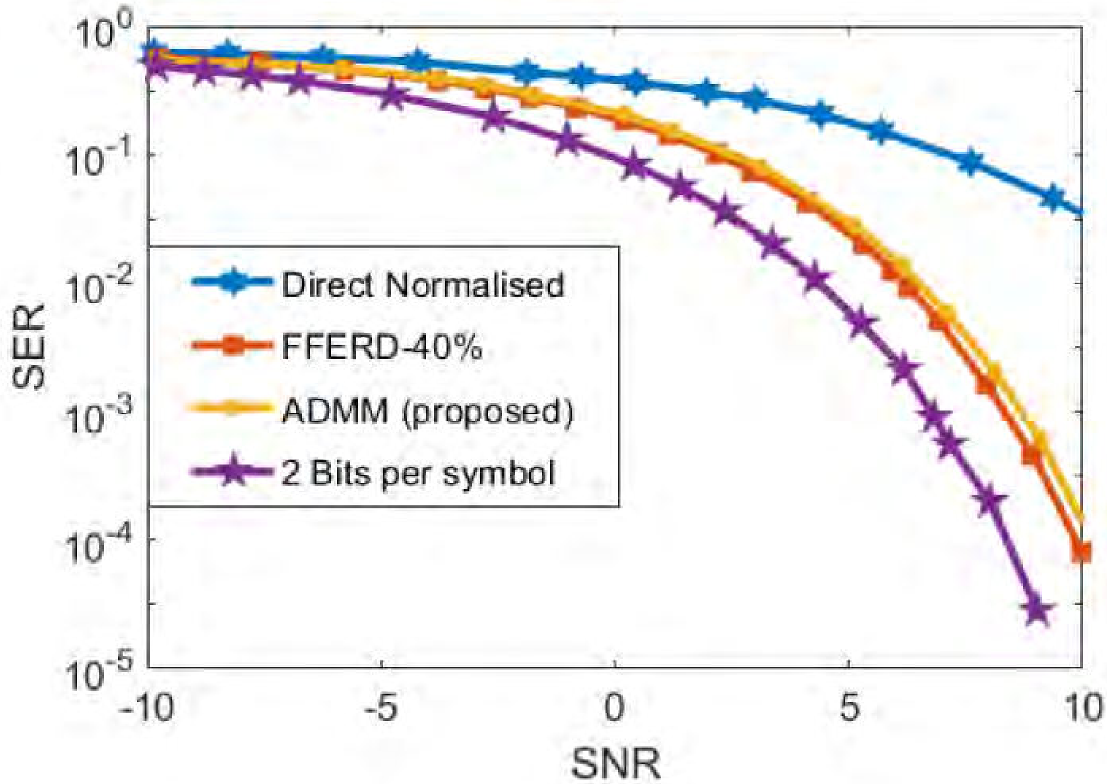

Figure 3.23: Comparison of different methods: SER vs SNR

3.3 Summary

This chapter addressed the waveform design problem for MIMO DFRC systems, proposing two methods. The first focused on designing constant modulus waveforms, formulated as an optimization problem with constraints on waveform synthesis and constant modulus. Due to the problem's non-convex and NP-hard nature, an iterative solution using the ADMM framework was developed. The resulting waveforms approximated a desired beampattern, achieving a high-gain radar beam and a slightly high-gain communication beam, with low sidelobe levels. This design improved radar detection probability and communication bit error rate (BER), as validated by simulations.

The second method tackled the challenge of designing constant power waveforms for joint radar-communication systems. The optimization problem minimized power radiation in undesired directions while maintaining waveform similarity and power constancy. An ADMM-based algorithm solved this, and a novel penalty parameter selection method was introduced. The designed waveforms effectively approximated the desired beampattern, ensuring both radar and communication waveforms were accurately received. Simulation results demonstrated the scheme's efficacy. This research advanced waveform design for dual-function radar-communication systems and provided robust methods to handle system complexities, contributing significantly to the field.

Chapter 4

ADMM based Beamspace Design for Dual-Function Radar-Communication

In this chapter, we consider the constant modulus beamspace design problem for MIMO based joint radar-communication systems and come with an efficient solution. First, we formulate the beamspace design problem as a non-convex optimization problem. Due to the non-convex and NP-hard nature of the problem caused by the constant modulus constraint, conventional methods are impractical for solving it. Hence, we employ the ADMM algorithm to tackle the problem iteratively. ADMM combines the principles of the augmented Lagrangian method (ALM) and dual decomposition, resulting in enhanced performance. The proposed method ensures enhanced detection probability for radar and better BER for the communications components. Finally, through simulation results, we demonstrate the effectiveness of our design in terms of different metrics like convergence and beampattern synthesis.

4.1 Joint Radar-Communication System Model

Traditional systems model utilize element-space for processing signals in array systems, where each antenna element's signal contribution is processed individually. However, the Beamspace represents an alternative approach element-space for processing signals in array systems. Processing in element-space leads to high computational complexity, especially in large antenna arrays. In contrast, beamspace processing exploits the spatial sparsity of signals by transforming them into a domain where signal energy is concentrated in a few dominant directions, known as beams. This transformation significantly reduces computational complexity, making beamspace processing particularly advantageous in scenarios with large antenna arrays or dense interference. By focusing on the dominant signal components, beamspace processing enables efficient extraction of relevant information while mitigating computational overhead, thus offering a powerful tool for enhancing the performance of array processing systems. In the following subsections, the conventional MIMO model based on element space for joint radar-communication is elucidated, followed by the introduction of the beamspace-based system model.

4.1.1 Element-space System Model

A MIMO system is considered consisting of M antennas, with a distance of $d = \lambda/2$ between the antenna elements, as shown in Figure (4.1). All the M antennas transmit M waveforms, given, for the mth antenna, by

$$s_m(t) = \sqrt{\frac{E}{M}}\phi_m(t), \quad m = 1, \cdots, M \tag{4.1}$$

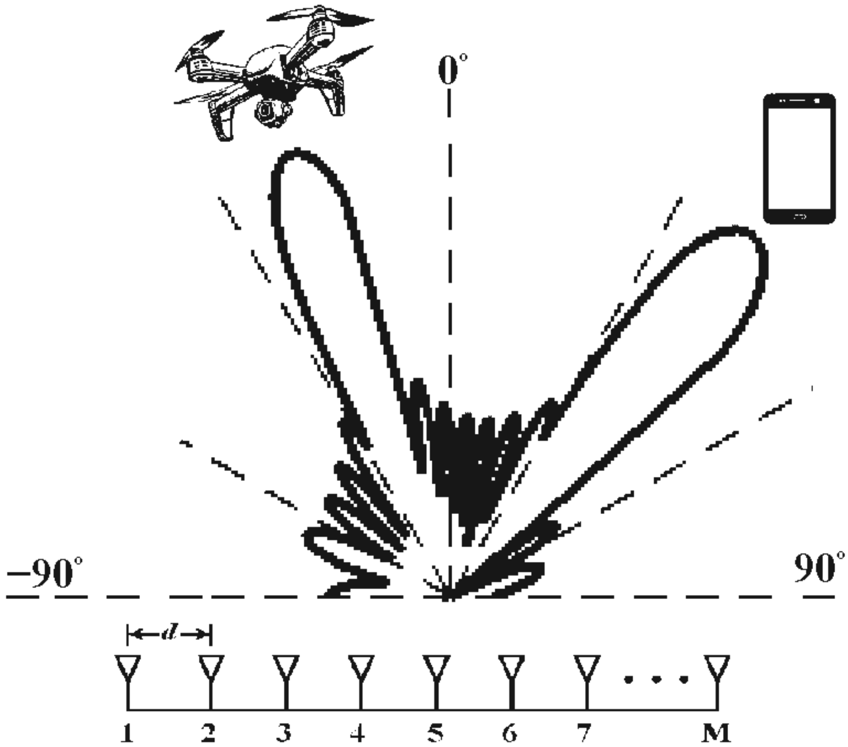

Figure 4.1: A representation of the joint radar-communication MIMO system

where E is transmit energy per pulse, $\phi_m(t)$ is mth transmit waveform, and t is fast time. All the waveform are considered to be orthogonal, i.e.,

$$\int_T |\phi_m(t)|^2 dt = 1, \qquad m = 1, \cdots, M \tag{4.2}$$

where T is the pulse duration. The signal transmitted by all antennas is, then, given by

$$s(t) = \sqrt{\frac{E}{M}} \sum_{m=1}^{M} \mathbf{a}^*(\theta)\phi_m(t), \quad m = 1, \cdots, M \tag{4.3}$$

or

$$s(t) = \sqrt{\frac{E}{M}} \mathbf{a}^H(\theta)\phi(t) \tag{4.4}$$

where $\phi(t) \triangleq [\phi_1(t), \cdots, \phi_M(t)]^T$ is the waveform vector. Some of these waveforms are for radar purposes and the rest for communication.

The signal at the receiver side, either radar or communication, can be expressed as

$$\mathbf{x}_m(t,\tau) = \sqrt{\frac{E}{M}}\left(\mathbf{a}^H(\theta)\phi_m(t)\right)\mathbf{b}^H(\theta) + \mathbf{z}(t,\tau) \tag{4.5}$$

where τ represents the slow time index, or equivalently, the pulse number. The radar and communication sides decode the received signal by match-filtering with their respective waveforms. Due to the mutual orthogonality of the waveforms, the undesired signals get cancelled and only the desired signal survives. This is expresses as

$$\mathbf{x}_m(\tau) \triangleq \int_T \mathbf{x}_m(t,\tau)\phi_m^*(t)dt, \quad m = 1,\ldots,M \tag{4.6}$$

Stacking the individual vectors, as obtained in Equation (4.6) together, an $MN \times 1$ is obtained as

$$\mathbf{y}(\tau) \triangleq \left[\mathbf{x}_1^T(\tau),\ldots,\mathbf{x}_M^T\right]^T \tag{4.7}$$

where N is the waveform length. While $\mathbf{y}(\tau)$ here is shown at a single receiver, but some of it is the radar side and some at communication sides.

4.1.2 Beamspace based System Model

Rather than transmitting omnidirectional, the energy transmission can be concentrated within a specific sector where the radar targets and communication users are situated. This is achieved by forming K directional beams, with each beam transmitting an independent waveform. A beamspace transformation matrix $\mathbf{W}$ can be designed as required to minimized the amount of energy transmitted within the sector(s) of interest and minimized the energy transmitted towards undesired directions. Let $W \triangleq [\mathbf{w}_1,\cdots,\mathbf{w}_K]^T$ be the beamspace transformation matrix, of dimension $M \times K$ where $K \leq M$. The kth column of $\mathbf{W}$ is used to form a transmit beam for transmitting the kth waveform $\phi_k(t)$. The signal transmitted towards a target/user in the direction θ through the kth beam can be expressed as

$$s_k(t,\theta) = \sqrt{\frac{E}{K}} \left(\mathbf{w}_k^H \mathbf{a}(\theta)\right) \phi_k(t), \qquad k = 1,\cdots,K \tag{4.8}$$

The signal transmitted via all beams towards the direction θ is expressed as

$$s_k(t,\theta) = \sqrt{\frac{E}{K}} \sum_{k=1}^{K} \left(\mathbf{w}_k^H \mathbf{a}(\theta)\right) \phi_k(t) = \sqrt{\frac{E}{K}} \left(\mathbf{W}^H \mathbf{a}(\theta)\right) \phi_k(t), \quad k = 1,\cdots,K \tag{4.9}$$

The beamspace transformation matrix changes the $M \times 1$ steering vector $\mathbf{a}(\theta)$ into a $K \times 1$ vector $\mathbf{W}^H \mathbf{a}(\theta)$. It can be observed that because of this transformation, the actual waveforms transmitted from the antennas are

$$\Psi^*(t) = \mathbf{W}^* \phi_K(t) \tag{4.10}$$

At the receiver side, the array observations can be expressed as a complex vector of size $N \times 1$as

$$\mathbf{x}_{beam}(t,\tau) = \sqrt{\frac{E}{K}} \sum_{l=1}^{L} \alpha_l(\tau) \left(\left(\mathbf{W}^H \mathbf{a}(\theta)\right)^T \phi_K(t) \right) \times \mathbf{b}(\theta_l) + \mathbf{z}(t,\tau) \tag{4.11}$$

By matched-filtering $\mathbf{x}_{beam}(t,\tau)$ to each of the waveforms, the received signal component associated with each waveform can be obtained as

$$\mathbf{x}_{m,beam}(\tau) \triangleq \int_T \mathbf{x}_{beam}(t,\tau) \phi_m^*(t) dt, \quad m = 1,\ldots,M \tag{4.12}$$

By stacking the individual vector components into a single vector, a virtual data vector of size $KN \times 1$, is obtained, represented as

$$\mathbf{y}_{beam}(\tau) \triangleq \left[\mathbf{x}_{1,beam}^T(\tau),\ldots,\mathbf{x}_{M,beam}^T\right]^T \tag{4.13}$$

4.2 Beamspace Design Problem Formulation

The problem at hand is to design a beamspace matrix $\mathbf{W}$ with the objective of minimizing power radiation in undesired directions, while satisfying certain constraints. Two such constraints are to ensure that the power radiation in the radar and communication directions aligns with desired specifications. An additional constraint is the constant modulus constraint to inhibit non-linear signal distortion, thereby enhancing the transmitter's efficiency.

Two of the constraints are given as

$$\mathbf{w}^T \mathbf{a}_r \mathbf{a}_r^T \mathbf{w} = 1 \tag{4.14}$$

and

$$\mathbf{w}^T \mathbf{a}_c \mathbf{a}_c^T \mathbf{w} = 1, \tag{4.15}$$

where $\mathbf{w}$ is vector that stacks the different columns of the beamspace matrix $\mathbf{W}$. Without loss of generality, we consider that there are two vectors in $\mathbf{W}$, *i.e.* $\mathbf{w}_r$ and $\mathbf{w}_c$ representing a radar and a communication beam. Then

$$\mathbf{w} = \begin{bmatrix} \mathbf{w}_r \\ \mathbf{w}_c \end{bmatrix} \tag{4.16}$$

Similarly, $\mathbf{a}_r$ and $\mathbf{a}_c$ are given by

$$\mathbf{a}_r = \begin{bmatrix} \mathbf{a}(\theta_R) \\ \mathbf{0} \end{bmatrix}, \tag{4.17}$$

and

$$\mathbf{a}_c = \begin{bmatrix} \mathbf{0} \\ \mathbf{a}(\theta_C) \end{bmatrix} \tag{4.18}$$

respectively, where $\mathbf{0}$ is an $M \times 1$ vector of zeros, and $\mathbf{a}(\theta_C)$ and $\mathbf{a}(\theta_C)$ are the $M \times 1$ steering vectors in the radar and communication directions. The constant modulus (or, in this case, uni-modular) constraint is expressed as

$$|\mathbf{w}(m,1)| = 1,0 \qquad 1 \leq m \leq 2M. \tag{4.19}$$

The the overall beamspace design problem can be formulated as

$$\begin{aligned}
&\underset{\mathbf{w}}{\text{minimize}} && \mathbf{w}^T \mathbf{A}(\widetilde{\Theta}) \mathbf{A}^T(\widetilde{\Theta}) \mathbf{w} \\
&\text{subject to} && \mathbf{w}^T \mathbf{a}_r \mathbf{a}_r^T \mathbf{w} = 1 \\
&\& && \mathbf{w}^T \mathbf{a}_c \mathbf{a}_c^T \mathbf{w} = 1 \\
&\& && |\mathbf{w}(m,1)| = 1, \quad 1 \leq m \leq 2M.
\end{aligned} \tag{4.20}$$

where the $2M \times L$ matrix $\mathbf{A}(\widetilde{\Theta})$ collects the steering vectors in L undesired locations, given by

$$\mathbf{A}(\widetilde{\Theta}) = \begin{bmatrix} \mathbf{a}(\theta_1) & \mathbf{a}(\theta_2) & \dots & \mathbf{a}(\theta_L) \\ \mathbf{a}(\theta_1) & \mathbf{a}(\theta_2) & \dots & \mathbf{a}(\theta_L) \end{bmatrix}. \tag{4.21}$$

For the ease of computation, especially in dealing with the constant modulus constraint, it is better to convert the all the variables in the formulated problem to their real-valued versions.

4.2.1 Conversion to real-valued variables

To convert a complex-valued vector its real-valued version, its real and complex parts are stacked together in another vector that is double in size compared to the original vector. Thus, real-valued versions of the vector variables $\mathbf{w}$, $\mathbf{a}_r$, and $\mathbf{a}_c$ are given as

$$\mathbf{u} = \begin{bmatrix} \Re\{\mathbf{w}\} \\ \Im\{\mathbf{w}\} \end{bmatrix}, \tag{4.22}$$

$$\mathbf{a}_R = \begin{bmatrix} \Re\{\mathbf{a}_r\} \\ \Im\{\mathbf{a}_r\} \end{bmatrix}, \tag{4.23}$$

and

$$\mathbf{a}_C = \begin{bmatrix} \Re\{\mathbf{a}_c\} \\ \Im\{\mathbf{a}_c\} \end{bmatrix}. \tag{4.24}$$

Similarly, the real-valued version of $\mathbf{A}(\tilde{\Theta})$ is given by

$$\mathbf{A} = \begin{bmatrix} \Re\{\mathbf{A}(\widetilde{\Theta})\} & -\Im\{\mathbf{A}(\widetilde{\Theta})\} \\ \Im\{\mathbf{A}(\widetilde{\Theta})\} & \Re\{\mathbf{A}(\widetilde{\Theta})\} \end{bmatrix}. \tag{4.25}$$

In terms of the real-valued variables the CM constraint, consisting of $2M$ equations in Eq. (4.19), is expressed as

$$\mathbf{u}^T \mathbf{E}_i \mathbf{u} = 1, \quad i = 1, 2, \cdots, 4M \tag{4.26}$$

where $\mathbf{E}_i$ is a $4M \times 4M$ matrix given by

$$\mathbf{E}_i(m,m) = \begin{cases} 1 & ;\ m = i \\ 1 & ;\ m = i + 2M \\ 0 & ;\ otherwise \end{cases} \tag{4.27}$$

The Equation (4.26) can be expressed more compactly as

$$\mathbf{T}(\mathbf{u})\mathbf{u} = \mathbf{1} \tag{4.28}$$

where

$$\mathbf{T}(\mathbf{u}) = \left[\mathbf{u}^T\mathbf{E}_1; \mathbf{u}^T\mathbf{E}_2; \cdots; \mathbf{u}^T\mathbf{E}_{2M}\right] \in \mathbb{R}.^{2M\times 4M} \tag{4.29}$$

The overall beamspace design problem can then be formulated as

$$\begin{aligned}
&\underset{\mathbf{u}}{\text{minimize}} && \mathbf{u}^T\mathbf{A}\mathbf{A}^T\mathbf{u} \\
&\text{subject to} && \mathbf{u}^T\mathbf{a}_R\mathbf{a}_R^T\mathbf{u} = 1 \\
&\& && \mathbf{u}^T\mathbf{a}_C\mathbf{a}_C^T\mathbf{u} = 1 \\
&\& && \mathbf{T}(\mathbf{u})\mathbf{u} = \mathbf{1}
\end{aligned} \tag{4.30}$$

This non-convex optimization problem can be solved to obtain u, which gives the beamspace transformation matrix. While conventional convex optimization techniques fail to solve such problems, different non-conventional methods, especially iterative methods like ADMM, can be used to obtain a solution. An ADMM based formulation of the problem is presented in the following section.

4.3 ADMM based Beamspace Design

The optimization problem described in Equation (4.30) shares similarities with Eq. (4.20), being non-convex and NP-hard. Obtaining analytical solutions for such problems poses significant challenges, leading to the adoption of numerical methods to approximate solutions. Even with these and other heuristic approaches like genetic algorithms (GA), formulating the constant modulus (CM) constraint can be problematic. Hence, we utilize an ADMM-based method, which is iterative in nature, to approximate a solution to the problem.

As a requirement for ADMM, a variable $\mathbf{v}$ can be introduced in Equation

(4.30), leading to the following equivalent version

$$
\begin{aligned}
&\underset{\mathbf{v},\mathbf{u}}{\text{minimize}} && \mathbf{v}^T\mathbf{A}\mathbf{A}^T\mathbf{u} \\
&\text{subject to} && \mathbf{v}^T\mathbf{a}_R\mathbf{a}_R^T\mathbf{u} = 1 \\
&\& && \mathbf{v}^T\mathbf{a}_C\mathbf{a}_C^T\mathbf{u} = 1 \\
&\& && \mathbf{T}(\mathbf{v})\mathbf{u} = \mathbf{1} \\
&\& && \mathbf{v} = \mathbf{u}
\end{aligned}
\tag{4.31}
$$

The augmented Lagrangian corresponding Equation (4.31) can be expressed as

$$
\begin{aligned}
\mathscr{L}\{\mathbf{v},\mathbf{u},\alpha,\beta,\gamma,\delta\} \;=\;& \mathbf{v}^T\mathbf{A}\mathbf{A}^T\mathbf{u} \\
+\;& \tfrac{\rho_1}{2}\left\|\mathbf{v}^T\mathbf{a}_R\mathbf{a}_R^T\mathbf{u} - 1 + \alpha\right\|_2^2 \\
+\;& \tfrac{\rho_2}{2}\left\|\mathbf{v}^T\mathbf{a}_C\mathbf{a}_C^T\mathbf{u} - 1 + \beta\right\|_2^2 \\
+\;& \tfrac{\rho_3}{2}\left\|\mathbf{T}(\mathbf{v})\mathbf{u} - \mathbf{1} + \gamma\right\|_2^2 \\
+\;& \tfrac{\rho_3}{2}\left\|\mathbf{v} - \mathbf{u} + \delta\right\|_2^2
\end{aligned}
\tag{4.32}
$$

where $\alpha \in \mathbb{R}^{1\times 1}, \beta \in \mathbb{R}^{1\times 1}$, $\gamma \in \mathbb{R}^{2M\times 1}$ and $\delta \in \mathbb{R}^{4M\times 1}$ are the dual variables and $\rho_1,\rho_2,\rho_3,\rho_4 > 0$ are the penalty parameters.

The algorithm's $(m+1)$th iteration is expressed as follows

$$\mathbf{u}^{m+1} := \arg\min_{\mathbf{u}} \mathscr{L}\left(\mathbf{u},\mathbf{v}^m,\alpha^m,\beta^m,\gamma^m,\delta^m\right) \tag{4.33a}$$

$$\mathbf{v}^{m+1} := \arg\min_{\mathbf{v}} \mathscr{L}\left(\mathbf{u}^{m+1},\mathbf{v},\alpha^m,\beta^m,\gamma^m,\delta^m\right) \tag{4.33b}$$

$$\alpha^{m+1} := \mathbf{v}^{m+1,T}\mathbf{a}_R\mathbf{a}_R^T\mathbf{u}^{m+1} - 1 + \alpha^m \tag{4.33c}$$

$$\beta^{m+1} := \mathbf{v}^{m+1,T}\mathbf{a}_C\mathbf{a}_C^T\mathbf{u}^{m+1} - 1 + \beta^m \tag{4.33d}$$

$$\gamma^{m+1} = \mathbf{T}(\mathbf{v}^{m+1})\mathbf{u}^{m+1} - \mathbf{1} + \gamma^m \tag{4.33e}$$

$$\delta^{m+1} = \mathbf{v}^{m+1} - \mathbf{u}^{m+1} + \delta^m \tag{4.33f}$$

As evident from Equation (4.33), the updates outlined in Equations (4.33c), (4.33d), (4.33e), and (4.33f) are straightforward. Moreover, the sub-equations (4.33a) and (4.33b), being convex, yield closed-form solutions. The forthcoming section elaborates on the update procedures for variables **v** and **w**.

4.3.1 Update of u

To obtain the $(m+1)$th update of **u**, the gradient of subequation (4.33a) with respect to **u** is computed and equate the result with 0, *i.e.*,

$$\nabla_{\mathbf{u}}\mathscr{L}(\mathbf{u},\mathbf{v}^m,\alpha^m,\beta^m,\gamma^m,\delta^m)=\mathbf{0}. \tag{4.34}$$

The solution to Eq. (4.34) is given by

$$\mathbf{u}^{m+1}=\Xi_1^{-1}\xi_1 \tag{4.35}$$

where

$$\Xi_1=\rho_1\mathbf{a}_R\mathbf{a}_R^T\mathbf{v}\mathbf{v}^T\mathbf{a}_R\mathbf{a}_R^T+\rho_2\mathbf{a}_C\mathbf{a}_C^T\mathbf{v}\mathbf{v}^T\mathbf{a}_C\mathbf{a}_C^T+\rho_3\mathbf{T}^T(\mathbf{v})\mathbf{T}(\mathbf{v})-\rho_4\mathbf{I} \tag{4.36}$$

and

$$\begin{aligned}\xi_1=\;&\rho_1(1-\alpha)\mathbf{a}_R\mathbf{a}_R^T\mathbf{v}\\&+\rho_2(1-\beta)\mathbf{a}_C\mathbf{a}_C^T\mathbf{v}\\&+\rho_3\mathbf{T}^T(\mathbf{v})(\mathbf{1}-\gamma)\\&+\rho_4(\mathbf{v}-\delta)\\&-\mathbf{A}\mathbf{A}^T\mathbf{v}.\end{aligned} \tag{4.37}$$

4.3.2 Update of $\mathbf{v}$

Similarly, in $\mathbf{v}$ update, the gradient of (4.33b) with respect to $\mathbf{v}$ is computed and the result is equated with 0, *i.e.*,

$$\nabla_{\mathbf{v}}\mathscr{L}\left(\mathbf{u}^{m+1},\mathbf{v},\alpha^m,\beta^m,\gamma^m,\delta^m\right)=\mathbf{0}. \tag{4.38}$$

The solution to Eq. (4.38) is given by

$$\mathbf{v}^{m+1}=\Xi_2^{-1}\xi_2 \tag{4.39}$$

where

$$\Xi_1=\rho_2\mathbf{a}_R\mathbf{a}_R^T\mathbf{u}\mathbf{u}^T\mathbf{a}_R\mathbf{a}_R^T+\rho_2\mathbf{a}_C\mathbf{a}_C^T\mathbf{u}\mathbf{u}^T\mathbf{a}_C\mathbf{a}_C^T+\rho_3\mathbf{T}^T(\mathbf{u})\mathbf{T}(\mathbf{u})+\rho_4\mathbf{I} \tag{4.40}$$

and

$$\begin{aligned}\xi_2=&\,\rho_1(1-\alpha)\mathbf{a}_R\mathbf{a}_R^T\mathbf{u}\\&+\rho_2(1-\beta)\mathbf{a}_C\mathbf{a}_C^T\mathbf{u}\\&+\rho_3\mathbf{T}^T(\mathbf{u})\left(\mathbf{1}-\gamma\right)\\&+\rho_4(\mathbf{u}+\delta)\\&-\mathbf{A}\mathbf{A}^T\mathbf{u}.\end{aligned} \tag{4.41}$$

To summarize, the vectors $\mathbf{u}$ and $\mathbf{v}$ are derived using Equations (4.34) and (4.38), respectively. Following a specific number of iterations, both $\mathbf{u}$ and $\mathbf{v}$ gradually converge. Consequently, they collectively represent the real version of the beamspace vector $\mathbf{w}$. Subsequently, the beamspace matrix $\mathbf{W}$ is obtained through a straightforward process of converting from real to complex, followed by a conversion from vector to matrix.

4.3.3 Algorithm Termination Criteria

The termination criteria determine when the algorithm should stop its execution. These criteria ensure that the algorithm completes its task efficiently and correctly. The stopping criteria in this algorithm depend on the primal and dual residuals. The primal residuals can be defined as

$$d_{pr1}^{m+1} = \left|\mathbf{u}^T \mathbf{a}_R \mathbf{a}_R^T \mathbf{v} - 1\right| \tag{4.42a}$$

$$d_{pr2}^{m+1} = \left|\mathbf{u}^T \mathbf{a}_C \mathbf{a}_C^T \mathbf{v} - 1\right| \tag{4.42b}$$

$$d_{pr3}^{m+1} = \|\mathbf{T}(\mathbf{u})\mathbf{v} - \mathbf{1}\|_2^2 \tag{4.42c}$$

$$d_{pr4}^{m+1} = \left\|\mathbf{u}^{m+1} - \mathbf{v}^{m+1}\right\|_2^2 \tag{4.42d}$$

Similarly, the dual residuals are be defined as

$$d_{rs1}^{m+1} = \mathbf{u}^{m+1} - \mathbf{u}^m \tag{4.43a}$$

$$d_{rs2}^{m+1} = \mathbf{v}^{m+1} - \mathbf{v}^m. \tag{4.43b}$$

As proposed by [84], suitable termination criteria include

$$\| d_{pr1}^{m+1} \|_2^2 \leq \varepsilon_1^{pri}, \tag{4.44a}$$

$$\| d_{pr2}^{m+1} \|_2^2 \leq \varepsilon_2^{pri}, \tag{4.44b}$$

$$\| d_{pr3}^{m+1} \|_2^2 \leq \varepsilon_3^{pri}, \tag{4.44c}$$

$$\| d_{pr4}^{m+1} \|_2^2 \leq \varepsilon_4^{pri}, \tag{4.44d}$$

$$\| d_{dr1}^{m+1} \|_2^2 \leq \varepsilon^{dual}, \tag{4.44e}$$

$$\| d_{dr2}^{m+1} \|_2^2 \leq \varepsilon^{dual}. \tag{4.44f}$$

where ε_1^{pri}, ε_2^{pri}, ε_3^{pri} and ε_4^{pri} are the primal residual's tolerances and ε_1^{dual}, the dual residual's tolerance. As described by [84], these tolerances are specified as

$$\varepsilon_1^{pri} = \sqrt{4M}\varepsilon^{abs} + \varepsilon^{rel}\max\{\left|\mathbf{u}^T\mathbf{a}_R\mathbf{a}_R^T\mathbf{v}\right|, 1\} \tag{4.45a}$$

$$\varepsilon_2^{pri} = \sqrt{4M}\varepsilon^{abs} + \varepsilon^{rel}\max\{\left|\mathbf{u}^T\mathbf{a}_C\mathbf{a}_C^T\mathbf{v}\right|, 1\} \tag{4.45b}$$

$$\varepsilon_3^{pri} = \sqrt{4M}\varepsilon^{abs} + \varepsilon^{rel}\max\left\{\| \mathbf{T}(\mathbf{u}^{m+1})\mathbf{v}^{m+1} \|_2, \| \mathbf{1} \|_2\right\} \tag{4.45c}$$

$$\varepsilon_4^{pri} = \sqrt{4M}\varepsilon^{abs} + \varepsilon^{rel}\max\left\{\| \mathbf{u}^{m+1} \|_2, \| \mathbf{v}^{m+1} \|_2\right\} \tag{4.45d}$$

$$\varepsilon^{dual} = \sqrt{4M}\varepsilon^{abs} + \varepsilon^{rel} \| \mathbf{u} \|_2 \tag{4.45e}$$

Provided following is a summary of the steps of the algorithm.

Steps of the proposed method
Input:
Step 1) **Initialize:** $\mathbf{u}^0$, $\mathbf{v}^0$, α^0, β^0, γ^0, δ, ρ_1, ρ_2, ρ_3, ρ_4 and ε_1^{pri}, ε_2^{pri}, ε_3^{pri}, ε_4^{pri}, ε^{dual}, $m = 1$.
Step 2) **While** the termination criteria, Eq. 4.44, are not satisfied, do
Step 3) Update $\mathbf{u}^{m+1}$, with 4.35
Step 4) Update $\mathbf{v}^{m+1}$, with 4.39
Step 5) Update α^{m+1} , with 4.33c
Step 6) Update β^{m+1} , with 4.33d
Step 7) Update γ^{m+1} , with 4.33e
Step 8) Update δ^{m+1} , with 4.33f
Step 8) $m = m + 1$
Step 9) **End while - WORD HERE NEEDED**

For clarity, Table 4.1 presents a list of symbols along with their descriptions.

Symbol	Dimension	Description
K	1×1	number of beams
L	1×1	number of side lobes
M	1×1	number of antennas
N	1×1	number of waveform samples
d	1×1	antenna inter-element spacing
$\mathbf{I}_N$	$N\times N$	identity matrix
λ	1×1	wavelength
$s_m(t)$	1×1	signal transmitted by m-th antenna at time instant t
t	1×1	fast time, *i.e.* time within each transmit pulse
τ	1×1	slow time, *i.e.* pulse number
T	1×1	pulse duration
$\mathbf{s}(t)$	$M\times1$	overall signal transmitted by all antennas at time instant t
$\mathbf{W}$	$M\times K$	beamspace transformation matrix
$\mathbf{w}$	$MK\times1$	beamspace vector, $\mathbf{w}$ = vec($\mathbf{W}$a)
$\mathbf{u}$	$2MK\times1$	real-valued version of $\mathbf{w}$
$\mathbf{v}$	$2MK\times1$	auxiliary variable, $s.t.$ $\mathbf{u}=\mathbf{v}$
$\phi_m(t)$	1×1	m-th waveform at time t
$\mathbf{a}(\theta_R)$	$M\times1$	steering vector in radar direction
$\mathbf{a}(\theta_C)$	$M\times1$	steering vector in communication direction
$\mathbf{A}\left(\widetilde{\Theta}\right)$	$2M\times L$	combination of the L side lobe steering vectors
$\mathbf{A}$	$4M\times2L$	real-valued version of $\mathbf{A}\left(\widetilde{\Theta}\right)$
α	1×1	dual variable
β	1×1	dual variable
γ	$2M\times1$	dual variable
δ	$4M\times1$	dual variable
η, μ	1×1	positive constants
ρ_1, ρ_2, ρ_3 , ρ_4	1×1	penalty parameters

Table 4.1: List of symbols

4.3.4 Penalty Parameter Selection

Selecting appropriate penalty parameters holds significant importance in the smooth functioning of algorithms like ADMM. These parameters can be dynamically adjusted, either decreasing or increasing, based on some predefined tolerances. Various strategies, such as trial-and-error approaches, are employed for this purpose. Another approach involves linking the penalty parameter values to iteration counts, incrementing or decrementing them in discrete steps from their initial values. A commonly adopted technique involves associating the penalty parameter values with residual norms and tolerances through the principle of residual balancing as

$$\rho_{k+1} = \begin{cases} \eta \rho_k & \text{if} \quad d_{pr_k}^{m+1} > \mu \varepsilon_k^{pri} \\ \rho_k / \eta & \text{if} \quad \varepsilon_k^{pri} > \mu d_{pr_k}^{m+1} \\ \rho_k & otherwise \end{cases} \tag{4.46}$$

where ρ_k is the penalty parameter, and $\mu > 1$ and $\eta > 1$ are constants, $d_{pr_k}^{m+1}$ is the primary residual and ε_1^{pri} is the tolerance.

4.4 Results and Discussion

This section examines the algorithm's performance and presents the results of numerical examples to assess the effectiveness of the proposed waveform design methodology. Across all examples, a Uniform Linear Array (ULA) comprising either $M = 16$ or $M = 32$ antenna elements, each separated by a half-wavelength inter-element spacing, is utilized at both the transmitter and receiver ends. The radar target is assumed to be located at $\theta_R = 0°$, while the communication user is positioned at $\theta_C = 45°$. Within this context, each transmit beam is tailored to convey $N_s = 1$ symbol, with $N_b = 2$ bits assigned per symbol. Consequently, each waveform transmits 2 information bits in every pulse repetition interval (PRI). Additional simulation parameters are summarized in Table 4.2.

Various experiments are conducted to analyze performance across diverse scenarios. Monte Carlo simulations are performed to evaluate communication performance across different signal-to-noise ratio (SNR) conditions. The suggested methodology is contrasted with several existing approaches, including the far-field radiated emission design (FFRED) [85], and an iterative optimiza-

Table 4.2: A tabulation of the simulation parameters used in the algorithm

Parameter	Value	Description
M	16	Number of antennas elements in the ULA
d	$\lambda/2$	Enter-elements distance in the ULA
θ_R	$0°$	Direction of radar target
θ_C	$45°$	Direction of communication user
α	Random	Dual variable associated with ρ_1
β	Random	Dual variable associated with ρ_2
γ	Random	Dual variable associated with ρ_4
δ	Random	Dual variable associated with ρ_4
η	1.5	Positive constant 1
μ	1.5	Positive constant 2
ρ_1	1, $1e^{12}$	Penalty parameter 1
ρ_2	1, $1e^{12}$	Penalty parameter 2
ρ_3	1, $1e^{12}$	Penalty parameter 3
ρ_4	1, $1e^{12}$	Penalty parameter 4

tion technique utilizing directly normalized waveforms [86]. In the FFRED approach, 0%, 10%, and 40% of the total power are allocated to the orthogonal complement waveform, with FFRED-40% demonstrating superior performance. Authors of [86] introduced several waveform design methodologies. One method involved designing non-constant modulus waveforms with a closed-form solution to the waveform design problem. Additionally, they proposed an iterative approach for constant modulus waveforms. However, due to computational complexity, they leveraged the outcomes of the first method employing non-constant modulus waveforms and employed iterative optimization for further waveform refinement. The authors referred to this approach as "directly normalized".

4.4.1 Computational Complexity Analysis

The analysis of computational complexity gauges the computational resources, like time and memory, and is necessary for assessing the efficacy of any algorithm. This examination provides insights into behavior of the algorithm across varying input sizes. In evaluating the computational complexity of the proposed method, every segment of the code underwent scrutiny to ascertain the count of operations or iterations relative to the input size. The primary loop within the code executed 'iter' times, wherein numerous calculations and operations transpired during each iteration, inclusive of matrix multiplications, norm computations, and variable updates. The complexity associated with these operations underwent meticulous analysis and amalgamation to deduce an overarching complexity estimate for the code. Furthermore, considerations were extended to factors influenced by the input size, such as M and L, to evaluate their impact on complexity. It is important to note that the proposed algorithm has significant computational complexity. This is mainly due to its cubic nature, with the matrix inversion operation being the primary contributor. After matrix inversion, matrix multiplication also requires considerable time, adding to the overall computational burden.

Regarding the updates for vector $\mathbf{u}$, computing Ξ_1 requires $O(KM^2N^2)$, while computing γ requires $O(M^2N^2)$. Consequently, the complexity of updating $\mathbf{u}$ using Equation (4.35) amounts to $O(KM^2N^2 + M^2N^2 + M^3N^3)$. Summing these complexities, the overall complexity of the method is $O(2(KM^2N^2 + M^2N^2 + M^3N^3))$ per iteration.

Regarding $\mathbf{u}$ updates, the calculation of Ξ_1 takes $O(KM^2N^2)$, while computation of γ takes $O(M^2N^2)$. Consequently the complexity of $\mathbf{u}$ update using Eq (4.35) is $O(KM^2N^2 + M^2N^2 + M^3N^3)$. The overall computational complexity of the algorithm is $O(2(KM^2N^2 + M^2N^2 + M^3N^3))$.

4.4.2 Communication Data Rate Performance

The data rate can be expressed as

$$R = N_s \times N_b \times K_b \times f_{PRF}, \tag{4.47}$$

where N_s is the number of symbols in one pulse, N_{bits} is the number of bits per symbol, K_b is the number of communication beams and f_{PRF} is the pulse repetition frequency (PRF).

4.4.3 ADMM Convergence Analysis

The convergence property demonstrates that the algorithm functions effectively, with the residuals diminishing over time until certain stopping criteria are met. Figure 4.2 shows the plots of the norms of primal residuals d_{pr1}, d_{pr2}, d_{pr3}, and d_{pr3}, Equation (4.42), and the stopping criteria limits ε_1^{pri}, ε_2^{pri}, ε_2^{pri}, ε_3^{pri}, and ε_4^{pri}, Equation (4.44), against the iteration numbers. The subplots show that the stopping criteria are satisfied within just a few iterations.

Similarly, Figure 4.3 shows the plots of the norms of dual residuals d_{rs1}, and d_{rs2}, Equation (4.43), and the stopping criteria limits ε^{dual}, last subequation in Equation (4.45), against the iteration numbers. The subplots too show that the stopping conditions are satisfied within the first few iterations.

The objective function, represented by the first line of Equation (4.31), was designed to minimize the power transmission in undesired direction. Figure 4.4 depicts a plot of the objective function values across various iterations. As evident from the figure, the objective function stabilizes within 20 iterations.

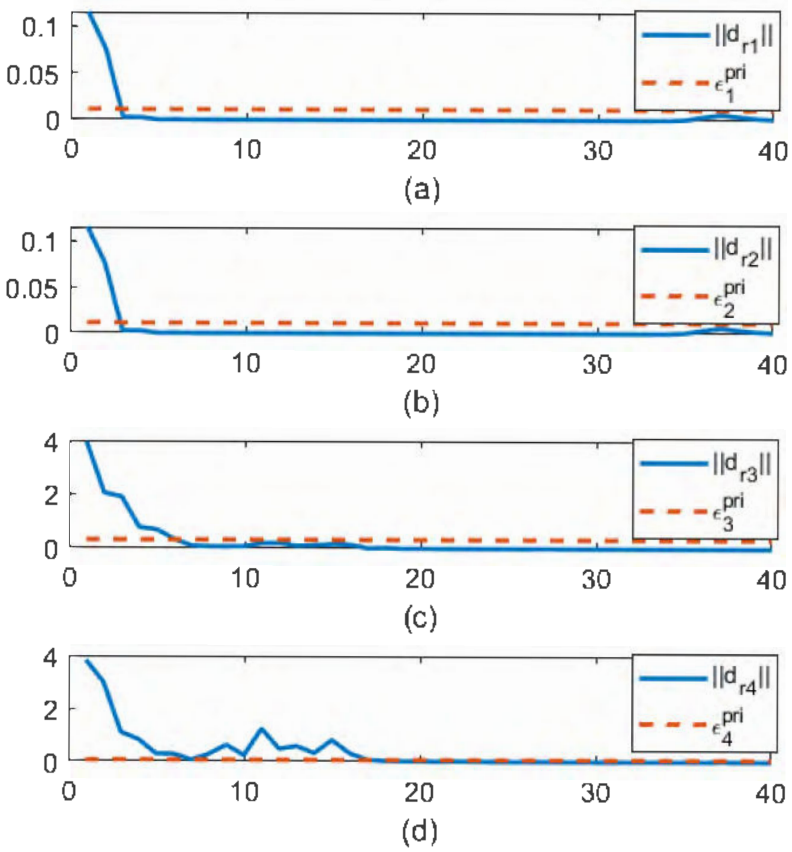

Figure 4.2: Gradual settling of the norms of primary residuals

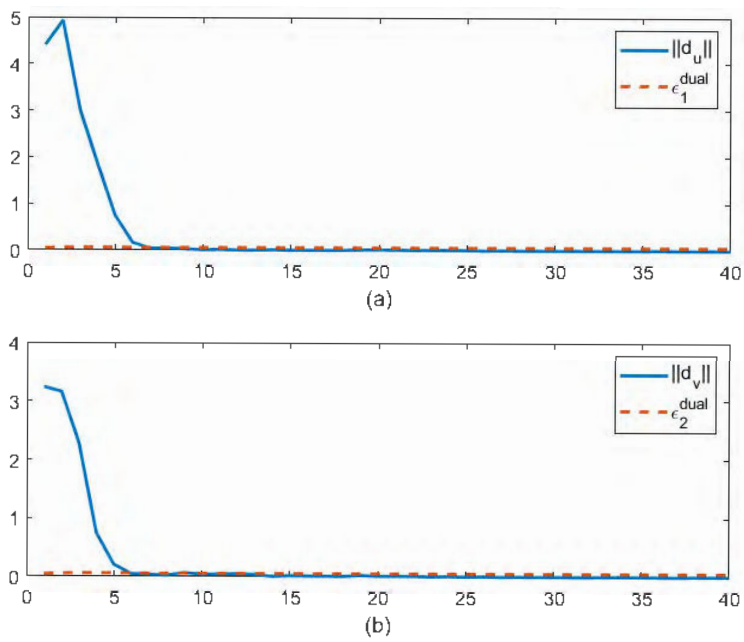

Figure 4.3: Gradual settling of the norms of dual residuals

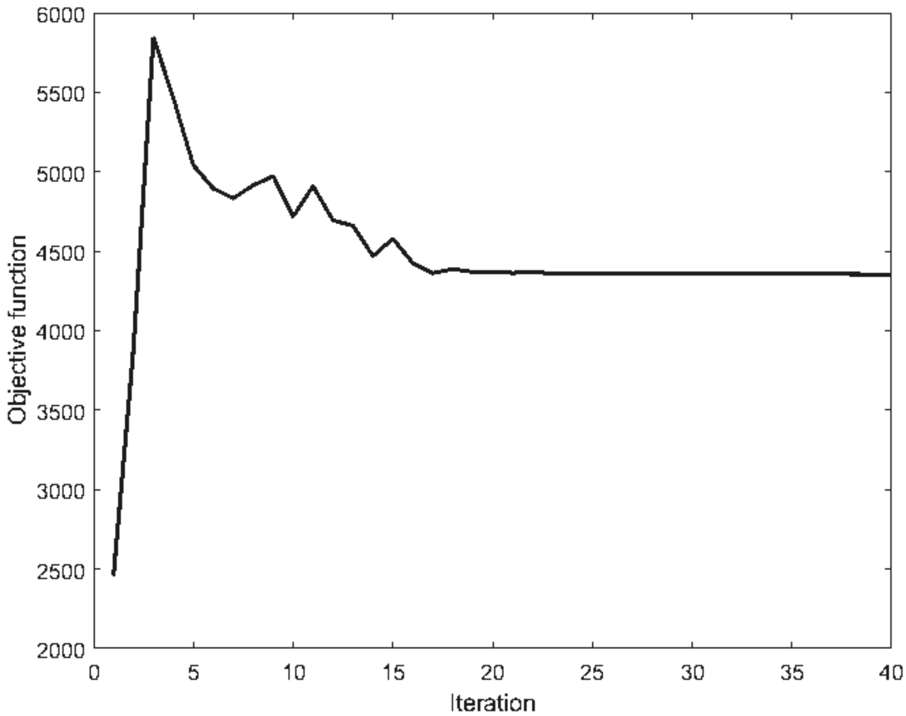

Figure 4.4: Settling of the Objective function, i.e, first line of Eq. (4.31)

4.4.4 Beampattern Analysis

Utilizing beamspace processing enhances the precision of the beampattern, enabling targeted signal detection and suppression in spatial domains. Figure 4.5 illustrates the beampattern at the transmitter produced by the beamspace matrix **W** using the proposed ADMM-based approach for a DFRC system featuring 32 antenna elements.

Figure 4.6 shows how the constant modulus constraint is satisfied. The plots in the figure indicate the maximum and the minimum values of **u**, which was another representation for the real version of the beamspace matrix **W**, and the desired uni-modular samples. As depicted in the graphs, both the maximum and minimum values stabilize around 10 by approximately the 20th iteration.

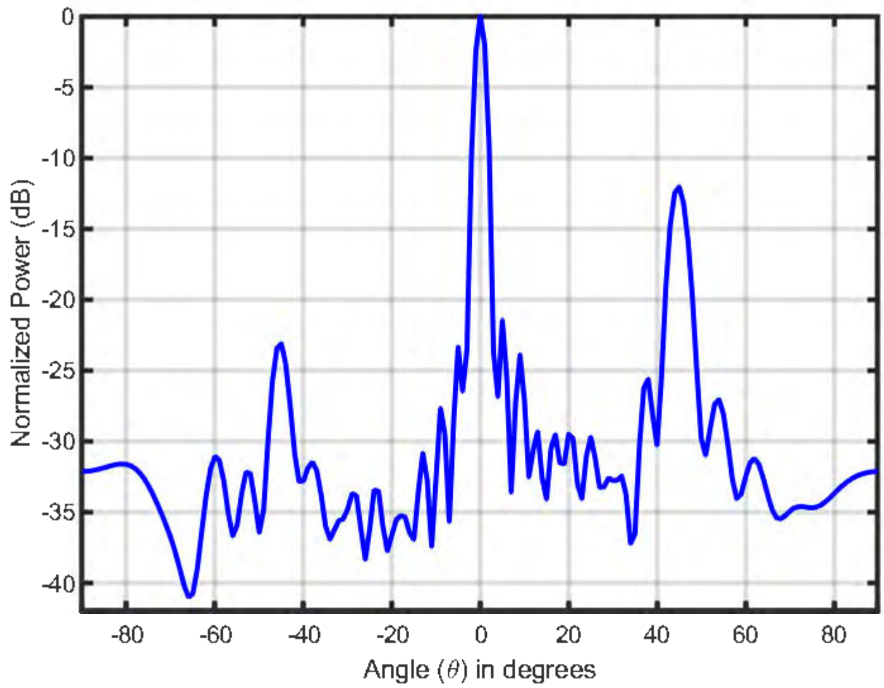

Figure 4.5: The transmit beampattern achieved through the proposed method

4.4.5 Radar Performance Analysis

An evaluation of radar performance through two key metrics is presented in this subsection. First, an analysis of the detection probability (pD) relative to SNR is provided. Then, probability of target resolution counterpart vs SNR is explored.

Figure 4.7 illustrates the graph of detection probability plotted against SNR, with the probability of false alarm set at 10^{-4}. Additionally, for comparison, pD versus SNR graphs of other methods are provided. As depicted in the figure, the proposed ADMM based method and FFRED-40% [85] exhibits the good pD, with ADMM slightly outperforming FFRED-40%. However, the graph of directly normalized method [86] closely follows, however its lower performance as compared with the other methods is obvious in the plot.

Moreover, we assess the performance of the proposed system under conditions where both the target and the communication receiver are in close prox-

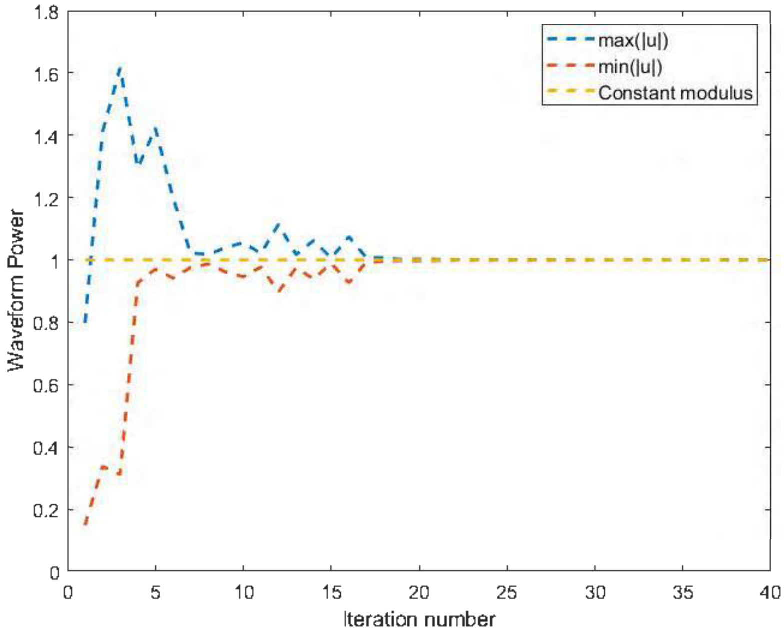

Figure 4.6: The moduli of beamspace weights approaching unity

imity. Specifically, the radar target is positioned at $\theta_r = 0^o$, while the communication receiver is located at $\theta_c = 3^o$. As depicted in Figure 4.8, the results demonstrate the superior performance of the ADMM-based approach proposed herein compared to the FFRED-40 % scheme previously introduced in[85].

4.4.6 Communication Performance Analysis

Communication performance is assessed using a comparison between the ADMM-based method and the FFRED, using the symbol error rate (SER) as a function of the signal-to-noise ratio (SNR) as a metric. Figure 4.9 displays the SER plotted against SNR. As is obvious in the plots, ADMM-based proposed methods exhibit best performance. FFRED-40% [85] has the next best performance. While the directly normalized waveform method [86] has the worst word performance.

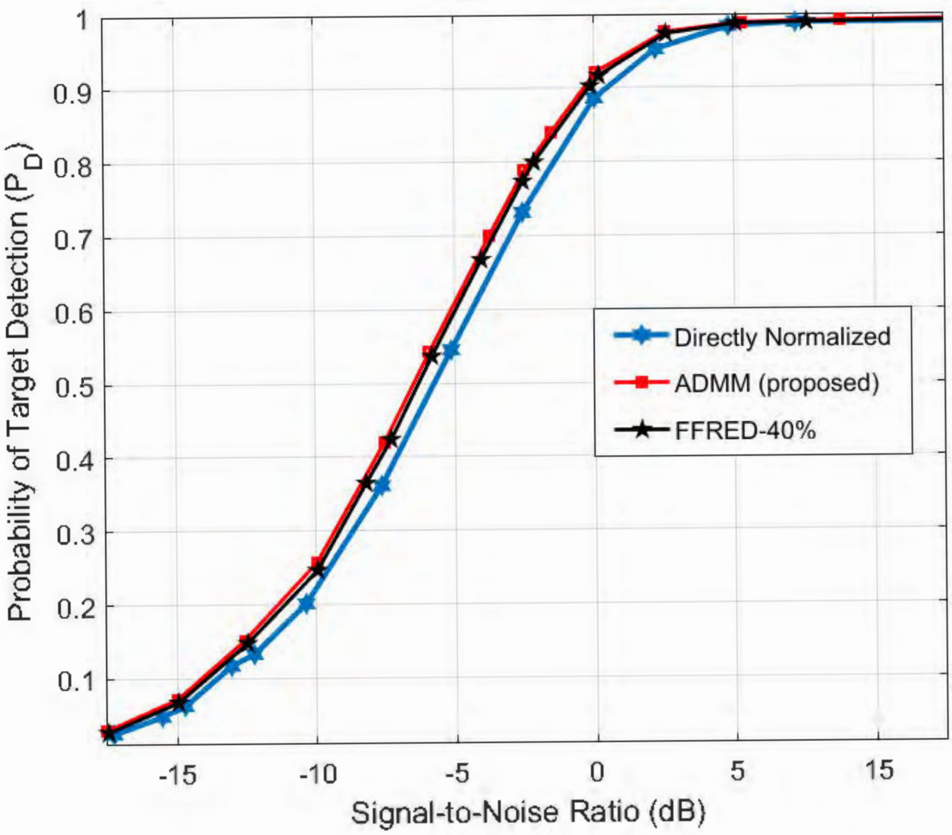

Figure 4.7: Comparison of different methods: detection probability vs SNR

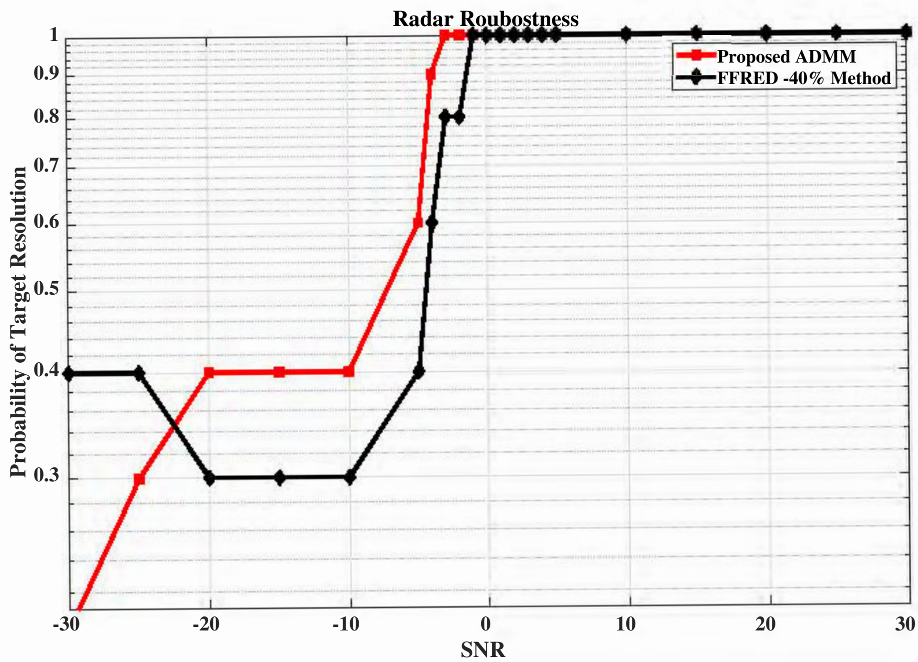

Figure 4.8: Comparison of different methods: target resolution vs SNR

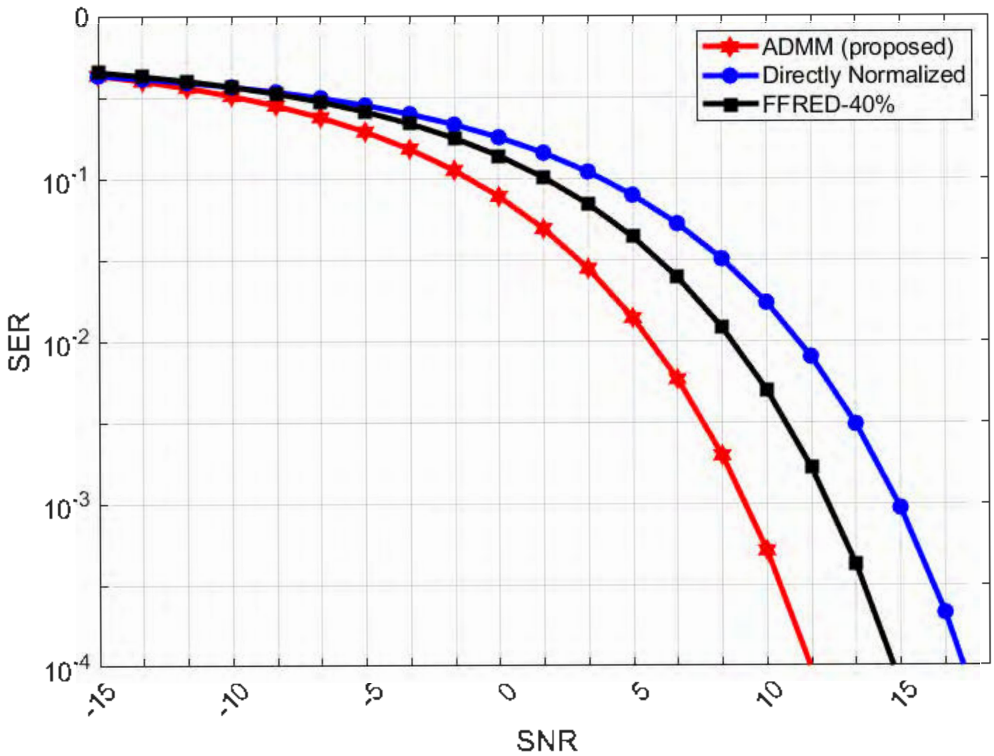

Figure 4.9: Comparison of different methods: SER vs SNR

4.5 Summary

This chapter has introduced an ADMM based design method of constant modulus beamspace transformation matrix design DFRC systems within a MIMO framework. Through formulating a non-convex optimization problem, the objective was to minimize power emission in undesired locations while maintaining desired power levels in target areas, all while adhering to a constant modulus constraint. To address this, an ADMM algorithm was utilized to solve the formulated optimization problem iteratively. Notably, the resultant waveforms approximate a desired beampattern, incorporating high-gain radar beams and slightly elevated gain communication beams, while also maintaining low sidelobe levels. The resulting beamspace matrix has shown promise in improving detection probability for radar functions and reducing bit error rates (BER) for communication tasks. The effectiveness of our proposed method has been demonstrated through simulation results, affirming its potential for enhancing the performance of DFRC systems.

Chapter 5

Conclusion and Future Work

5.1 Summary and Future Directions

This dissertation investigated the convergence of radar and communication functionalities within a unified system, with a focus on optimizing system performance through waveform design and beamspace processing. The research was structured into four chapters, briefly introduced as follows.

Chapter 1 provided an overview of the thesis, discussing the background of joint radar-communication and the motivation for addressing research challenges such as waveform design and beamspace processing in this domain. It defined the research problem, outlined research objectives, and discussed the contributions of the study.

Chapter 2 presented a thorough review of the relevant literature on radar, communication, and joint radar-communication, encompassing historical developments and contemporary trends. Additionally, it analyzed literature pertaining to waveform design and beamspace processing, supported by citations from various reports and articles detailing different techniques and methodologies.

Chapter 3 delved into detailed discussions on two waveform design methods for joint radar-communication. Both methods utilized ADMM-based optimization techniques to achieve specific objectives while adhering to various constraints. The first method focused on designing constant-modulus waveforms for MIMO-based dual-function radar-communication systems. Meanwhile, the second method was dedicated to designing constant-power waveforms for similar integrated systems.

Chapter 4 explored a beamspace design method for joint radar-communication. This approach employed ADMM-based optimization techniques to achieve defined objectives while addressing multiple constraints. Specifically, the method concentrated on designing a constant-modulus beamspace transformation matrix for MIMO-based dual-function radar-communication systems.

Chapter 5 concluded the thesis by presenting the outcomes of the research and evaluating the extent to which the research objectives had been achieved. It compared these results with contemporary research findings, highlighting the significant contributions made. The chapter also proposed future research directions in the field, emphasizing opportunities for further advancements in dual-function radar and communication systems. Additionally, it included a list of publications resulting from this work.

The dissertation concludes with a discussion on future research directions and a summary of key findings. The potential for further advancements in dual-function radar and communication systems is highlighted, emphasizing the importance of continued research in this rapidly evolving field.

Overall, this thesis advances the field of DFRC systems by proposing innovative methods in waveform design and beamspace processing. By employing optimization techniques such as ADMM, the research addresses challenges related to constant modulus and constant power waveform designs, enhancing the performance of MIMO-based dual-function systems. Additionally, the work on beamspace processing provides efficient solutions for reducing computational complexity while maintaining high performance standards. These contributions pave the way for more efficient, adaptive, and robust multifunctional systems, capable of meeting the growing demands of contemporary radar and communication applications.

5.2 Future Directions

Despite the extensive research being conducted, new challenges continuously emerge, necessitating future work to address these evolving challenges. Some of the challenges in the field include the following.

5.2.1 AI based Approaches

Constraint-based multi-objective optimization problems in waveform design and beamspace processing for DFRC systems often struggle with high computational complexity and slow convergence. Some solutions, like using recurrent neural networks, have been proposed to speed up waveform design. However, there is still considerable potential in using advanced machine learning and deep learning techniques to address computational challenges in both waveform optimization and beamspace design. Moreover, there are significant improvements needed in receiver signal classification. A key challenge is distinguishing between target echoes and communication signals in the presence of interference, noise, and clutter. Methods such as independent component analysis (ICA) or deep learning-based techniques could provide effective solutions to these problems, improving system performance. With the rapid advancements in artificial intelligence, particularly deep learning, exploring new technical approaches is highly promising. These approaches could lead to breakthroughs in both beamspace design and waveform optimization for RadCom systems.

5.2.2 Compressive Sensing based Approaches

Compressive sensing methods have been applied to address key challenges in DFRC systems. A primary challenge in DFRC is the accurate extraction of critical information from sparse and noisy signals. Compressive sensing techniques tackle this by exploiting signal sparsity, enabling accurate reconstruction with fewer measurements. This reduces data sampling requirements and computational burden, which are significant challenges in waveform design. Additionally, in beamspace processing, compressive sensing aids in precisely determining parameters such as range, velocity, and angle, even amidst noise and interference. By enhancing the efficiency and accuracy of both waveform design and beamspace processing, compressive sensing methods play a crucial role in overcoming the inherent challenges in DFRC systems.

5.2.3 Cognitive Radar-Communication

Cognitive radar-communication face several challenges that must be addressed to achieve optimal performance. One significant challenge is the dynamic adaptation of waveforms and beam patterns in real-time to varying environmental conditions and operational requirements, requiring advanced algorithms capable of quickly and accurately sensing the spectrum, detecting changes, and adjusting parameters without causing significant delays or errors. Another challenge lies in managing the trade-off between radar and communication functionalities, necessitating sophisticated resource management strategies and decision-making algorithms to balance the competing demands. Interference management is also critical, as cognitive systems and beamspace processing must distinguish between useful signals and noise in high-interference environments, requiring advanced signal processing techniques and robust algorithms for interference mitigation. Security is another concern, as dynamic adaptation can make CRC systems vulnerable to spoofing and jamming attacks, thus requiring robust encryption methods, authentication protocols, and strategies to detect and counteract malicious activities. Additionally, the computational complexity associated with cognitive processing and beamspace transformation can be significant, demanding powerful computing resources and efficient algorithms to process large volumes of data rapidly. Addressing these challenges is essential for the successful deployment of cognitive radar-communication systems and beamspace processing, paving the way for more intelligent and adaptive solutions in modern wireless communication and radar applications.

5.2.4 Security Challenges

Security challenges in DFRC systems are significant and multifaceted, demanding robust solutions to ensure reliable and secure operations. One primary concern is the vulnerability to jamming and spoofing attacks, where adversaries deliberately interfere with radar and communication signals to degrade system performance or mislead operations. This dual functionality increases the attack surface, as both radar and communication components can be targeted. Additionally, the dynamic nature of DFRC systems, which adapt in real-time to changing environments, presents opportunities for attackers to exploit these adaptive mechanisms. Ensuring secure data transmission and reception in such a scenario requires advanced encryption techniques and robust authentication protocols to prevent unauthorized access and data breaches. Furthermore, the integration of radar and communication functions necessitates the protection of sensitive information related to both domains, which can be challenging given the shared use of spectrum and hardware. Addressing these security challenges is critical for the development of resilient DFRC systems capable of withstanding and counteracting sophisticated threats in diverse and hostile environments.

5.2.5 Quantum technologies and DFRC

Quantum technologies are revolutionizing various fields, including communication and sensing. Quantum communication leverages principles of quantum mechanics, such as superposition and entanglement, to enhance secure data transmission. Quantum sensing, on the other hand, exploits quantum states to achieve unprecedented sensitivity and precision in measuring physical quantities. The convergence of these technologies leads to the emerging field of quantum DFRC, which aims to integrate quantum communication and quantum sensing capabilities into a single framework. This integration promises significant improvements in performance, security, and efficiency for next-generation radar and communication systems.

The advancement of quantum DFRC faces several challenges, particularly in the areas of waveform design and beamspace processing. Designing waveforms for quantum DFRC systems involves a higher level of complexity compared to classical systems. Quantum waveforms must maintain coherence and entanglement properties, which are essential for leveraging quantum advantages. Ensuring these properties while meeting practical constraints such as bandwidth, power, and robustness to noise requires advanced optimization techniques and a deep understanding of quantum mechanics. Beamspace processing in quantum

DFRC systems involves manipulating quantum states to direct and shape the radar beams. This process must account for the quantum nature of the signals, ensuring that entanglement and superposition states are preserved. Achieving precise beamforming and beam steering while maintaining quantum coherence presents significant technical challenges.

5.2.6 Intelligent Reflecting Surfaces Aided DFRC

Intelligent Reflecting Surfaces (IRS) are revolutionizing integrated radar-communication systems by enabling dynamic control over electromagnetic waves. These surfaces consist of passive elements that manipulate incoming signals to enhance transmission efficiency and coverage. In IRS-aided integrated radar-communication, challenges in waveform design arise from optimizing signals to interact effectively with IRS for improved radar detection and communication throughput. Beamforming and beamspace processing must adapt to IRS characteristics, ensuring coherent phase alignment and efficient wave reflection to achieve desired radar beam patterns and communication links. Overcoming these challenges involves developing sophisticated algorithms that can harness the full potential of IRS while mitigating complexities associated with signal interference and environmental variations.

5.2.7 mmWave Technology and DFRC

Millimeter-wave (mmWave) technology is transforming integrated radar-communication systems by leveraging high-frequency electromagnetic waves. In mmWave-based integrated radar-communication, challenges in waveform design emerge from optimizing signals to exploit the unique propagation characteristics of mmWave frequencies. Beamspace processing must be tailored to efficiently form and steer beams in dense environments with potentially high path loss and atmospheric absorption. Designing waveforms that mitigate these challenges while ensuring robust radar detection and reliable communication links requires innovative approaches in signal processing, antenna design, and modulation techniques. Successful implementation hinges on overcoming obstacles such as beamforming limitations, signal interference, and complex environmental interactions inherent to mmWave frequencies.

5.3 Bibliography

[1] A. Basit, "Hybrid cognitive phased and frequency diverse array radar," Ph.D. dissertation, Department of Electronic Engineering Faculty of Engineering and Technology ..., 2016.

[2] J. Li and P. Stoica, *MIMO radar signal processing*. John Wiley & Sons, 2008.

[3] Y. Liu and Y. C. Eldar, "Joint radar-communications strategies for autonomous vehicles," *IEEE Signal Processing Magazine*, vol. 1053, no. 5888/20, 2020.

[4] F. Liu and C. Masouros, "Communication and radar systems: Spectral coexistence and beyond," *Spectrum Sharing: The Next Frontier in Wireless Networks*, pp. 213–227, 2020.

[5] R. Yang, "Beam space signal processing for directional transmission phased arrays," Ph.D. dissertation, 2018.

[6] R. M. Mealey, "A method for calculating error probabilities in a radar communication system," *IEEE Transactions on Space Electronics and Telemetry*, vol. 9, no. 2, pp. 37–42, 1963.

[7] P. K. Hughes and J. Y. Choe, "Overview of advanced multifunction rf system (amrfs)," in *Proceedings 2000 IEEE International Conference on Phased Array Systems and Technology (Cat. No. 00TH8510)*. IEEE, 2000, pp. 21–24.

[8] F. Liu, L. Zheng, Y. Cui, C. Masouros, A. P. Petropulu, H. Griffiths, and Y. C. Eldar, "Seventy years of radar and communications: The road from

separation to integration," *IEEE Signal Processing Magazine*, vol. 40, no. 5, pp. 106–121, 2023.

[9] S. Mazahir, S. Ahmed, and M.-S. Alouini, "A survey on joint communication-radar systems," *Frontiers in Communications and Networks*, vol. 1, p. 619483, 2021.

[10] F. Liu, C. Masouros, A. P. Petropulu, H. Griffiths, and L. Hanzo, "Joint radar and communication design: Applications, state-of-the-art, and the road ahead," *IEEE Transactions on Communications*, vol. 68, no. 6, pp. 3834–3862, 2020.

[11] T. K. Sarkar and M. S. Palma, "A history of the evolution of radar," in *2014 44th European Microwave Conference*. IEEE, 2014, pp. 734–737.

[12] C. Süsskind, "Who invented radar?" *Endeavour*, vol. 9, no. 2, pp. 92–96, 1985.

[13] L. Brown, "A radar history of world war ii," *J. Am. Hist. Res*, 1999.

[14] R. J. Mailloux, "Phased array theory and technology," *Proceedings of the IEEE*, vol. 70, no. 3, pp. 246–291, 1982.

[15] P. Antonik, M. C. Wicks, H. D. Griffiths, and C. J. Baker, "Frequency diverse array radars," in *2006 IEEE Conference on Radar*. IEEE, 2006, pp. 3–pp.

[16] S. Haykin, "Cognitive radar: a way of the future," *IEEE signal processing magazine*, vol. 23, no. 1, pp. 30–40, 2006.

[17] O. Boric-Lubecke, V. M. Lubecke, A. Host-Madsen, D. Samardzija, and K. Cheung, "Doppler radar sensing of multiple subjects in single and mul-

tiple antenna systems," in *TELSIKS 2005-2005 uth International Conference on Telecommunication in ModernSatellite, Cable and Broadcasting Services*, vol. 1. IEEE, 2005, pp. 7–11.

[18] J. Das and P. Venkateswaran, "Design and development of multiple antenna based system for radar applications," in *2015 IEEE MTT-S International Microwave and RF Conference (IMaRC)*. IEEE, 2015, pp. 143–146.

[19] W. P. Delaney and W. W. Ward, "Radar development at lincoln laboratory: An overview of the first fifty years," *Lincoln Laboratory Journal*, vol. 12, no. 2, pp. 147–166, 2000.

[20] A. J. Fenn, D. H. Temme, W. P. Delaney, and W. E. Courtney, "The development of phased-array radar technology," *Lincoln laboratory journal*, vol. 12, no. 2, pp. 321–340, 2000.

[21] E. Brookner, "Phased-array radars," *Scientific American*, vol. 252, no. 2, pp. 94–103, 1985.

[22] A. Ludvig-Osipov, J.-M. Hannula, P. Naccachian, and B. L. G. Jonsson, "Physical limitations of phased array antennas," *IEEE Transactions on Antennas and Propagation*, vol. 69, no. 9, pp. 5512–5523, 2021.

[23] P. Antonik, "An investigation of a frequency diverse array," Ph.D. dissertation, UCL (University College London), 2009.

[24] A. Basit, W. Khan, S. Khan, and I. M. Qureshi, "Development of frequency diverse array radar technology: a review," *IET Radar, Sonar & Navigation*, vol. 12, no. 2, pp. 165–175, 2018.

[25] W.-Q. Wang, "Overview of frequency diverse array in radar and navigation applications," *IET Radar, Sonar & Navigation*, vol. 10, no. 6, pp. 1001–1012, 2016.

[26] W. Khan and I. M. Qureshi, "Frequency diverse array radar with time-dependent frequency offset," *IEEE Antennas and Wireless Propagation Letters*, vol. 13, pp. 758–761, 2014.

[27] H. Shao, J. Li, H. Chen, and W.-Q. Wang, "Adaptive frequency offset selection in frequency diverse array radar," *IEEE Antennas and Wireless Propagation Letters*, vol. 13, pp. 1405–1408, 2014.

[28] E. Fishler, A. Haimovich, R. Blum, D. Chizhik, L. Cimini, and R. Valenzuela, "Mimo radar: An idea whose time has come," in *Proceedings of the 2004 IEEE Radar Conference (IEEE Cat. No. 04CH37509)*. IEEE, 2004, pp. 71–78.

[29] E. Fishler, A. Haimovich, R. S. Blum, L. J. Cimini, D. Chizhik, and R. A. Valenzuela, "Spatial diversity in radars—models and detection performance," *IEEE Transactions on signal processing*, vol. 54, no. 3, pp. 823–838, 2006.

[30] K. Forsythe, D. Bliss, and G. Fawcett, "Multiple-input multiple-output (mimo) radar: Performance issues," in *Conference Record of the Thirty-Eighth Asilomar Conference on Signals, Systems and Computers, 2004.*, vol. 1. IEEE, 2004, pp. 310–315.

[31] T. K. Sarkar, R. Mailloux, A. A. Oliner, M. Salazar-Palma, and D. L. Sengupta, *History of wireless*. John Wiley & Sons, 2006.

[32] L. Coe, *Wireless radio: A brief history*. McFarland, 1996.

[33] V. K. Nassa, “Wireless communications: Past, present and future,” *Dronacharya Research Journal*, vol. 50, 2011.

[34] K. G. Beauchamp, *History of telegraphy*. Iet, 2001, no. 26.

[35] H. N. Casson, *The history of the telephone*. AC McClurg & Company, 1910.

[36] G. Marconi, “Radio telegraphy,” *Journal of the American Institute of Electrical Engineers*, vol. 41, no. 8, pp. 561–570, 1922.

[37] J. B. Andersen, “History of communications/radio wave propagation from marconi to mimo,” *IEEE Communications Magazine*, vol. 55, no. 2, pp. 6–10, 2017.

[38] C. Fortuna and M. Mohorcic, “Trends in the development of communication networks: Cognitive networks,” *Computer networks*, vol. 53, no. 9, pp. 1354–1376, 2009.

[39] Y. Rahmat-Samii and A. C. Densmore, “Technology trends and challenges of antennas for satellite communication systems,” *IEEE Transactions on Antennas and Propagation*, vol. 63, no. 4, pp. 1191–1204, 2014.

[40] N. Navet, Y. Song, F. Simonot-Lion, and C. Wilwert, “Trends in automotive communication systems,” *Proceedings of the IEEE*, vol. 93, no. 6, pp. 1204–1223, 2005.

[41] F. Liu, L. Zhou, C. Masouros, A. Li, W. Luo, and A. Petropulu, “Toward dual-functional radar-communication systems: Optimal waveform design,” *IEEE Transactions on Signal Processing*, vol. 66, no. 16, pp. 4264–4279, 2018.

[42] C. Sturm and W. Wiesbeck, “Waveform design and signal processing aspects for fusion of wireless communications and radar sensing,” *Proceedings of the IEEE*, vol. 99, no. 7, pp. 1236–1259, 2011.

[43] M. Bică and V. Koivunen, “Radar waveform optimization for target parameter estimation in cooperative radar-communications systems,” *IEEE Transactions on Aerospace and Electronic Systems*, vol. 55, no. 5, pp. 2314–2326, 2018.

[44] M. Alaee-Kerahroodi, E. Raei, S. Kumar, and B. S. MRR, “Cognitive radar waveform design and prototype for coexistence with communications,” *IEEE Sensors Journal*, vol. 22, no. 10, pp. 9787–9802, 2022.

[45] Y. Yao, P. Miao, and Z. Chen, “Cognitive waveform optimization for phase-modulation-based joint radar-communications system,” *IEEE Access*, vol. 8, pp. 33 276–33 288, 2020.

[46] S. K. Agrawal, A. Samant, and S. K. Yadav, “Spectrum sensing in cognitive radio networks and metacognition for dynamic spectrum sharing between radar and communication system: A review,” *Physical Communication*, vol. 52, p. 101673, 2022.

[47] J. Wang, S. Guan, C. Jiang, D. Alanis, Y. Ren, and L. Hanzo, “Network association in machine-learning aided cognitive radar and communication co-design,” *IEEE Journal on Selected Areas in Communications*, vol. 37, no. 10, pp. 2322–2336, 2019.

[48] A. C. Mahipathi, B. Pardhasaradhi, T. Purushottama, P. Srihari, J. D’Souza, and L. R. Cenkeramaddi, “A survey on waveform design for radar-communication convergence,” *IEEE Access*, 2024.

[49] M. Roberton and E. Brown, “Integrated radar and communications based on chirped spread-spectrum techniques,” in *IEEE MTT-S International Microwave Symposium Digest, 2003*, vol. 1. IEEE, 2003, pp. 611–614.

[50] X. Shaojian, C. Bing, and Z. Ping, “Radar-communication integration based on dsss techniques,” in *2006 8th international Conference on Signal Processing*, vol. 4. IEEE, 2006.

[51] B. Donnet and I. Longstaff, “Combining mimo radar with ofdm communications,” in *2006 European radar conference*. IEEE, 2006, pp. 37–40.

[52] G. N. Saddik, R. S. Singh, and E. R. Brown, “Ultra-wideband multifunctional communications/radar system,” *IEEE Transactions on Microwave Theory and Techniques*, vol. 55, no. 7, pp. 1431–1437, 2007.

[53] D. W. Bliss, “Cooperative radar and communications signaling: The estimation and information theory odd couple,” in *2014 IEEE Radar Conference*. IEEE, 2014, pp. 0050–0055.

[54] A. Hassanien, M. G. Amin, Y. D. Zhang, and F. Ahmad, “Dual-function radar-communications: Information embedding using sidelobe control and waveform diversity,” *IEEE Transactions on Signal Processing*, vol. 64, no. 8, pp. 2168–2181, 2015.

[55] X. Wang, Z. Fei, J. Guo, Z. Zheng, and B. Li, “Ris-assisted spectrum sharing between mimo radar and mu-miso communication systems,” *IEEE Wireless Communications Letters*, vol. 10, no. 3, pp. 594–598, 2020.

[56] S. K. Dehkordi, L. Gaudio, M. Kobayashi, G. Colavolpe, and G. Caire, “Beam-space mimo radar with otfs modulation for integrated sensing and

communications," in *2022 IEEE International Conference on Communications Workshops (ICC Workshops)*. IEEE, 2022, pp. 509–514.

[57] P.-C. Chen and P. Vaidyanathan, "Channel estimation for mmwave using the convolutional beamspace approach," *IEEE Transactions on Signal Processing*, 2024.

[58] J. Brady, N. Behdad, and A. M. Sayeed, "Beamspace mimo for millimeter-wave communications: System architecture, modeling, analysis, and measurements," *IEEE Transactions on Antennas and Propagation*, vol. 61, no. 7, pp. 3814–3827, 2013.

[59] X. Wei, C. Hu, and L. Dai, "Deep learning for beamspace channel estimation in millimeter-wave massive mimo systems," *IEEE Transactions on Communications*, vol. 69, no. 1, pp. 182–193, 2020.

[60] R. Pal and K. Sarawadekar, "Distributed ris-assisted mmwave multi-user mimo beamspace system," *AEU-International Journal of Electronics and Communications*, vol. 161, p. 154560, 2023.

[61] J. He, H. Wymeersch, T. Sanguanpuak, O. Silvén, and M. Juntti, "Adaptive beamforming design for mmwave ris-aided joint localization and communication," in *2020 IEEE Wireless Communications and Networking Conference Workshops (WCNCW)*. IEEE, 2020, pp. 1–6.

[62] J. Wang, W. Tang, S. Jin, C.-K. Wen, X. Li, and X. Hou, "Hierarchical codebook-based beam training for ris-assisted mmwave communication systems," *IEEE Transactions on Communications*, vol. 71, no. 6, pp. 3650–3662, 2023.

[63] J. Sun, M. Jia, Q. Guo, and X. Gu, “Joint user grouping and beam selection for beamspace mmwave multi-user mimo system,” *IEEE Communications Letters*, vol. 26, no. 5, pp. 1170–1174, 2022.

[64] R. Wei, Q. Xue, Y. Xu, L. Yan, and S. Ma, “Joint beamforming design for cooperative double-ris aided mmwave multi-user mimo communications,” in *2023 IEEE 98th Vehicular Technology Conference (VTC2023-Fall)*. IEEE, 2023, pp. 1–6.

[65] X. Cheng, Y. Yang, B. Xia, N. Wei, and S. Li, “Sparse channel estimation for millimeter wave massive mimo systems with lens antenna array,” *IEEE Transactions on Vehicular Technology*, vol. 68, no. 11, pp. 11 348–11 352, 2019.

[66] R. Pal, K. Srinivas, and A. K. Chaitanya, “A beam selection algorithm for millimeter-wave multi-user mimo systems,” *IEEE Communications Letters*, vol. 22, no. 4, pp. 852–855, 2018.

[67] M. A. L. Sarker, M. F. Kader, and D. S. Han, “Hybrid beam selection scheme in millimeter-wave beamspace mimo-noma with lens antenna array,” *AEU-International Journal of Electronics and Communications*, vol. 120, p. 153204, 2020.

[68] Z. Cheng, B. Liao, S. Shi, Z. He, and J. Li, “Co-design for overlaid mimo radar and downlink miso communication systems via cramér–rao bound minimization,” *IEEE Transactions on Signal Processing*, vol. 67, no. 24, pp. 6227–6240, 2019.

[69] Z. Cheng, S. Shi, Z. He, and B. Liao, “Transmit sequence design for dual-

function radar-communication system with one-bit dacs," *IEEE Transactions on Wireless Communications*, vol. 20, no. 9, pp. 5846–5860, 2021.

[70] C. Xu, B. Clerckx, S. Chen, Y. Mao, and J. Zhang, "Rate-splitting multiple access for multi-antenna joint radar and communications," *IEEE Journal of Selected Topics in Signal Processing*, vol. 15, no. 6, pp. 1332–1347, 2021.

[71] R. Liu, M. Li, Y. Liu, Q. Wu, and Q. Liu, "Joint transmit waveform and passive beamforming design for ris-aided dfrc systems," *IEEE Journal of Selected Topics in Signal Processing*, vol. 16, no. 5, pp. 995–1010, 2022.

[72] X. Yu, X. Yao, J. Yang, L. Zhang, L. Kong, and G. Cui, "Integrated waveform design for mimo radar and communication via spatio-spectral modulation," *IEEE Transactions on Signal Processing*, vol. 70, pp. 2293–2305, 2022.

[73] T. Wei, L. Wu, K. V. Mishra, and M. B. Shankar, "Multiple irs-assisted wideband dual-function radar-communication," in *2022 2nd IEEE International Symposium on Joint Communications & Sensing (JC&S)*. IEEE, 2022, pp. 1–5.

[74] Z. Cheng and B. Liao, "Qos-aware hybrid beamforming and doa estimation in multi-carrier dual-function radar-communication systems," *IEEE Journal on Selected Areas in Communications*, vol. 40, no. 6, pp. 1890–1905, 2022.

[75] A. Murtada, B. S. M. R. Rao, and U. Schroeder, "Distributed radar imaging based on accelerated admm," *arXiv preprint arXiv:2307.08606*, 2023.

[76] X. Zhao, H. Liu, S. Gong, X. Ju, C. Xing, and N. Zhao, "Dual-functional mimo beamforming optimization for ris-aided integrated sensing and communication," *IEEE Transactions on Communications*, 2024.

[77] Y. Yao, F. Shu, X. Cheng, H. Liu, P. Miao, and L. Wu, "Automotive radar optimization design in a spectrally crowded v2i communication environment," *IEEE Transactions on Intelligent Transportation Systems*, vol. 24, no. 8, pp. 8253–8263, 2023.

[78] B. K. Chalise, D. M. Wong, K. T. Wagner, and M. G. Amin, "Enhancing distributed radar detection performance with reliable communications," *IEEE Transactions on Aerospace and Electronic Systems*, vol. 59, no. 4, pp. 4118–4133, 2023.

[79] Y. Chen, C. Wen, Y. Huang, L. Liang, J. Li, H. Zhang, and W. Hong, "Joint design of isac waveform under papr constraints," *arXiv preprint arXiv:2311.11594*, 2023.

[80] J. Liu, K. V. Mishra, and M. Saquib, "Co-designing statistical mimo radar and in-band full-duplex multi-user mimo communications–part ii: Joint precoder, radar code, and receive filters design," *arXiv preprint arXiv:2403.19119*, 2024.

[81] S. Zhang, Z. Xiao, R. Liu, M. Li, W. Wang, and Q. Liu, "Multipath exploitation for fluctuating target detection in ris-assisted isac systems," *arXiv preprint arXiv:2406.00604*, 2024.

[82] P. Li, M. Li, R. Liu, Q. Liu, and A. L. Swindlehurst, "Mimo-ofdm isac waveform design for range-doppler sidelobe suppression," *arXiv preprint arXiv:2406.17218*, 2024.

[83] B. Lee, A. B. Das, D. Love, C. Brinton, and J. Krogmeier, “Constant modulus waveform design with interference exploitation for dfrc systems: A block-level optimization approach,” *arXiv preprint arXiv:2406.18951*, 2024.

[84] S. Boyd, N. Parikh, E. Chu, B. Peleato, J. Eckstein *et al.*, “Distributed optimization and statistical learning via the alternating direction method of multipliers,” *Foundations and Trends® in Machine learning*, vol. 3, no. 1, pp. 1–122, 2011.

[85] P. M. McCormick, S. D. Blunt, and J. G. Metcalf, “Simultaneous radar and communications emissions from a common aperture, part i: Theory,” in *2017 IEEE Radar Conference (RadarConf)*. IEEE, 2017, pp. 1685–1690.

[86] L. Han and K. Wu, “24-ghz integrated radio and radar system capable of time-agile wireless communication and sensing,” *IEEE Transactions on Microwave Theory and Techniques*, vol. 60, no. 3, pp. 619–631, 2012.

[87] M. Jiang, G. Liao, Z. Yang, Y. Liu, and Y. Chen, “Integrated radar and communication waveform design based on a shared array,” *Signal Processing*, vol. 182, p. 107956, 2021.

[88] B. Wohlberg, “Admm penalty parameter selection by residual balancing,” *arXiv preprint arXiv:1704.06209*, 2017.